Weight & Balance Estimation with Automated Structural Analysis for Subscale Flight Models

A Knowledge Based Engineering Approach

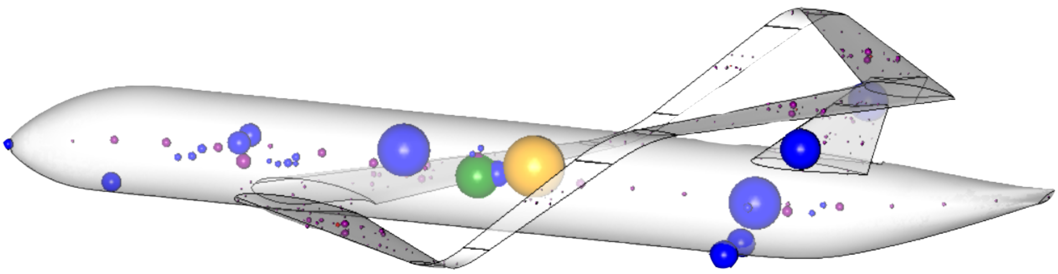

L.N. de Ruiter

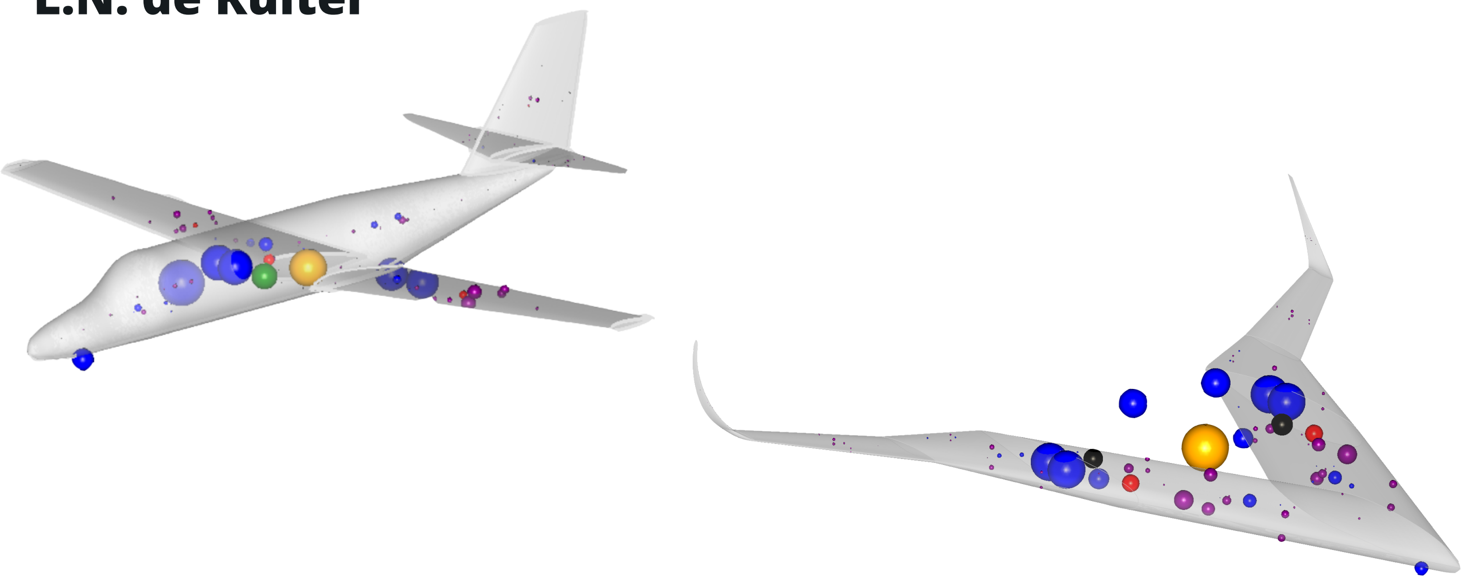

WEIGHT & BALANCE ESTIMATION WITH AUTOMATED STRUCTURAL ANALYSIS FOR SUBSCALE FLIGHT MODELS

A thesis submitted to the Delft University of Technology in partial fulfillment
of the requirements for the degree of

Master of Science in Aerospace Engineering
to be defended publicly on Friday October 16, 2020 at 09:30.

Author

Luc de Ruiter

Student number

4223500

Master Thesis Student, Faculty of Aerospace Engineering

September 2020

The research project is funded by the Clean Sky 2 project, part of the European Union Research Framework Program:

Work Package 1.3 & 1.6
Novair project
European Union Research Framework Program

This research is done at Delft University of Technology:

Department of Flight Performance & Propulsion
Faculty of Aerospace Engineering
Delft University of Technology

Supervisors: Prof.dr.ir. Leo Veldhuis
Prof.dr.ir. Gianfranco La Rocca
PhD Candidate. Akshay Raju Kulkarni
Dr.ir. Daniel Peeters

PREFACE

This report shows the research steps taken to conclude my master's thesis at the division of Flight Performance and Propulsion of the faculty of Aerospace Engineering at the Delft University of Technology in Delft, The Netherlands.

First of all I would like to thank my daily supervisor Akshay Kulkarni (PhD candidate TU Delft, Netherlands) for all his effort and support in guiding me through this research project. Also, special thanks to Max Baan from ParaPy (Delft, Netherlands), who assisted me during this period even when on holidays and moving to another house. Moreover, I would like to thank Vivek Ahuja from Flightstream company (Texas, USA), for the support on Aerodynamics and Paul Lancelot (PhD candidate TU Delft, Netherlands) and Noël Bijl (MSC software) for the support on structural problems.

Undoubtedly, I owe the deepest gratitude to my parents. They provide me with the greatest possible support for all decisions I take in my life, and always give me a safe home and unlimited love. I am truly thankful for this.

Moreover, studying in Delft made it possible to do a minor abroad as Erasmus exchange student at the Universidad Politécnica de Madrid during the bachelor. To stay and live for 5 months in Madrid was a memorable time. In the master I had the privilege to be part of the construction of a new airport in Abu Dhabi. I was based on project location for three months. I experienced this as very enriching, as I experienced to live and work in a country which is extreme in many ways, not only for the temperatures, but also where the western-thinking has not yet been the standard. More importantly, I am very grateful to have not only developed technically during my study, but also personally, especially during these periods abroad.

Luc de Ruiter
Delft, October 7, 2020

ABSTRACT

Unconventional aircraft designs have the potential to lower the impact of aviation on emissions and climate as compared to conventional aircraft designs. However, the flight dynamics behaviour of such unconventional configurations must be carefully evaluated by studying Stability and Control (S&C) characteristics to design safe aircraft and mitigate risks in flight. Various methods, that are a combination of numerical and experimental methods, have been used in the literature to predict the S&C characteristics. Sub-scale Flight Testing (SFT) is one such method that can predict aircraft flight behaviour, especially in the case of unconventional designs for which legacy information is unavailable and wind tunnel tests can partially predict aircraft dynamics.

In order to successfully use SFT, the Sub-scale Model (SM) used in SFT must be carefully designed such that the results of SFT can be scaled-up to predict full-scale flight behavior. Furthermore, the SM should be able to complete the required SFT mission safely (the model is trimmable, statically stable and dynamically stable throughout the flight envelope). Finally, the SM must be designed with a short lead-time, as the time available for SFT in the overall design cycle is limited. Thus, the design of sub-scale models is a multidisciplinary task. In this thesis, an appropriate methodology is identified and developed to design the structural components of SM, position Commercial Off-The-Shelf (COTS) components and estimate the mass, inertia and the associated Center of Gravity (CG) of the SM. These are important inputs to determine the flight dynamics behaviour of the SM. Secondly, the structural analysis capabilities are automated to ensure that the structure does not fail in flight under critical load conditions.

To shorten the design lead-time, methodologies developed in this thesis are formalized using a Knowledge Based Engineering (KBE) system. This KBE application automates the estimation of the weight & balance of a SM, which includes software modules for structure generation, flight equipment selection and positioning and the automated pre/post-processing task for Finite-Element (FE) analysis. Such a KBE application enables structural studies for different SM scale sizes, design variables such as rib pitch or frame pitch, and load cases. This KBE application to estimate the weight & balance properties of the SM can be coupled with other disciplines such as aerodynamic analysis, flight dynamics toolbox, etc. as part of a Multidisciplinary Design Analysis and Optimization (MDAO) workflow to quickly design sub-scale models that can be used to predict full-scale flight behaviour.

Three different case studies are performed to demonstrate the effectiveness of the methodology and the KBE application. Each case study predicts the different aircraft configuration namely, a conventional Citation II and two unconventional models being the Prandtl-Plane and the Flying V. The methodologies can therefore be used for future SFT activities and can help in successfully comparing the sub-scale aircraft model behavior to the full-scale aircraft behavior, thereby making Sub-scale Flight Testing a step closer to reality.

CONTENTS

LIST OF FIGURES

LIST OF TABLES

NOMENCLATURE

ACRONYMS

CAD Computer Aided Design

CFD Computational Fluid Dynamics

CG Center of Gravity

COTS Commercial Off-The-Shelf

DEE Design and Engineering Engine

DNS Direct Numerical Simulation

DOE Design of Experiment

DoS Degree of Similitude

EOM Equations of Motion

FD Full-scale Design

FE Finite-Element

FER Full-scale Experimental Response

FFT Full-scale Flight Test

FPP Flight Performance & Propulsion

FRP Fibre-Reinforced Polymers

FSA Full-scale Aircraft

FVR Full-scale Virtual Response

HFQ Handling and Flying Qualities

HLP High-Level Primitives

KBE Knowledge Based Engineering

LES Large-Eddy Simulation

MMG Multi-Model Generator

MDAO Multidisciplinary Design Analysis and Optimization

OML Outer Mold Line

RANS Reynolds-averaged Navier–Stokes

S&C Stability and Control

SD Sub-scale Design

SFC Specific Fuel Consumption

SFT Sub-scale Flight Testing

SM Sub-scale Model

TLR Top Level Requirement

TUD Technical University Delft

xDSM eXtended Design Structure Matrix

3DPM 3D Panel Method

ROMAN SYMBOLS

b	Wing span	$[m]$
c	Mean aerodynamic chord	$[m]$
c_l	Coefficient of the lift distribution	$[-]$
C_L	Lift coefficient	$[-]$
C_{L_α}	$\frac{\delta C_L}{\delta \alpha}$	$[1/rad]$
$C_{L_{\dot{\alpha}}}$	$\frac{\delta C_L}{\delta \dot{\alpha}}$	$[1/rad]$
$C_{L_{\delta e}}$	$\frac{\delta C_L}{\delta e}$	$[1/rad]$
$C_{L_{\dot{\delta} e}}$	$\frac{\delta C_L}{\dot{\delta} e}$	$[1/rad]$
C_{L_u}	V $\frac{\delta C_L}{\delta u}$	$[1/rad]$
C_{L_q}	$\frac{\delta C_L}{\delta (qc/2V)}$	$[1/rad]$
C_{m_α}	$\frac{\delta C_m}{\delta \alpha}$	$[1/rad]$
$C_{m_{\dot{\alpha}}}$	$\frac{\delta C_m}{\delta \dot{\alpha}}$	$[1/rad]$
C_{m_q}	$\frac{\delta C_m}{\delta q}$	$[1/rad]$
C_{z_α}	$\frac{\delta C_z}{\delta \alpha}$	$[1/rad]$
$C_{z_{\dot{\alpha}}}$	$\frac{\delta C_z}{\delta \dot{\alpha}}$	$[1/rad]$
C_{z_q}	$\frac{\delta C_z}{\delta q}$	$[1/rad]$
D	Drag force	$[N]$
g	gravitational constant	$[m/s^2]$
i	Imaginary number	$[-]$
$I_{xx,yy,zz}$	Mass moment of inertia	$[kgm^2]$
I_{xz}	Product moment of inertia	$[kgm^2]$
$K_{X,Y,Z}$	Non-dimensional radius of gyration	$[-]$
K_{XZ}	Non-dimensional product of inertia	$[-]$
L	Lift force	$[N]$
M	Mach number	$[-]$
m	Mass	$[kg]$
n	Scale factor	$[-]$
n_z	Load factor in z-direction	$[-]$
p	roll rate	$[rad/s]$
q	Pitch rate	$[rad/s]$
r	yaw rate	$[rad/s]$
Re	Reynolds number	$[-]$
S	Surface area	$[m^2]$
V	Flight speed	$[m/s]$
W	Aircraft weight	$[-]$

GREEK SYMBOLS

α	angle of attack	$[rad]$
$\dot{\alpha}$	rate of change of angle of attack	$[rad/s]$
β	angle of sideslip	$[rad]$
γ	shear strain	$[rad]$
δ	deflection angle	$[rad]$
ϵ	normal strain	$[-]$
η	frequency coefficient	$[-]$
λ	Eigenvalue	$[-]$
μ_c	Relative density for symmetric motions	$[m/\rho Sc]$
ξ	damping coefficient	$[-]$
ρ	Air density	$[-]$
σ	Density ratio	$[-]$

DEFINITIONS

bdf	Input file for Nastran (FEM analysis)
bulkhead	Member of a fuselage in lateral direction, to distribute concentrated loads into the fuselage skin
card	Text line in the bdf (Nastran) file that describes a property e.g. grid point or mass property
floor	Member of a wing or fuselage on which the flight equipment is placed
frame	Member of a fuselage in lateral direction, to maintain the circumferential fuselage shape and prevent instability of the structure
MTOM	maximum take-off mass
nastran	NASA structural analysis; FEM solver used for structural analysis
python	Open source programming language
rib	Member of a wingbox either in flow direction, at an angle, or perpendicular to the spars
riblet	Special type of rib, in which portions of the rib at the leading edge or the trailing edge can have different orientations
segment	Structure between two neighbouring ribs
skin	Supporting the aerodynamic pressure distribution
SOL101	MSC.Nastran solver for static loads analysis
spar	Structural member of the wingbox running in spanwise direction between rib elements
wingbox	Main structural element in a wing to take torsional loads

1 INTRODUCTION

Unconventional aircraft designs have the potential to accommodate the expected growth of flights worldwide as compared to conventional aircraft designs [1]. That is needed because the impact of the aviation industry on the emission of pollutants and noise annoyance will increase [2]. Environmental concerns and growing oil scarcity are stimulating advanced and radically new transportation technologies [3].

Although all disciplines for conventional aircraft evolved over time, it seems to have reached a plateau in terms of fuel efficiency [4]. From the simplified Breguet-Formula, Equation 1.1, a lower Specific Fuel Consumption (SFC) can be obtained by using more efficient engines, secondly the lift and drag can be improved due to aerodynamic improvements, and weight improvements are obtained by the development of novel airframe technologies such as advanced composite materials and active load alleviation of wing structures [5].

$$\frac{\text{Trip Fuel}}{\text{Distance}} \approx \frac{SFC}{M_\infty} \approx \frac{W}{L/D} \tag{1.1}$$

However, the design changes due to aerodynamic-, engine-, or structural- improvements can have large influence on the Stability & Control (S&C) of the aircraft, and thus the safety. A good example is the recent crash of two Boeing 737 Max's in October 2018 and later in March 2019 due to a software error. When Boeing set out to develop the 737 Max, engineers had to find a way to fit the much larger and more fuel efficient engine under the wing of the aircraft. By moving the engine slightly forward and higher up and extending the nose landing gear by eight inches, Boeing was able to reach another 14% improvement in fuel consumption [6]. The displacement of components changed how the aircraft responded in certain situations regarding the flight mechanics. The relocated engines and their refined nacelle shape caused an upward pitching moment at high angles of attack. A new system was added to compensate for the upward pitching moment to help pilots bring the nose down in the event the aircraft angle of attack became too high when flying manually, putting the aircraft at risk of stalling.

From this example it becomes clear that small improvements to the design can affect the S&C due to the weight & balance properties of the aircraft. If the effect of changes on the S&C characteristics and the associated Handling and Flying Qualities (HFQ) is difficult to predict for conventional aircraft, it is a lot more difficult for the design of unconventional aircraft [7]. Also there is no legacy information available for these aircraft and at the same time airliners and passengers demand to fly the same distance from A to B in the shortest time possible. This is a challenging task for aircraft manufacturers, which all emphasizes the need for unconventional aircraft design. Numerous conceptual designs of unconventional aircraft promising lower environmental impact can be found in the literature. Examples of unconventional aircraft are the Blended Wing Body, Prandtl-plane aircraft, the flying V, or DUUC hybrid-electric aircraft [8]–[10].

Not only to ensure safe and risk-free flight to estimate the S&C of the unconventional aircraft, but also due to the high costs and risk involved, the aircraft designs have not yet entered into market and are still mainly designs on paper [11]. Various

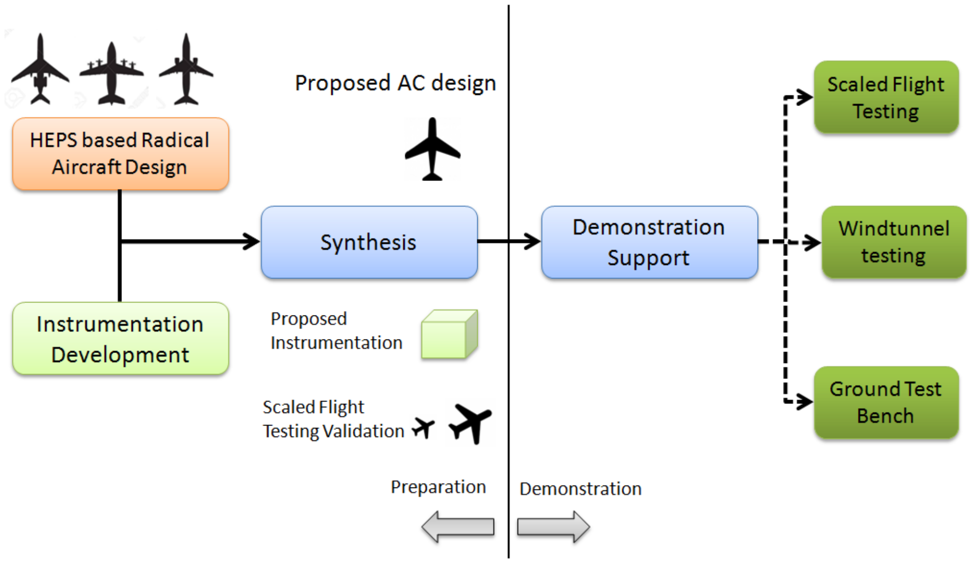

Figure 1.1: Development logic and long-term vision in the aircraft design cycle [1].

methods that are a combination of numerical and experimental methods have been used in the literature to predict the S&C characteristics of unconventional aircraft [12]–[14].

Computational methods have their uncertainties when using Computational Fluid Dynamics (CFD) models, such as Large-Eddy Simulation (LES) or Reynolds-averaged Navier–Stokes (RANS) methods. Most accurate is Direct Numerical Simulation (DNS), but the computational effort scales with Reynolds number to the third power in this method (Re^3). Low fidelity methods like 2D panel codes are very fast (few seconds per case) but inaccurate. An adequate trade-off between simulation accuracy and time is important in design and therefore a medium-fidelity 3D Panel Method (3DPM) can be used, like commercial 3DPM software called VSAERO or Flightstream [15], [16]. The problem with these aerodynamic solvers it that all these models will have low accuracy outside the normal flight envelope. This is because computer simulations have prediction problems in the nonlinear region where flow separation occurs [17], [18]. Analyzing unconventional aircraft with numerical methods thus have difficulties and disadvantages.

Alternatively, experimental methods can be used to predict the flight dynamics. Sub-scale Flight Testing (SFT) is one such experimental method which can be used to quantify the S&C and HFQ of unconventional FD. This is also explicitly stated in the Flightpath 2050 long term vision by the European Commission [4], see Figure 1.1. By actually flying the design it can be shown that the design is not only promising on paper. Experimental methods typically require to scale down the Full-scale Aircraft (FSA) and test the aircraft in different flight conditions. Aerodynamic experimental testing can be divided in ground based testing, wind tunnel testing and free-flight testing.

Ground based testing and wind tunnel testing, are suitable for static testing and in some cases also dynamic testing, if the wind tunnel allows it [18]. In another thesis work by Marco Palermo conducted at the TUD a sub-scale model of the Flying V is designed and the aerodynamic characteristics were assessed by wind tunnel testing [19]. Testing in a wind tunnel requires a sophisticated and expensive experimental setup. Although wind tunnel free-flight testing facilities can provide unique and valuable information regarding the flying characteristics of unconventional air-

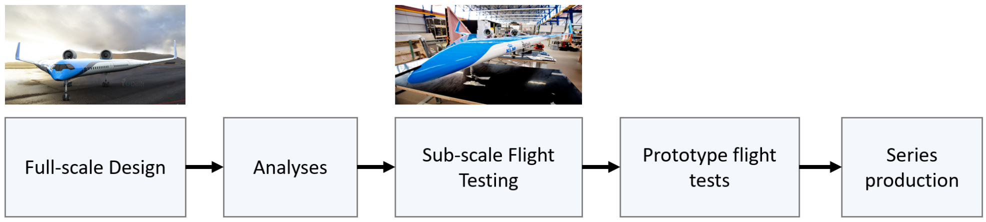

Figure 1.2: SFT as testing technique in the full-scale aircraft development cycle [20].

craft, the tests that can be performed are limited, due to the wind-tunnel walls which puts a physical limit to the test, or is unsuitable to test certain situations.

For example, as a result of the limited physical size of some wind tunnels and therefore the relatively small size of a scaled model, the motions of the models are very fast and difficult to control. Moreover, vehicle motions for other than 1g flight, involving large manoeuvres or out-of-control conditions, result in significant changes in flight trajectory and altitude, which can only be studied in larger outdoor facilities. In addition, research at high-speed dynamic stability and control problems or heavy gusts or turbulence, can not be tested in all wind tunnels.

Thus, testing the sub-scale aircraft model in a real free-flight is important because it is only really known how the aircraft design performs if the aircraft model is flown in dynamic circumstances in case windtunnel testing or numerical methods are challenging. Moreover, SFT is a relatively cheap testing method compared to Full-scale Flight Test (FFT). Therefore it can potentially be integrated at early stages of the design process of the Full-scale Aircraft, see Figure 1.2 [20]. Not only because SFT is cheaper, but also because of the miniaturization of electronics and improved manufacturing methods and materials over the last years, SFT has the potential to become an integral part of the full-scale aircraft design process. Moreover, wind tunnel testing can only partially predict aircraft dynamics and computational methods have their disadvantages and shortcomings. Therefore SFT could supplement the results found from wind tunnel tests.

SFT involves the design of Sub-scale Model (SM) followed by its flight test. Then, the results of SFT must be suitably scaled-up to predict the behaviour of the full-scale aircraft, which is a complex task. The process of scaling-up the results is challenging because of differences in the flight condition, the mass, inertia, CG and the propulsion unit of the FD and the SM. All these disciplines will affect the flight dynamics of both the FD and the SM, see Figure 1.3.

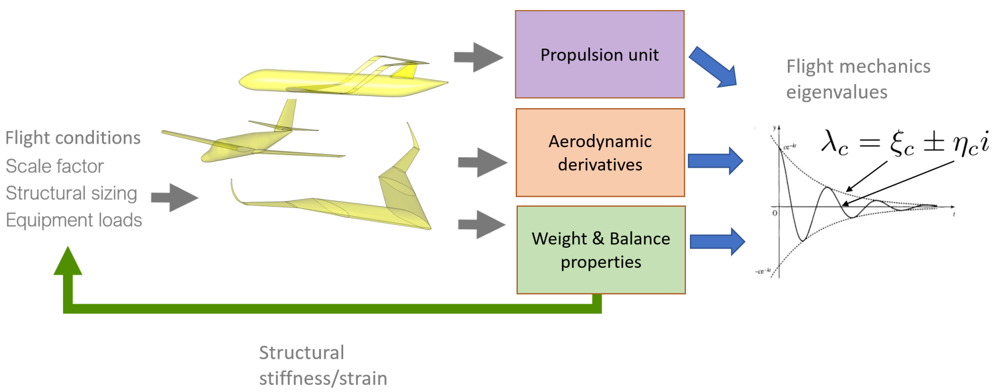

Figure 1.3: Design changes due to structural analysis results and possible impact on flight dynamics.

The discipline's effect on the flight dynamics is a complex interaction, because a change in mass or the center of gravity, and therefore possibly the inertia, will effect the trim conditions for the SM. If the mass and inertia properties are known the results can be used for two purposes.

First of all the aerodynamic derivatives of the sub-scale aircraft model can be gathered from wind tunnel or from real flight tests based on the mass and inertia properties and are used to improve the parameters in the numerical simulation to validate the model. When the model is validated it shows that the results can be used for further development of SD [21]. Secondly, if these results can be validated for the SM and the full-scale eigenvalue can also be estimated, the flight mechanics behaviour of the sub-scale model can be compared with the full-scale eigenvalue. If the eigenvalue is the same for the motion to be tested, the sub-scale model mimics the flight behavior of the full-scale aircraft.

However, even in case the behavior of the sub-scale model perfectly mimics the full-scale aircraft, the SM needs adequate flight performance and handling qualities to enable the execution of flight tests. For example, the SM must be designed such that the center of gravity results in a trimmable model and also the structure of the sub-scale model must not fail in flight under critical load conditions. Moreover, depending on specific regulations of the country, the authorities can put a maximum design weight for the model to be tested for example. If these constraints for the design of SM can be met, the proposed method of using SFT is potentially useful in the study of:

- dynamic control and stability of aircraft
- loss of control/equipment failure situation
- regimes outside the normal flight envelope

SFT has been used in different forms in the last decades by various organisations of which an example is the X-48B, which is an 8.5% geometrically scaled aircraft. Another example is the AirSTAR geometrically scaled 5.5% aircraft built by NASA. When looking at Europe, applications of scaled flight testing are very limited. In Europe, the university of Linköping built a 13.8% geometrically scaled model and was mainly built for educational purposes, see Figure 1.4, but not to investigate the flight dynamics behaviour. Most SM that were built could not fully represent the dynamics that the full-scale aircraft will encounter. This is further explained in more detail in Chapter 2.

Figure 1.4: **Left:** X-48B (NASA) 8.5% geometrically scaled SM. **Center:** Raven (University of Linköping) 13.8% geometrically and Froude's scaled SM. **Right:** AirSTAR (Air-Force Research Laboratory USA) 5.5% geometrically scaled tube-wing SM with Froude's scaling.

1.1 RELEVANCE OF WEIGHT & BALANCE IN SM DESIGN FRAMEWORK

Only if a short design lead time for sub-scale aircraft models can be managed, it can make real impact and be effective in the full-scale aircraft design cycle. This is because the time available for SFT in the overall design cycle is limited, see Figure 1.2. The design of sub-scale aircraft models is a multidisciplinary task. Moreover, finding an optimum SM design is a rather time consuming, error prone and labour intensive task. Describing a complete framework is not in the scope of this research, but it should aim to clarify how the work could fit in a larger MDAO framework performed at the Flight Performance & Propulsion (FPP) department of the TUD. Figure 1.5 is just one example of different types of MDAO workflows. The framework may include an optimiser, or disciplines can be left out or added for the specific problem. In the current work, the aerodynamic, structure, weight & balance and flight mechanics disciplines are of main interest.

When designing the SM it must be designed correctly with the structure and measurement equipment in place. This means it must be trimmable around the center of gravity in different flight phases, statically & dynamically stable and also controllable. Table 1.1 gives an overview of parameters when used in a larger MDAO framework. *x(0)* could represent the initial sub-scale vector with scale factor, mission design variables and flight conditions. *y(0)* is the initial structural input with a certain defined rib spacing, frame spacing and number of mounting floors in the fuselage and/or wings. The full-scale geometry design variable description is represented by *z*. *y1* represents the sub-scale aerodynamic analysis outputs, with VSAERO or Flightstream for example. *y2* represents the positioning of structural components & strain/model criteria or deflection as a measure for stiffness. FE analysis is done to ensure a safe SFT.

Different failure criteria exist when performing FE analysis: one such frequently used failure criteria for composite laminates is the 2D maximum principal strain. Major 2D principal strain is the strain resolved in the principal direction. The major and minor directions are the most important as they often work in the direction of the fibers. Fibers are typically superior on tensile and not so effective on compression. For AS4-tape an allowable strain is between 1000μ (conservative) and 3500μ, adviced by an expert from industry. The definition of the 2D principal strain is given in Equation 1.2 [22]:

$$\epsilon_{max}, \epsilon_{min} = \frac{\epsilon_{xx} + \epsilon_{yy}}{2} + - \sqrt{(\frac{\epsilon_{xx} + \epsilon_{yy}}{2})^2 + (\frac{\gamma_{xy}}{2})^2} \quad (1.2)$$

Table 1.1: Overview of parameters when used in an MDAO framework.

Parameter	Description
x(0)	initial sub-scale vector with flight conditions, scale factor, mission design variables
y(0)	initial structural input (rib spacing, frame spacing, number of floors)
x	sub-scale geometry design variable description
z	full-scale geometry design variable description
y1	sub-scale aerodynamic analysis outputs
y2	positioning of structural components and strain & deflection criteria
y3	positioning and mass properties of flight equipment
y4	mass, inertia and cg
y5	flight mechanics eigenvalues and neutral point
y0	full-scale aerodynamic analysis output
f	Objective function to have similitude between full-scale and sub-scale models
g	Flyability constraints (weight requirements, equipment fit, S&C)

Where ϵ_{max} and ϵ_{min} are the maximum and minimum normal strain, and γ_{xy} the maximum shear strain. In general then the following should hold for a safe design:

$$\epsilon_{max} \leq \epsilon_{permissible} = \frac{\text{yielding strain under tensile test}}{\text{factor of safety}} \tag{1.3}$$

In design sometimes design iterations are necessary. It can be the case that the weight & balance properties can not result in a trimmable, statically stable and dynamically stable sub-scale aircraft model throughout the flight envelope. The Mass, Inertia and CG are given by $y4$. $y5$ represents the eigenvalues, the trim condition and neutral point of the SM. The designer needs to re-position the COTS components, $y3$ is the location of COTS equipment. Moreover a maximum allowed mass or the flight-speed could impose constraints on the SM. The designed SM can also appear to be not stiff or strong enough based on the failure criteria. In that case the model needs to be reinforced with structural elements (more spars or ribs make the structure stiffer) or use different materials. The structural response (strains/stresses and displacements) are calculated by MSC NASTRAN software. If the aircraft is stiff enough and the material strength is sufficient to withstand aerodynamic loads during a defined critical loadcase and support the equipment inside, the sized SM is passed to PHALANX. This is a multi-fidelity non-linear flight dynamics toolbox developed within the FPP research group. Depending on the type of MDAO problem studied, PHALANX can evaluate the control and stability properties of the aircraft, to size the control surfaces or determine if the aircraft is stable.

This process is continued until a satisfactory result is obtained for the mass, CG and its corresponding inertia such that it satisfied control-ability and stability requirements.

The solution is assessed by what is called a converger, a piece of logic that compares subsequent solutions in order to determine whether convergence is reached, i.e. the convergence criteria have been met. If the converger satisfies the constraint for the SM, the results could be further used in an optimization loop to maximize similarity between SD and the corresponding FD. In the xDSM work-flow constraints can be imposed on the S&C characteristics and the HFQ. Of these disciplines, the aerodynamic analysis for both FSA and SM is performed as described by Raju Kulkarni et al. [23]. The objective function of this MDAO process is the DoS as described in more detail in Chapter 2 in Equation 2.12. Furthermore, the non-linear flight dynamics analysis can be used to construct a simulator which can be used by pilots to practice and assess the flying qualities of the SM design.

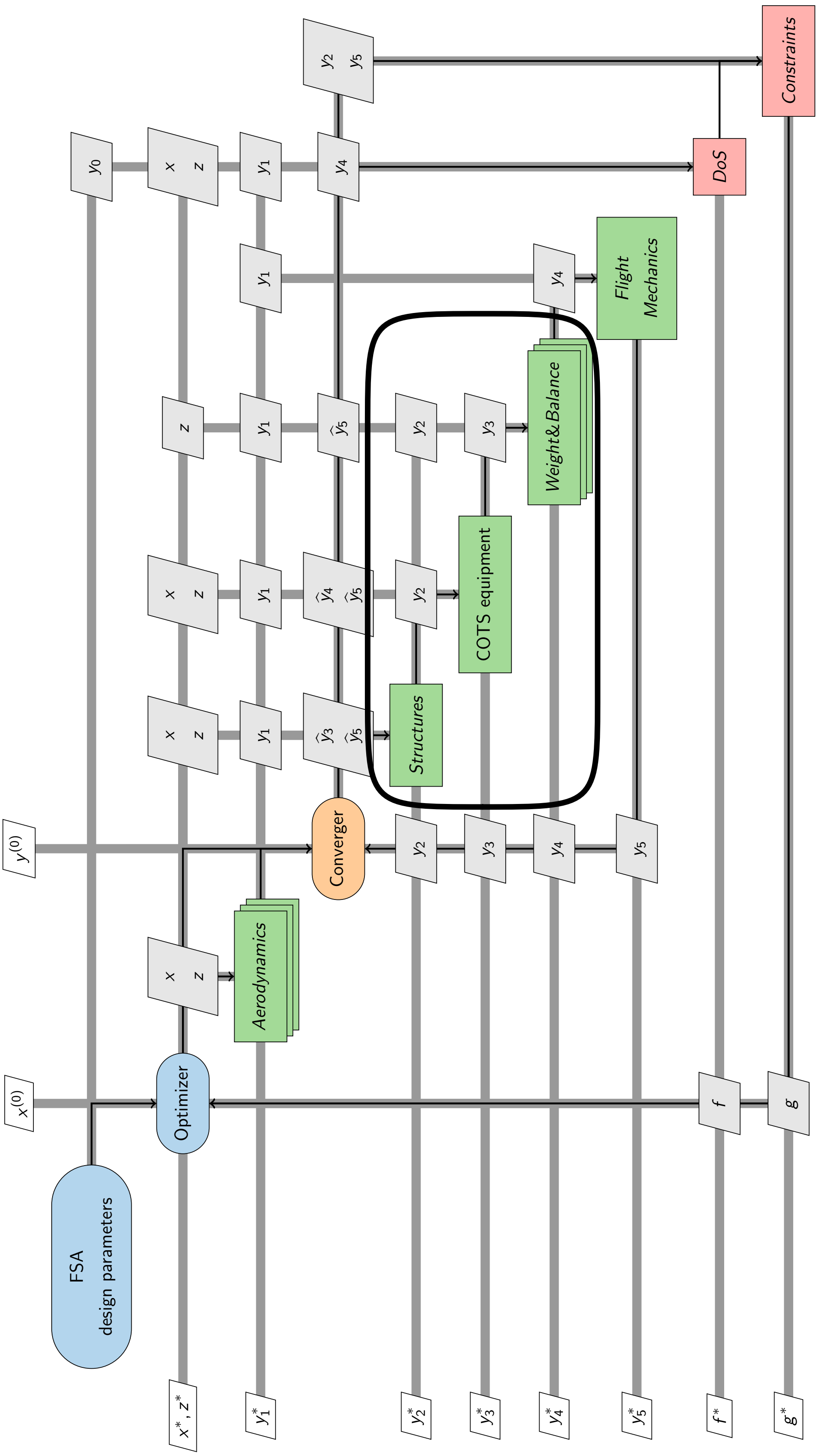

Figure 1.5: An example xDSM representation of the optimization problem for the maximization of DoS while ensuring a safe SM.

1.2 RESEARCH OBJECTIVES AND SCOPE

Even in case the behavior of the sub-scale aircraft model can perfectly mimic the full-scale aircraft, taking into account all disciplines as previously explained and visualized in Figure 1.5, it still needs to be flyable to enable the execution of flight tests. Flyable means that the model is trimmable, statically stable and dynamically stable. There are two main challenges. The first concerns estimating the mass, center of gravity and inertia accurately as well as quickly for the SM in order to determine the HFQ and the trim conditions of an SM. These derivatives are a direct result of the scale size and internal configuration of the structure and equipment that is chosen. The second is about ensuring the structure does not fail in flight under critical load conditions.

The developed methodology in this work should be used in an MDAO framework currently under development in the FPP research group of the TUD. The MMG is a KBE application to support MDAO of aircraft configurations that uses a HLP build-up approach and parametric rules to automate process knowledge. The MMG is further explained in more detail in section 2.2.

Different positioning of internal structural elements and COTS components can be used in SM. The resulting weight & balance properties and its sensitivity on the flight mechanics for different scale factors and design variables are important to have a flyable design. Design variables are for example rib pitch, frame pitch or choice of material properties. Currently, the HFQ and S&C assessment for SM is strongly influenced by the aerodynamic dataset provided as input to the flight mechanics toolbox. The combined effect from the aerodynamic analysis together with the weight & balance properties can be used to evaluate the flight mechanics of the aircraft, see Figure 1.6.

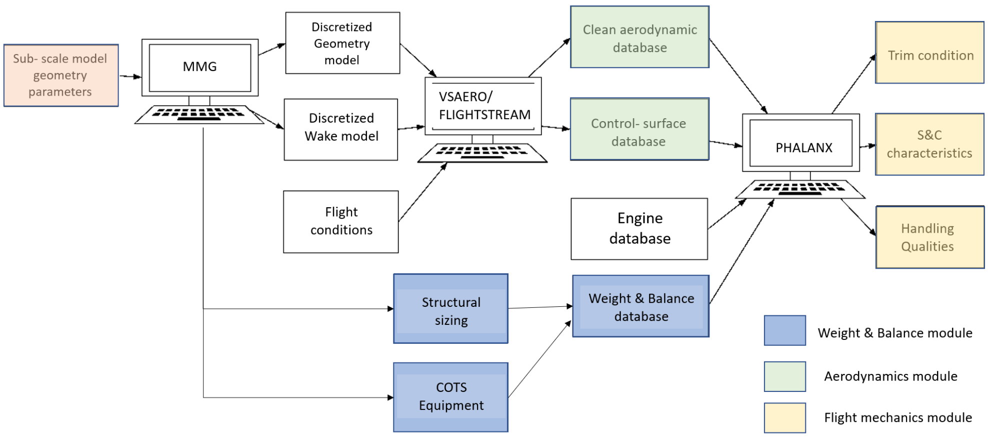

Figure 1.6: Key factors needed to determine the stability and controls of an aircraft model.

Therefore, the aim of this research project is to develop physics-based design and analysis tools which allow to rapidly and accurately estimate the weight & balance properties. This then makes to module able to react rapidly to changes in top-level requirements of the full-scale design and its scaled SM. The weight & balance properties come from structural elements or COTS components that are placed inside the SM. The properties are then calculated in two possible ways: by having positioning control about the COTS components or by having control about the placement of structural elements and their assigned material properties. If also the requirement on stiffness and strength to withstand aerodynamic loads during a critical loadcase can be met, the weight & balance properties can be used to estimate the dynamic characteristics of different SM and compare with the FD.

The following research objective has been formulated for this master's thesis:

Estimate the mass, CG and inertia of SM configurations by designing its structural elements and selecting and positioning appropriate COTS components such to ensure a stiff and safe SM structure.

The main research question is:

How to design, integrate and analyse the structure and COTS components for SM in the preliminary design phase and to create an automated finite element model generation for structural investigation?

The first part of this work is an overview introducing the framework to solve sub-scale flight testing problems in Chapter 2. This includes the assessment of similitude between the full-scale model and sub-scale aircraft model and the explanation of the use of a KBE platform to reduce the design lead time. Second, the general methodology to demonstrate how the research is conducted and extending previous works is explained in Chapter 3. An appropriate methodology is identified and developed to design the structural components of SM, position COTS components and estimate the mass, inertia and the associated CG of SM in Chapter 4. The pre-processing steps regarding automated structural analysis capabilities are presented in Chapter 5. The methodology is verified and validated in Chapter 6. Finally, a DOE is then presented for the conventional Cessna Citation II, Flying V and Prandtl-Plane as a proof of concept showing the sensitivity of the scale size and design variables on the estimated weight & balance properties in Chapter 7.

2 BACKGROUND ON SUB-SCALE FLIGHT DESIGN METHODS

An important question to be answered is how to scale representative SM, when SM is used to compare it with FD. As was already mentioned in the introduction the FD of an unconventional aircraft design is possibly the best way to test the flight mechanics behaviour (upper right corner of Figure 2.1). However, the associated risk and cost make this impossible in early stages of design cycle. Therefore designers can use computational models to predict the flight dynamics behaviour of a given design (upper left corner of Figure 2.1).

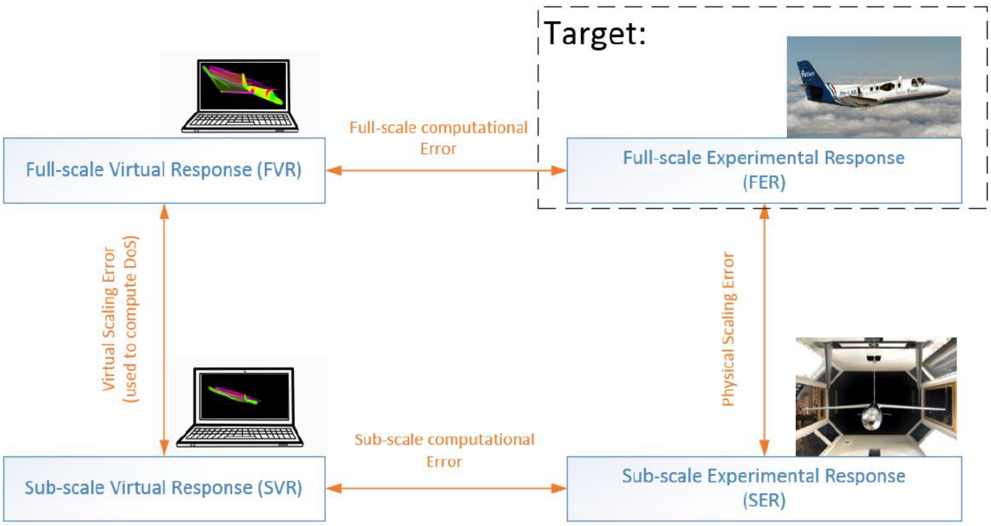

Figure 2.1: Overview of errors when comparing different models.

These computational models take the FSA as input. In an ideal case, the Full-scale Virtual Response (FVR) is the same as the results obtained from the FFT performed, defined as Full-scale Experimental Response (FER). However due to assumptions made in for example the exclusion of viscous and compressibility effects and the turbulence model choice, as explained in Chapter 1, this is hard to achieve. Therefore a substitute to the impractical FD, SM can be designed and manufactured such that their behavior is similar as possible to the FD. SM's can then be used to perform wind-tunnel testing or free-flight testing (lower right corner of Figure 2.1). This is less expensive and already feasible to manufacture at the end of the conceptual design phase, see Figure 1.2. This data can again be used to improve the parameters that were difficult to predict in the numerical simulation model. Ideally, the aerodynamics of the SM are similar to the full-scale aircraft in terms of coefficients. The key parameters that play a role in aerodynamic similarity are the Reynolds number (inertia and viscous forces dominant), Mach number (inertia and elastic forces dominant) and Froude number (inertia and gravity forces dominant). Equations 2.1 and 2.2 would then approximate zero.

$$\text{Virtual Scaling Error} = f(FVR - SVR) \tag{2.1}$$

$$\text{Sub-scale Computational Error} = f(SVR - SER) \tag{2.2}$$

Conventional scaling laws

The design of a SM can be based on scaling laws that will directly influence the aerodynamic parameters and their derivatives instead of dimensionless numbers like the Reynolds, Froude and Strouhal number. The scaling laws were found to be classified into five types listed below [24]:

1. **Geometric scaling**: the relationship between the SM and the FSA is purely based on the shape and can be subdivided in:
   - Isotropic scaling - a linear transformation that enlarges or shrinks objects by one factor that is same in all directions. This factor is commonly known as the scale factor.
   - An-isotropic scaling - a non-uniform transformation where different factors are used in each axis direction. This non-uniform scaling mutates the shape of the object to be tested and thereby affects all the other relationships that depend on the shape of the object. Such an-isotropic scaling is often used in aerodynamic scaling (explained below).
2. **Kinematic scaling:** When the ratio of geometry and the time rate of change of fluid flow around both the SM and the FSA are the same, therefore yielding similar fluid streamlines.
3. **Dynamic scaling:** when all of the following ratios are the same simultaneously:
   - geometric size of SM and FSA
   - time rate of change of fluid flow around SM and FSA
   - the forces acting on the SM and FSA
4. **Aerodynamic scaling:** Since both dynamic scaling is restrictive and difficult to achieve, a variant of kinematic scaling called aerodynamic scaling can be chosen. Aerodynamic scaling requires the modification of the SM geometry (not necessarily geometrically scaled) to simulate the aerodynamics of the FSA to maintain the following ratios:
   - time rate of change of fluid flow around SM and FSA for the specific phenomena being tested
   - relevant forces acting on the SM and FSA for the phenomena being tested

   This is accomplished in three different ways:
   - using different scaling factors per axis of the FSA
   - using different scaling factors per component of the FSA (for example, making a 15% scaled wing while the rest of the components are 5% scaled)
   - using different relative distances between different components of the aircraft (for example, changing the tail volume coefficient)
5. **Mass & Inertia scaling:** Mass scaling requires the distribution of weight in the model to be scaled using a set of scaling laws, which are used to simulate aircraft motion and response. These scaling laws are an expansion of the square-cube law, with the addition of a density-scaling factor.

Regarding the mass & inertia scaling, regulations might limit the maximum mass to 25 kg or 150 kg, dependent on the certification rules that apply for the specific model and the country. Also the airspeed can be a constraint, as this is one of EASA regulations for flying drones. This regulation requires the aircraft model to fly in line-of-sight [25]. In practice it is therefore very difficult to achieve full dynamic scaling by Froude and Reynolds number similarity simultaneously.

For example in low speed flight, compressibility effects are not an issue and therefore the assumption of neglecting the Mach and Reynolds number effects are acceptable. The derivation will be shortly explained by an example for the lift and moment coefficients in the following section for dynamic motions in which dynamic scaling is used.

Dynamic scaling

This specific type of scaling law is done with the aim to scale the geometric and dynamic properties of the aircraft model. This means that the weight, inertia and control system responses must be scaled such that the dynamic response of the model corresponds to the full scale aircraft. For an airplane in steady, level, 1g flight, the lift coefficient is given by Equation 2.3:

$$C_L = \frac{W}{\frac{1}{2}\rho V^2 S} = 2(\frac{m}{\rho S\bar{c}})(\frac{g\bar{c}}{V^2}) \approx f(\frac{m}{\rho l^3}, \frac{gl}{V^2}) \tag{2.3}$$

If the Froude number is matched and lift similarity is desired, then the mass scales with a factor l^3. When the aircraft is subjected to a different load case, for example a pull-up maneuver with 2.5g, experiencing a linear acceleration along the z-axis as well as centrifugal acceleration, the lift equation becomes as in Equation 2.4.

$$C_L = \frac{m(\ddot{z} + qV + g)}{\frac{1}{2}\rho V^2 S} \approx C_{L_u}\frac{\Delta u}{V} + C_{L_\alpha}\Delta\alpha + C_{L_q}\frac{q\bar{c}}{2V} + C_{L_{\dot{\alpha}}}\frac{\dot{\alpha}\bar{c}}{2V} + C_{L_{\delta_e}}\delta_e + C_{L_{\dot{\delta}_e}}\frac{\dot{\delta}_e\bar{c}}{2V} \tag{2.4}$$

If the lift coefficient is considered an important parameter affecting a phenomenon, the lift coefficient for both FD and SD must be the same. Which means that the aerodynamic coefficients, C_{L_u}, C_{L_α},C_{L_q},$C_{L_{\dot{\alpha}}}$,$C_{L_{\delta_e}}$,$C_{L_{\dot{\delta}_e}}$, should be the same for SD and FD. These aerodynamic coefficients and their derivatives depend on forces such as fluid's viscous forces, inertial forces, gravitational forces, pressure forces, as is shown in Equation 2.5:

$$C_L = \frac{m(\ddot{z} + qV + g)}{\frac{1}{2}\rho V^2 S} = 2[\frac{m}{\rho S\bar{c}/2}](\frac{\ddot{z}\bar{c}}{2V^2} + \frac{q\bar{c}}{2V} + \frac{g\bar{c}}{2V^2}) \tag{2.5}$$

The similitude requirements now include reduced linear acceleration and reduced angular rate as well as relative density factor and Froude number. In the preceding discussion on Froude number the relative density factor, $\frac{m}{\rho l^3}$, was shown to be a basic similitude parameter in the aerodynamic force equations. When simulating a different load case than steady flight, this scale factor is not only dependent on Froude number. This parameter is important in model studies of stability and control characteristics [26].

For dynamic response the inertia of the SM is also important. The moment of inertia is defined as the measure of resistance of a body to angular acceleration about an axis of rotation. The mathematical expression of moment of inertia of a body is expressed as follows.

$$I = mr^2 + I_o \tag{2.6}$$

Table 2.1: Overview of the required scale factors for rigid dynamic models tested at sea level. Multiply full-scale values by the indicated scale factors to determine model values, where n is the ratio of model-to-full-scale dimensions, σ is the ratio of air density to that at sea level (ρ/ρ_0), and ν is the value of kinematic viscosity [18].

	Scale factor	
	symbol	froude scaling law
Linear dimension	l	n
Relative density ratio	RdR	1
Froude number	Fr	1
Angle of attack	α	1
Linear acceleration	a	1
Weight, mass	m	n^3/σ
Moment of inertia	I	n^5/σ
Linear velocity	V	$n^{1/2}$
Angular velocity	p, q, r	$1/n^{1/2}$
Time	t	$n^{1/2}$
Reynolds number	Re	$n^{1.5}\ v/v_0$

or in matrix notation written as,

$$I = \begin{bmatrix} I_{xx} & I_{xy} & I_{xz} \\ I_{yx} & I_{yy} & I_{yz} \\ I_{zx} & I_{zy} & I_{zz} \end{bmatrix} \tag{2.7}$$

The first term in the equation represents the resistance of the body to rotation about the remote axis, while the latter represents the resistance to rotation of each component about its own axes. From this simple equation, it can be stated that inertia depends on the model shape, amount, and distribution of mass. The moment of inertia of an aircraft is determined about its longitudinal, lateral and vertical axes which gives roll, pitch and yaw. The larger the moments of inertia, the greater will be the resistance to rotation.

To get a relation for the expression relating the moment coefficient to the mass moment of inertia is given in equation 2.8, here $\dot{q}$ is the dimensionless dynamic pressure. The derivatives of the moment coefficients have the same structure as for the lift coefficient.

$$I\dot{q} = C_m \frac{1}{2}\rho V^2 S\bar{c} \tag{2.8}$$

Where C_m can be rewritten as in Equation 2.9,

$$C_m = \frac{I\dot{q}}{qS\bar{c}} = C_{m_0} + C_{m_u}\frac{\Delta u}{V} + C_{m_\alpha}\Delta\alpha + C_{m_q}\frac{q\bar{c}}{2V} + C_{m_{\dot{\alpha}}}\frac{\dot{\alpha}\bar{c}}{2V} + C_{m_{\delta_e}}\delta_e + C_{m_{\dot{\delta}_e}}\frac{\dot{\delta}_e\bar{c}}{2V} \tag{2.9}$$

For the SM to have the same moment coefficient as the FD, relative mass moment of inertia parameters, $\frac{I}{\rho l^5}$, and the reduced angular accelerations, $\frac{\dot{q}l^2}{V^2}$, must be identical, see Equation 2.10. For a rigid airplane, mass moment of characteristics (including products of inertia) can be simulated on the SM by an appropriate distribution of masses. This will then give the same reduced radius of gyration, $\frac{k}{l}$ as on the FSA.

$$C_m = 2\left(\frac{I}{\rho S\bar{c}^3}\right)\left(\frac{\dot{q}\bar{c}^2}{V^2}\right) \approx f\left(\frac{I}{\rho l^5}\right)\left(\frac{\dot{q}l^2}{V^2}\right) \approx f\left(\frac{m}{\rho l^3}, \left(\frac{k}{l}\right)^2, \frac{\dot{q}l^2}{V^2}\right) \tag{2.10}$$

The value k represents the distance from the reference line to the point mass. The relative density factor $\frac{m}{\rho l^3}$, should also be satisfied as was already required for an equal lift coefficient. Thus if the similarity of the moment is required around a reference axis of the aircraft, the inertia scales with a factor l^5. An overview of the required scale factors n for dynamic scale models is given in Table 2.1. The equations of motions, as in Equations 2.4 and 2.9, include the relative density factor, relative mass moment of inertia, aircraft attitude, control surface position and reduced velocity and acceleration parameters.

To ensure static longitudinal stability, the CG has to be located in front of the neutral point of the aircraft which tends to shift forward at higher angles of attack. While for conventional aircraft stability is ensured at high angles of attack by the horizontal tail. For flying wings or the prandtl-plane aircraft this situation can be different. To avoid the pitching moment slope to turn positive, the location of the aerodynamic center has to be known and also very important the CG range has to be selected such that stability is ensured [21]. Moreover, the CG position is important for many aerodynamic derivatives of the SM. One very important derivative that depends on the CG position is the pitching moment due to angle-of-attack derivative C_{m_α}. Or $C_{m_{\delta_e}}$ indicate if the control surfaces can provide sufficient control to trim the SM. This latter depends on the arms of the control surfaces with respect to the CG. If an aircraft has static stability, the aircraft has an elevator input that can bring the aircraft in equilibrium, see Equation 2.11.

$$C_{m_\alpha} = C_{L_{\alpha w}} \left(\left(\frac{x_{cg}}{c} - \frac{x_{ac}}{c} \right) + C_{m_{\alpha_f}} - \eta V_H C_{L_{\alpha_t}} \left(1 - \frac{d\epsilon}{d\alpha}\right) \right) \tag{2.11}$$

Thus, knowing the CG of the designed sub-scale model is important. Shifting the wing is an effective method in order to achieve a convenient position of the CG. Another way to affect the aircraft balance is that of relocating other aircraft components, such as COTS engines, landing gear, battery & other instruments. When designing a SM that is carrying these instruments and batteries.

In conclusion, with the use of classical scaling law, see Table 2.1, it is not evident what the dependence of the aerodynamic coefficients and their derivatives from the equations of motion is on Reynolds number, Strouhal number, Mach number, and other non-dimensional parameters. This relationship is only known qualitatively, but not quantitatively. It is also shown that the CG has an implicit effect on some aerodynamic derivatives. Moreover, due to other practical limitations it is often not possible to satisfy full dimensionless similitude conditions of these derivatives.

For example, for a 1/9-scale model (n=1/9), the linear velocities of the SM (flight speeds) will only be 1/3 of those of the FSA, but the angular velocities encountered by the aircraft model in roll, pitch and yaw will be 3 times faster than those of the FSA. Because the model's angular motions are much faster than those of the FSA, the SM may be difficult to control. Another important result of dynamic scaling is the large differences in the magnitude of one of the non-dimensional aerodynamic parameter known as Reynolds number. A 1/9-scale dynamic model is typically tested at a value of Reynolds number that is only 1/27 that of the airplane for sea level conditions [18]. If for example, the mass distribution of the SM results in inertial nose-up loads that are too low compared with the aerodynamic loads, the model weight & balance dominate the motion. More specifically it then has larger influence on the damping or frequency of the motion regarding the S&C discpline.

2.1 DoS ESTIMATION FOR SFT

As was shown in the previous section dynamic scaling is almost impossible, due to weight constraints and the flying conditions in which the scale model must fly. Since both dynamic scaling is restrictive and difficult to achieve, a variant of kinematic scaling called aerodynamic scaling can be chosen. Aerodynamic scaling requires the modification of the SM geometry (not necessarily geometrically scaled) to simulate the aerodynamics of the FSA. A new design method for SD is proposed based on the previous mentioned scaling laws in a paper by Raju Kulkarni, et. al. (2018) [24]. The new method takes into account relevant aerodynamic coefficients derivatives affecting the phenomena that is tested, being the short period, phugoid or dutch-roll, for example.

A figure of merit, defined as the DoS, to support the new methodology to maximize similitude between the full-scale and sub-scale flight behavior is proposed. The objective function is given in Equation 2.12, in which n is the number of selected aerodynamic coefficients $C_{i_{SM}}$ and $C_{i_{FSA}}$ of the SM and FSA respectively, and where w_i represents the degree of influence of a given coefficient. The objective is to achieve a Degree of Similitude as close as possible to 1 for the flight motion that will be tested.

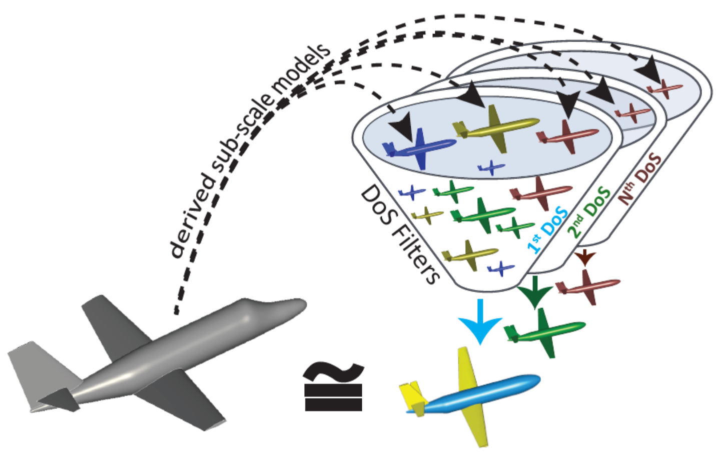

Figure 2.2: Derived sub-scale models when using DoS filters.

$$\text{DoS} = 1 - \frac{1}{n}\sum_{i=1}^{n} w_i \cdot \frac{|C_{i_{FSA}} - C_{i_{SM}}|}{|C_{i_{FSA}}|} \tag{2.12}$$

with respect to:

sub-scale flight test conditions (2.13)

geometric scaling factor of the model (2.14)

subject to:

sub-scale flight certification requirements (2.15)

limitations of COTS equipment (2.16)

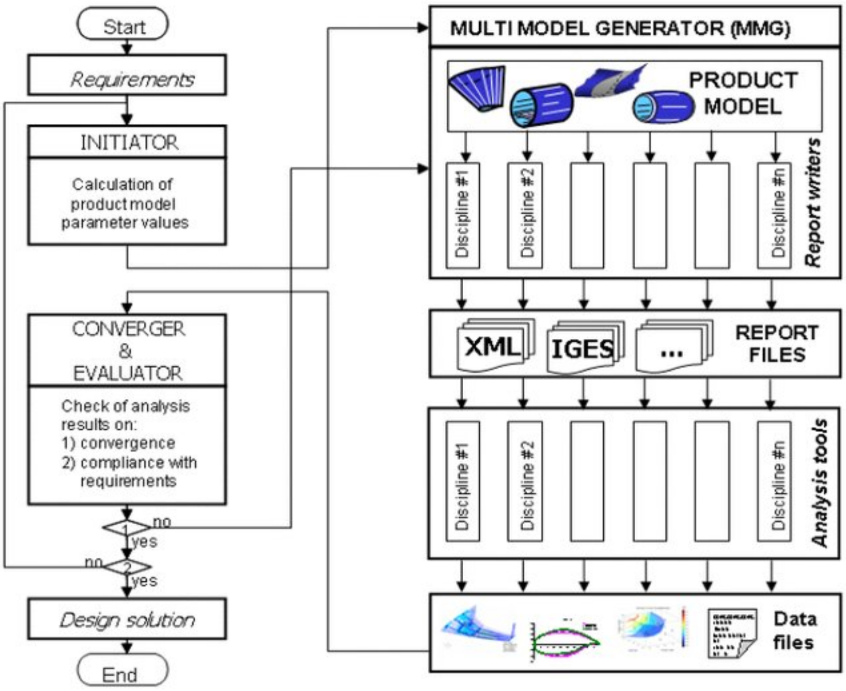

Figure 2.3: Design and Engineering Engine [27].

What is currently not included in this work is the inclusion of physics-based estimated weight & balance properties and its sensitivity on the flight mechanics between the FD and SD. The eigenvalues give an estimate for how strong the damping and frequency/oscillations are, given the aerodynamic derivatives and very important the mass and inertia properties. This provides a method to create multiple SM's taking into account the distribution of masses and the inertia, and is necessary to predict its flight dynamics. The objective is to identify a SM with maximum DoS for the phenomena to be studied, while ensuring that it can safely complete a mission by taking the S&C, structures and propulsion unit into account. This can then be used for three different purposes:

1. compare one or more SMs to select the best suited SM for testing the motion
2. filter-out unsuitable test cases or designs
3. optimize SM for a specified test case

2.2 MMG TO SUPPORT SM DESIGN

The design routine to examine and identify the SM design space uses the DEE as introduced by La Rocca and van Tooren [27] and schematically shown in Figure 2.3. The Multi-model Generator MMG is under development at the TUD and uses the ParaPy commercial KBE platform, see Appendix A for more details. The steps are made possible through object-oriented programming and makes the MMG flexible and generic such that different aircraft configurations can be modelled. The MMG has been developed such that it allows the generation of both conventional and unconventional designs.

The framework in Figure 2.3 starts with the specified Top Level Requirement (TLR)s. The workflow starts with an initial estimate of the aircraft under consideration by the Initiator based on full-scale aircraft design variables, such as range and other mission requirements. It gives an estimation of the full-scale aircraft mass, low

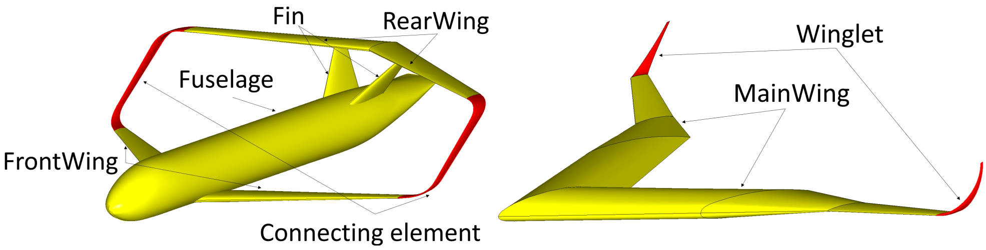

Figure 2.4: Left: Prandtl-plane connecting elements HLP in red. **Right:** Flying V winglets HLP in red.

fidelity aerodynamic performance and its initial geometry. In the current methodology this corresponds to the Full-scale Aircraft design properties: weight/mass, moment of inertia, linear velocity, reynolds number and linear dimensions. The initial full-scale design coming from the initiator is then scaled down to the desired sub-scale size and can be used to generate two types of sub-scale designs:

- Geometrically scaled design
- Aerodynamically scaled designs

The aircraft geometry is then further developed inside the MMG by making use of HLPs which together make the aircraft product model. These are distinct building blocks with which the different aircraft geometries are built. The terminology was conceived to make a distinction between HLPs and low-level primitives used by conventional Computer Aided Design (CAD) systems such as surfaces, solids and splines [28]. There are four different HLPs defined inside the MMG:

- Fuselage
- Wing
- Connecting element
- Wing extension (winglet)
- Engine

The Outer Mold Line (OML) are obtained from these HLP profiles and is considered as the starting baseline for the generation of structure and equipment. Figure 2.4 shows the HLPs.

Repetitive tasks such as meshing or making small geometrical changes can be carried out by the MMG, reducing the time required for the non-creative tasks. The aircraft models can be modified to generate automated discipline specific models for different analysis tools, see Figure 2.3. Different analysis tools requires a discretized geometry of the model, aerodynamically or structurally, which is for both disciplines preferably a structured mesh as input file for the analysis. Generating a structured mesh for an aircraft structure which has more than four edges everywhere is difficult. However, an algorithm is used and extended to develop and incorporate inside the MMG, which automatically splits the geometry of the conventional or unconventional aircraft in four sided faces.

Furthermore, the designers can modify the geometry via the graphical user interface of the MMG to perform what-if studies or execute scripts to interact with instances of the MMG thereby making use of the features of a KBE tool like ParaPy, such as dependency tracking and lazy evaluation, which makes the MMG a more efficient and powerful solution than using a conventional CAD tool in a loop [29].

3 DESIGN METHODOLOGY

In order to answer the research question to estimate the mass, CG and inertia for any SM configuration in the preliminary design phase a methodology should be developed to design the structural elements and to select and position the COTS components. This is explained in more detail in Chapter 4. Secondly, the structural analysis capabilities are automated to ensure that the structure does not fail in flight under critical load conditions. This is explained in more detail in Chapter 5.

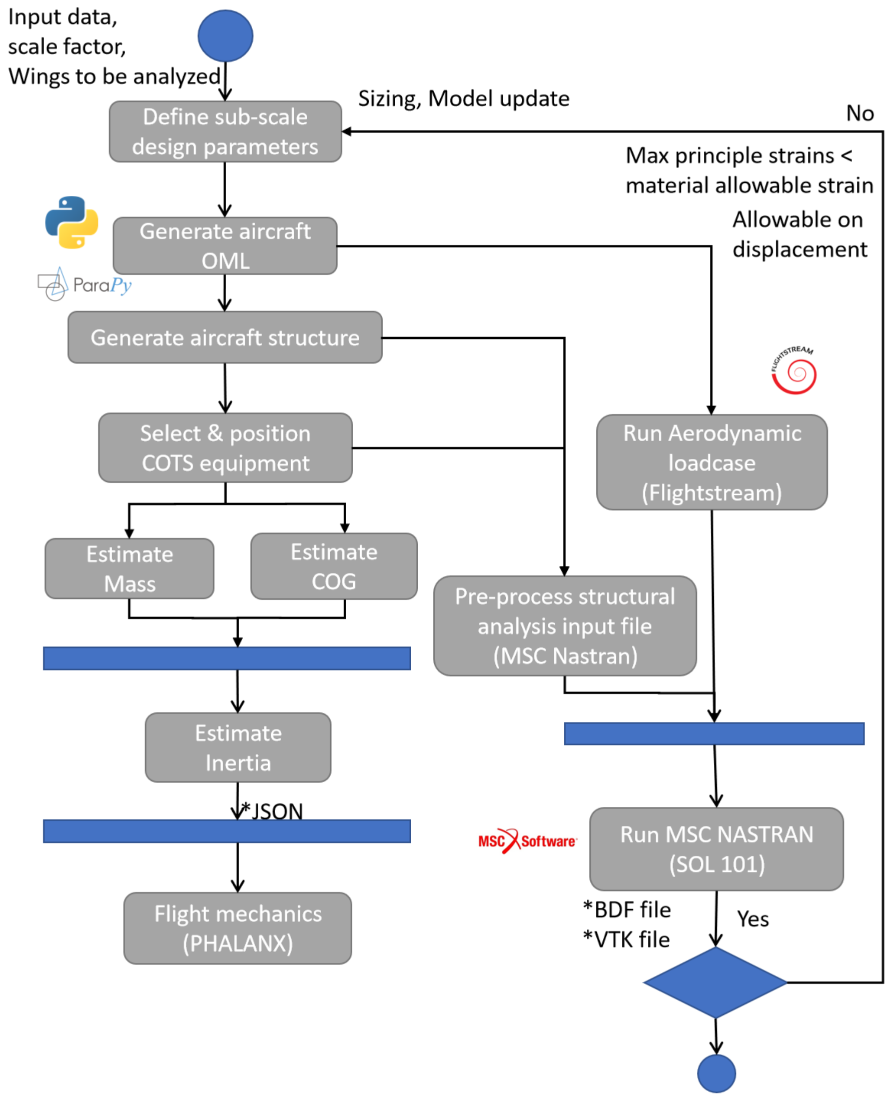

Figure 3.1: Activity diagram of the design and analysis framework describing the methodology to estimate the weight & balance properties and full-fill structural conditions for the SM.

DESIGN AND ANALYSIS FRAMEWORK

The activity diagram in the DEE framework is presented in Figure 3.1 showing the general approach to answer the research objective. The starting point of the module is the definition of SM design parameters. As explained in Section 2.2, any combination of HLP and scale factor of the full-scale aircraft can be given as input coming from TLR requirements.

The MMG is then able to model the geometry of various aircraft configurations by combining instances of Wing and Fuselage classes. The OML of the model is then created on which the structural elements can be parametrically defined. The aircraft structure and equipment module are reported in Chapter 4. The requirement for having an equipment module is build with the objective to build models with experimental flight test equipment, to measure the aerodynamic derivates during flight and for example batteries, engines and other equipment. The structural design and the selected components are then used to estimate the mass, CG and inertia of the SM. The MMG can prepare the specific discipline specific analysis reports. These include a json file with the weight & balance properties of the model, that can be directly used by other discipline specific tools such as PHALANX to assess the flight mechanics of the SM.

The integration with MSC Nastran is treated in Chapter 5, to create the input file the report includes the pressure load integration from an aerodynamic solver (Flightstream). For this a discipline specific file for the aerodynamic analysis in Flightstream is developed to map the aerodynamic loads on the structural mesh. The visualization of this pressure load mapping are facilitated by ParaPy built-in functions, see Appendix A. Verification of this load mapping is considered in Chapter 7. An input file is then automatically generated to perform structural analysis of (components of) the model. The input file that is used for static structural analysis is expanded to also include the stacking sequence and orthotropic material properties that are assigned to the structural components.

The final mass distribution for the structure can be iterated with structural analysis results based on requirements on stiffness and strain, this is known as structural sizing. This then can be used to check if the model is able to withstand some critical load cases, for example if it can meet stiffness requirements on maximum displacement and if the loads are within defined limits. In case the designed SM appears not to meet these requirements regarding structural stiffness and strain the designer needs to re-position some COTS components or to reinforce the model with structural elements or use different materials. This then can affect the weight & balance properties of the SM.

Therefore the following conditions are set for the code to automate the tasks:

1. The methodology must be configuration agnostic.

2. Able to interface with aerodynamic results from Flightstream

3. Able to interface with MSC Nastran

4. Being sufficient representative for the physics of the phenomena

5. Low computational time

KBE TO SUPPORT THE STRUCTURAL DESIGN OF THE SM

In order to meet these conditions the KBE approach is used. This is achieved by the development of a KBE application, as described in Section 2.2. Although structural analysis simulations take a few minutes per case, the preparation of the analysis input models is generally very time expensive. For each case, a few hours are needed to manually prepare the model: apply the discretization of the model, perform the load mapping, add the (material) properties and generate the analysis input file according to the prescribed format. This can be a critical bottleneck when hundred of cases must be evaluated. To solve this problem, the developed methodology can prepare the input model for structural analysis within a few seconds.

KBE allows the possibility of studying a large design space in a shorter time in early design stages. This is based on the important objective is that the design lead time of SM must be small, in order to be effective in the full-scale design cycle. In general the challenges of engineering design state that the broader the amount of proposed solutions, the higher will be the chance to include the most appropriate or to be closest to the best solution [29]- [30].

REFERENCE AIRCRAFT

To show the flexibility of the proposed methodology three SMs are used to demonstrate the study, being the conventional Citation II, and two unconventional models: the Prandtl-plane and Flying V. But the methodology is configuration agnostic, it can be used on different models, any scale size and different internal configurations.

The Cessna Citation II

In this research to verify that the methodology works first a conventional aircraft design is used. Hence, the TLRs of the FD conventional aircraft Cessna Citation II is used as baseline to test the framework, see Figure 3.2. This model is chosen because the full-scale aircraft is co-owned by the TUD and an aerodynamic and weight & balance database does also exist for this full-scale aircraft, from which the flight mechanics eigenvalues can be derived.

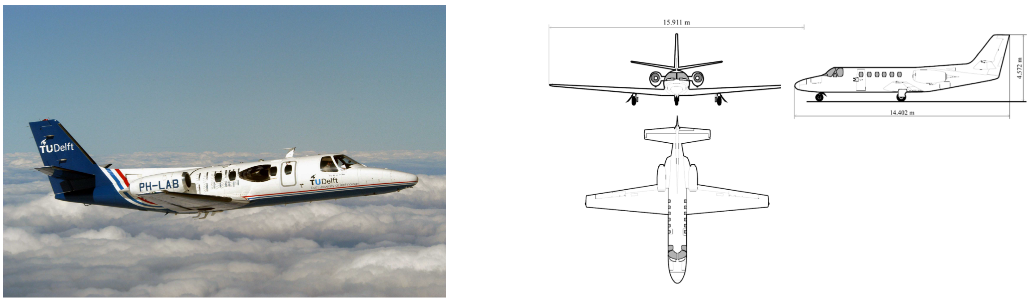

Figure 3.2: The Cessna Citiation II co-owned by the TUD.

The Prandtl-Plane aircraft

The Prandtl-plane aircraft is another unconventional model studied, see Figure 3.3. The FD Prandtl-plane, or also called box-wing aircraft, is expected that it could enter a new market segment by offering a higher payload capacity for a given range compared to current competitors. The FD is aimed to minimize the lift induced drag. In addition to the aerodynamic potential, the configuration offers several ad-

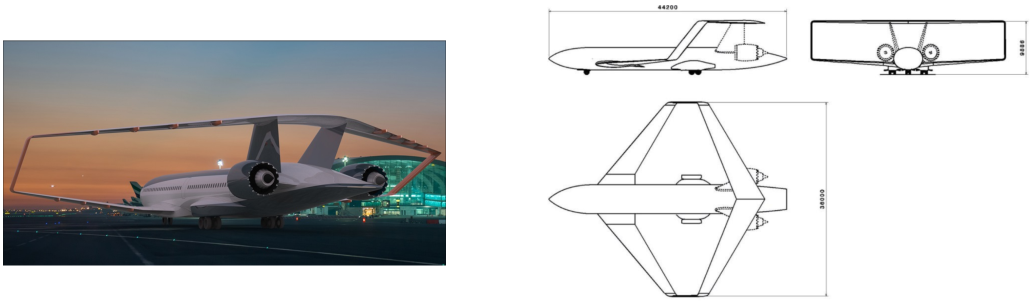

Figure 3.3: The Prandtl-plane configuration. **Left:** render view. **Right:** FD initial dimensions [32].

vantages and opportunities in the field of flight mechanics. The two relatively large wings, produce both positive lift and provide pitch control through pure couple, which is more efficient.

An initial investigation of a tool able to develop the definition of the internal structure of the box-wing full-scale aircraft is developed by Sansone [31]. The fuselage structural components (bulkheads & frames) and other subsystem components were not included in this thesis work, which are important to calculate the model mass and inertia. The aerodynamic loads in the work of Sansone are modelled as points loads to ribs. In this research it is chosen to apply lift loads as pressure loads which is expected a better representation of reality. Regarding the extension of the module by Sansone the following was identified in the literature study:

1. Add structural components such as bulkheads and frames for the fuselage
2. Introduction of composite materials
3. Selection and positioning of COTS equipment
4. Weight & balance estimation module
5. Aerodynamic load mapping based on pressure distribution

The Flying V

The Flying V is a promising unconventional aircraft configuration originally developed as a collaboration between TU Berlin and Airbus, see Figure 3.4. The FSA concept is intended to compete with the Airbus A350-900, with the possibility to transport about 315 passengers. It is claimed that the Flying V concept would operate with 10% greater aerodynamic efficiency in cruise and a 2% lower empty weight [33]. Beside the promising preliminary results of this study, still much has to be investigated on the proposed configuration, for which a a real-built SM of the Flying V is currently under construction at the TUD. This SM is used to determine for example engine integration location, the longitudinal shift of the aerodynamic center from low to high angles of attack, the identification of the most forward and aft center of gravity locations and their effects on aircraft flight envelope [34], [35].

In a MSc thesis work by Palermo an initial proposed mass breakdown of the required instrumentation was proposed [19]. A weight & balance sheet and also a detailed CATIA model is available of the Flying V model. The weight & balance sheet is manually edited, therefore sensitive for errors and labour intensive. The design knowledge that is put in this model is captured in this research work in the MMG to be used for other SM for future design activities in the preliminary design phase. The Flying V sub-scale model includes the airframe and COTS components and could therefore be used to validate how well the mass, inertia and center of gravity could be predicted for other models than the Flying V by the parametric model in the MMG. This can help to answer the research question.

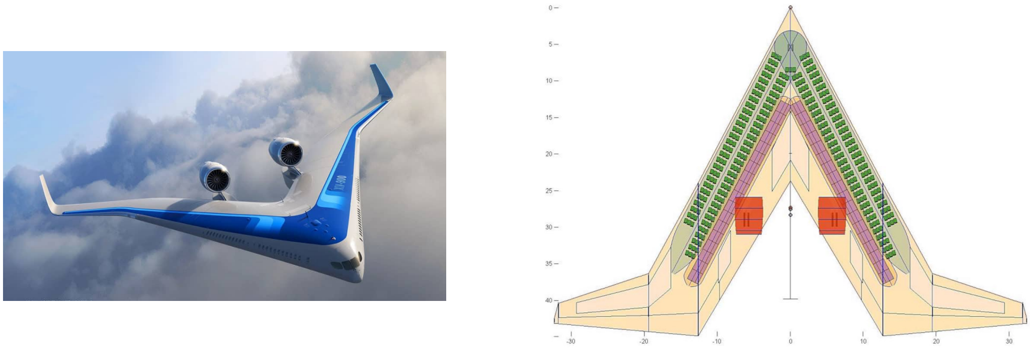

Figure 3.4: The Flying V configuration. **Left:** render view. **Right:** FD initial dimensions [33].

4 PARAMETRIC STRUCTURE GENERATION OF SUB-SCALE AIRCRAFT MODEL

The objective of the aircraft structure is to describe the internal structure of the SM for all possible lifting surfaces and the fuselage, known as HLP as explained in Section 2.2. In Section 4.2, after the definition of the inputs set by the user for the structural generation in Section 4.1, all the components are individually presented. Section 4.3 discusses the implementation of the equipment module.

4.1 INPUT FILE

A first definition of the full-scale aircraft is based on the TLRs, which is done in another module called Initiator. The values given by the Initiator represent the starting point for the MMG. The resulting OML of this aircraft can then be scaled down to any size around which the structure can be build and equipment can be placed inside the model. The inputs needed for building these structural components and equipment is fed to the MMG by having the user to fill an input file with the JSON format. The file has a prescribed structure that the user has to comply which is useful from a modelling perspective. An example JSON input file is given in Appendix G. The module will automatically read the file through an input reader class, collecting all the data that is stored regarding structures, equipment or mesh settings, see Figure 4.1.

The input values are normalized with respect to some aircraft's reference values, this is known to be parametrically defined. In case of the wings the reference value is the trailing edge and chord, for the fuselage this is the midline of the fuselage connecting the nose and tail, see Figure 4.2. This makes the module work for different scale factors of the model and also for connecting elements like in the Prandtl-Plane aircraft or winglets in the Flying V.

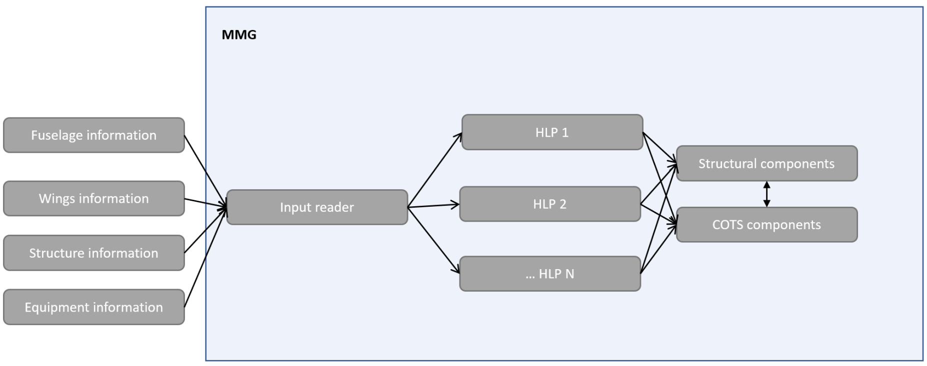

Figure 4.1: Information processing inside the MMG through the input file reader.

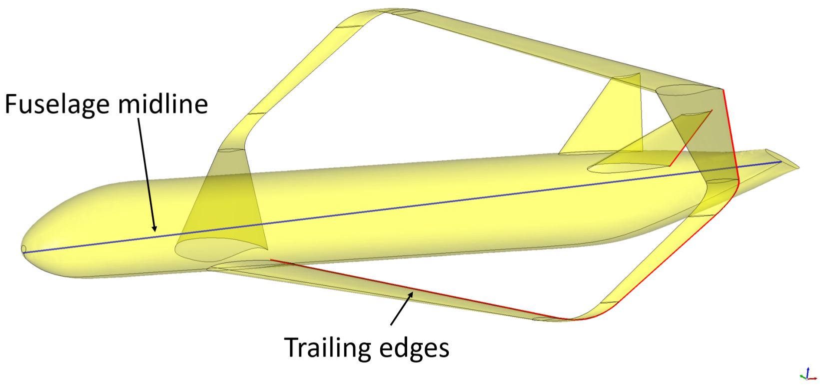

Figure 4.2: Reference value to define the fuselage and wing structural components.

4.2 AIRCRAFT STRUCTURE MODULE

The structural components considered for sub-scale aircraft model design include:

- spars
- ribs & riblets
- fuselage bulkheads
- fuselage frames
- floors
- skins

In Sections 4.2.1 to 4.2.6, the structural components that are used will be explained in more detail. A general overview of the structure generation class diagram is presented in Appendix B. For most SM the assumption can be made on a (semi-)monocoque structure, where the loads are mainly supported through the skin, and where spars and ribs assist in additional stiffness especially in case of high load cases. Stringers are another type of structural elements that can be used to strengthen the structure, but are therefore left out in the methodology.

The initial aircraft sizing rules for the structural components are based on data found by Raymer [36], which contains some design rules for sub-scale models or homebuilts. SM wings usually have the front spar at about 20-30% of the chord back from the leading edge. The rear spar is usually at about the 60-75% chord location. Additional spars can be located between the front and rear spars forming a "multispar" structure, but this is not common for SM. The models have typically just two spars, and some have one main spar which is then usually located at the point of maximum airfoil thickness. Wing ribs and fuselage frames are spaced to provide stability to the wing and fuselage skins and make the structure stiffer. See Table 4.1 with an overview of design rules for some initial structural sizing of SM for the the location of spars, rib pitch and frame pitch.

Topological rules, such as trailing edges & wing-fuselage intersections, are used to initialize the configuration on which the structures module is based. In case the wing intersects with a fuselage, a new geometry of the wing is created that takes

Table 4.1: Design rules for sub-scale models for double spar configuration, rib spacing and frame spacing [36].

	lower value	higher value	units
Front Spar	20%	30%	[-]
Rear Spar	60%	75%	[-]
Rib spacing	0.2	0.8	[m]
Frame spacing	0.2	0.8	[m]

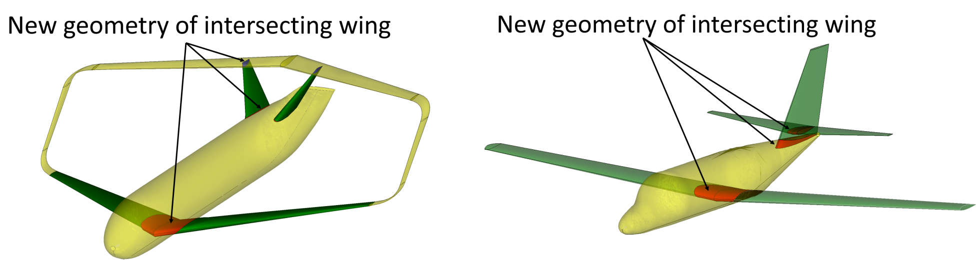

Figure 4.3: The new wing geometry after intersecting with the fuselage and/or another wing (**Left:** Prandtl-plane aircraft **Right:** Cessna Citation II).

in the original wing and splits it in a wing part that is internal to the fuselage and a wing part that is external to the fuselage, see Figure 4.3. This new geometry has more faces and edges of which all edges that belong to the leading edge and trailing edge and faces that belong to bottom or top face must be gathered. The new geometry subdivides the structure in parts that are internal and external to the flow. The division into internal and external wing part is especially useful for the mesh grid definition for the aerodynamic mesh and structural mesh coupling. This is further discussed in Chapter 5.

4.2.1 Spar

The spar is the main load carrying member of the wing. It resists shear and torsional loads and also supports the skin. There are several types of wing carry-through structures possible for SM. The wingbox can continue through the fuselage, while the fuselage itself is not exposed to the bending moment of the wing, which reduces the fuselage weight. If the wing intersects with the fuselage, the wingbox can be a constant-section straight part going perpendicularly to the fuselage midline or it can be an extension of the wings which meet at the center of the fuselage forming a "V" if the wing is swept [36], see Figure 4.4.

The location of the spar at both the end and start are normalized with the local chord. Typically, the spars run from root to tip for SM. A spar can be built in two different methods, named *2points* and *angle*. The first method sets the spar tip point, by specifying the chordwise and spanwise location at root and tip respectively. The latter solution sets the spar's root location together with its location and its extension in the spanwise direction with a certain defined angle.

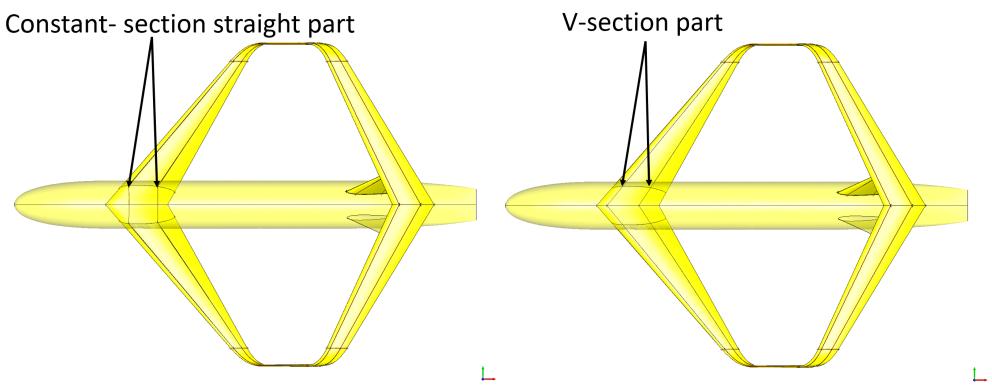

Figure 4.4: The type of box carry-through can be a constant-section straight part going perpendicularly to the fuselage midline or an extension of the spars following the wing that meet at the center of the fuselage forming a "V".

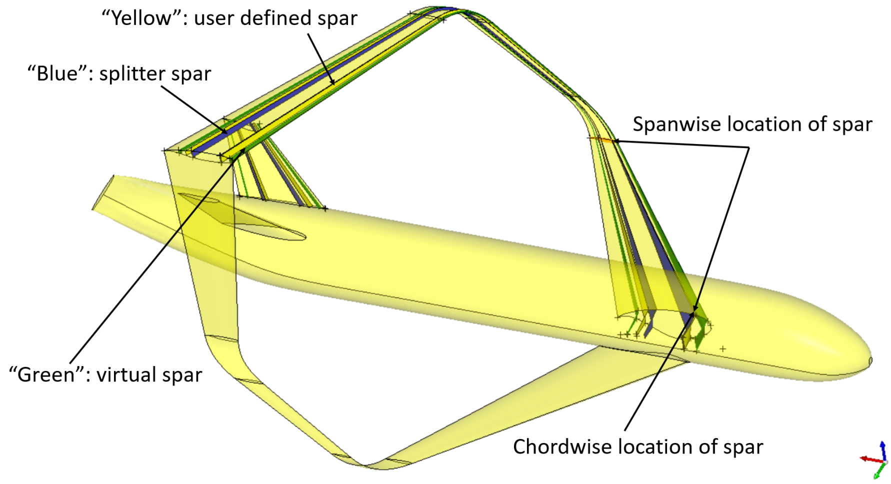

Figure 4.5: Example of spars generated for Prandtl-Plane Aircraft.

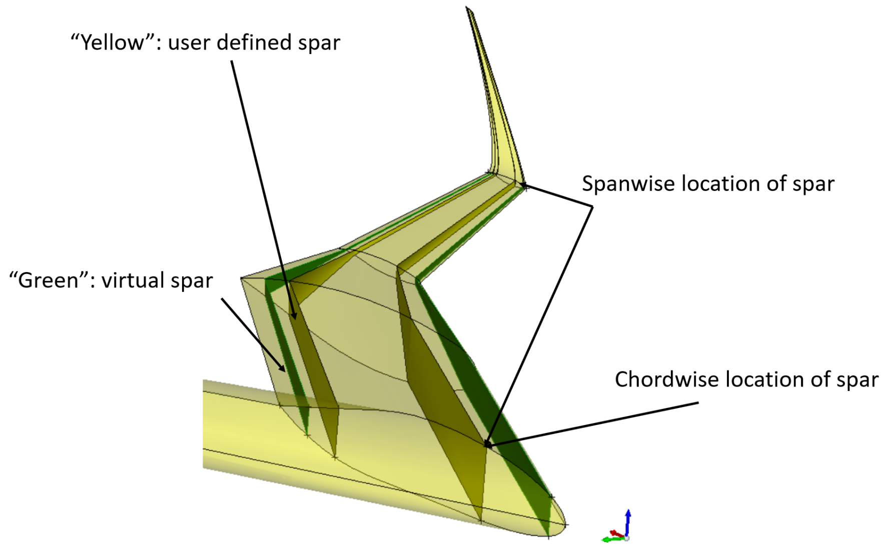

Figure 4.6: Example of spars generated for Flying V Aircraft (no splitter spars).

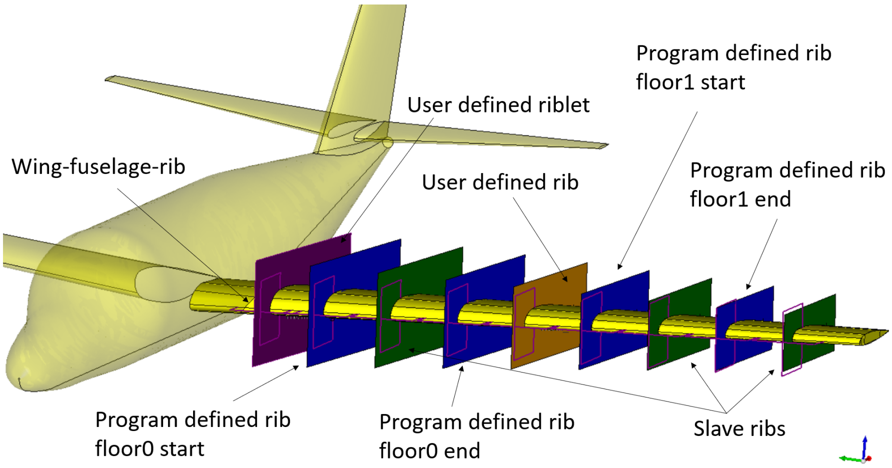

Figure 4.7: Visualization of the generated rib panels of a Cessna Citation II.

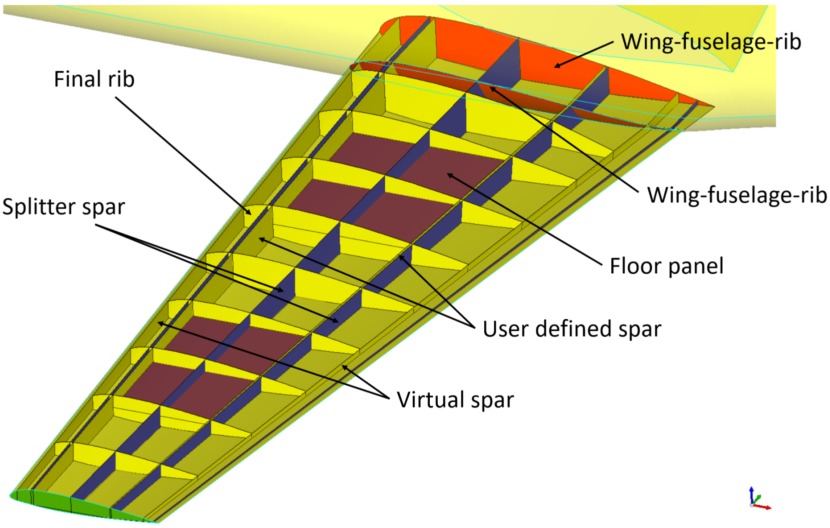

Figure 4.8: The final ribs after fusion with the user defined and virtual spars of a Cessna Citation II.

The data is read from the input file after which a few steps follow to actually build the spar. The spar generator class is divided in *user defined spars*, *virtual spars* and *splitter spars*, see Figures 4.5 & 4.6.

- *User defined spars* can be manually set by the user and have material properties assigned to the component, these components belong to the real load carrying structure.
- *Virtual spars* are generated to cut the rib faces to remove some faces to have a meshable shape with mostly cuad faces. The need to create a meshable shape is explaind in more detail in Chapter 5. This type of spars do not have assigned material properties.
- *Splitter spars* are generated to have a meshable shape too, but mainly in case one of the wings is intersected with a bulkhead or frame in the fuselage. Like virtual spars, splitter spars do not have assigned material properties.

Virtual spars and splitter spars are almost the same, but are defined differently because virtual spars are always used in wings and splitter spars are only used in case a wing intersects with the fuselage. Both type of spars are used and necessary to create a meshable shape for a structural mesh, but are not required for weight & balance estimation. More about the function of these spars is given in Chapter 5.

4.2.2 Rib

The ribs have the function to maintain the correct shape of the skin and resist buckling. The input value to create the rib is normalized with respect to the trailing edge length making them independent of scale size of the aircraft model. The rib is not always necessarily perpendicular to the leading edge, but might have a user defined input angle. Moreover, it is also possible to input the number of holes to create in the wingbox part of the rib, the type of hole and a corresponding rib height as a fraction of the frame diameter or rib height length. In SMs ribs are modelled to have the possibility to have holes to save weight or to have cabling passing through.

The rib generator class is divided into *user defined ribs*, *user defined rib set*, *program defined ribs* and *slave ribs*, see Figures 4.7 & 4.8. A special type of ribs, named riblets, is also defined in which the portions of the rib that are located at the leading edge or the trailing edge can have different orientations, these can also be generated as user defined, as set or program defined.

- *User defined ribs* can be manually set by the user and have different material properties assigned to every rib component. This type of ribs have assigned material properties to them.
- *Program defined ribs* are ribs which are automatically generated at locations where heavy equipment is placed. In this project the coupling has been chosen to automatically create a rib at locations where heavy components are located and externally connected to the SM such as the engines and landing gears. This minimizes the structural load flow in the wings.
- *slave ribs* can be created at spanwise locations based on a user defined pitch along the wing in the bays of the unique ribs.

The ribs can also be generated in a set defined by a start and end position of the set. There are two options to generate the ribs in the set: the first is the number or amount of ribs in the set that will be equally distributed between the start and end location of the rib set, the second is the amount of ribs that will be generated based on the relative start and end positions of the set.

It might also be the case that the user does not oversee the inputs for the positioning of user defined and program defined ribs at once and that some ribs might overlap each other. For example, it can be that a *program defined rib* is automatically generated in case the engine is positioned at the same spanwise location and that another *user defined rib* is generated to have a defined rib pitch along the wing. This will create double ribs at the same spanwise location. Therefore a simple algorithm is made to check if rib locations overlap with each other at the same spanwise location. After the check is performed only unique ribs are returned to the weight & balance module and structural analysis module.

4.2.3 Bulkhead

The bulkheads' are structural components of a fuselage in lateral direction, to distribute concentrated loads into the fuselage skin, see Figure 4.9. In case of full-scale aircraft structures the bulkheads might also be called pressure bulkheads to take the fuselage pressure loads in case of a cabin or are provided at points of introduction of concentrated forces such as those from the wings, tail surfaces and landing gear. In case of the SM the assumption is made that bulkheads are automatically placed at locations of relatively high loads. This is the case at location where groups of equipment (such as batteries, GPS, etc.), must be supported. Also at the location of nose or main- landing gears and at locations where engines are attached to the fuselage. The parametric inputs to create the bulkhead component are the longitudinal

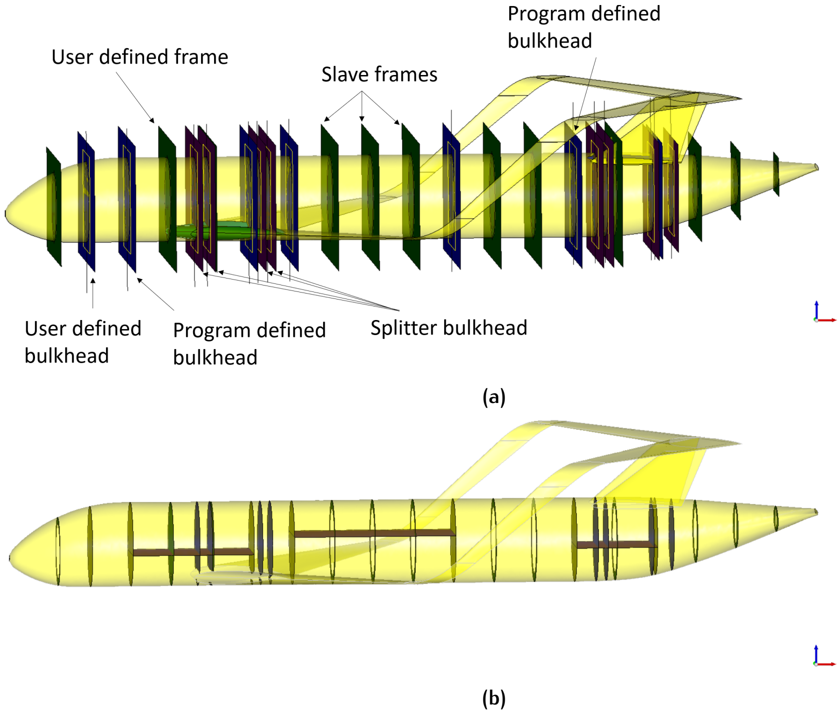

Figure 4.9: Example of a scaled model of the Prandtl-Plane aircraft (a) showing the bulkhead and frame panels (b) generating the final bulkheads and frames.

location as a percentage of the fuselage's midline length, see Figure 4.2.

The bulkheads are classified as *program defined bulkheads*, *user defined bulkheads* and *splitter bulkheads*. The *user defined bulkheads* can be manually placed by the user through the input file if needed. There is also the option to set a pack of bulkheads defined by the user. *splitter bulkheads* are automatically generated in case the user defined spars and virtual spars intersect with the fuselage. The splitter bulkheads do not have material properties, but assist in creating a meshable shape for the fuselage, this is discussed in more detail in Chapter 5.

4.2.4 Frame

The frames' are also structural components in the fuselage cross section. They primarily serve to maintain the shape of the fuselage and prevent instability of the structure. Fuselage frames are equivalent in function to wing ribs, except that local air loads will have a large influence on the design of wing ribs while the design of fuselage frames may be mainly influenced by loads resulting from equipment mounted in the fuselage. These frames can be automatically generated at fuselage locations based on a user defined pitch along the fuselage in the bays of the unique bulkheads and frames that are already contained in the fuselage. The parametric inputs to create the frame component are the longitudinal location as a percentage of the fuselage's midline length and likewise as for the ribs, the capability of generating holes inside the frame are used to reduce weight or simply to allow equipment or cabling to be positioned inside. The frame height input is defined as a fraction of the maximum frame diameter.

4.2.5 Floor

For the positioning of COTS components the analysis includes floors. The floor is the structural component to place groups of physical equipment and instruments.

This way is makes it easy to re-position the equipment around to enhance or decay the inertia or CG by indexing a classified group of equipment. Inside the wing the floors are created in between the spars and two ribs, inside the torsion wingbox, see Figure 4.8. In the fuselage the floor is created between two bulkheads, see Figure 4.9. In real sub-scale aircraft structures the floor or system board can be of very different sizes and the attachment to the structure can also be different, for example the floor can be based directly on the skin or mounted to the spars only. In this research the assumption is made that the loads from the equipment are taken by the ribs or bulkheads/frames and ultimately passed to the skin. The start and end location are given input as a fraction of the wing span or fuselage length. Also the floor height is given as input as a fraction of the wingbox height or the fuselage diameter in case of the fuselage.

4.2.6 Skin

The primary function of the wing skin is to form a surface for supporting the aerodynamic pressure distribution from which the lifting capability of the wing is derived. If the skin material is made of composite material, the skin of the wings and fuselage of SM in reality is in most cases made in moulds for composite fabrication. It could even be the case that in reality a foam layer in between the composite could be used to account for the relatively high bending loads in the wingbox section. Therefore, in case of the wing a division has been made between top and bottom skin, and additionally leading/trailing and wingbox sections. This allows to assign different material properties in each of these section. As observed in the real build Flying V SM this allows to strengthen the wingbox section with more layers or with a foam in between the layers. This makes it possible to strengthen the structure only in specific parts where needed, while this is not necessary for the whole wing skin, to save weight. The skin of the fuselage is divided into lateral faces, nose and tail face. The material groups chosen for the wing skin are summarized below:

- wingbox material in between the spars
- top skin material
- bottom skin material
- root material
- tip material

4.2.7 Material definition

In order to estimate the mass & inertia and CG of the assembly all previous *user defined* or *program defined* components have assigned material properties. Different materials might be used in SM, some of the options are wood, metal (isotropic), but most models in practice are built of composites. See Appendix C for more details on composite materials. As said before, in some models the wingbox has additional foam in the layup in the center in between the spars making a stiff wingbox, this is included to better estimate the weight & balance properties of the SM. The materail inputs for all these sub-assemblies are listed below:

- an isotropic/orthotropic or foam material type. Foam material can be added in between the ply layers
- the density of the corresponding material type. Input dimensions of density for fibers and foam are areal densities in $kg/m2$.
- the number of plies to be used for the component in case orthotropic is used.

- the thickness of the ply
- the resin mass fraction of the laminate

Additionally the strength properties are assigned to the component. These material properties are used to automatically write them to the FE input file in the structural analysis module, discussed in more detail in Chapter 5.

Based on the material data that is read and assigned to the structural component the mass is estimated. Also the inertia per component is estimated by projecting an element of area dA through the thickness of thin plate theory. The thickness of the plate itself in calculating the moments of inertia is neglected, since the coordinate of the element dm is $(x, y, 0)$. This assumption is based on the thin plate theorem, having zero thickness in the z-direction [37]. An element's moment of inertia about the x axis is:

$$I_{xx} = \int_m (y^2 + z^2) dm = \rho T \int_A y^2 dA = \rho T I_x \tag{4.1}$$

$$I_{yy} = \int_m (x^2 + z^2) dm = \rho T \int_A x^2 dA = \rho T I_y \tag{4.2}$$

$$I_{zz} = \int_m (x^2 + y^2) dm = \rho T \int_A (x^2 + y^2) dA = \rho T I_z \tag{4.3}$$

Where I_x is the moment of inertia of the element's cross-sectional area about the x axis, and for the other around the y and z axis. Since the mass of the thin plate is:

$$m = \rho \cdot thickness \cdot A \tag{4.4}$$

The 3D moment of inertia is then estimated as:

$$I_{xx} = \frac{m}{A} \cdot I_x \tag{4.5}$$

$$I_{yy} = \frac{m}{A} \cdot I_y \tag{4.6}$$

$$I_{zz} = \frac{m}{A} \cdot J_O \tag{4.7}$$

where $J_O = I_x + I_y$ is the polar moment of inertia of the cross-sectional area. The parallel-axis theorem is used to transform the object's inertia with its origin at the center of mass of the object around the CG of the aircraft [37].

4.3 AIRCRAFT EQUIPMENT MODULE

The aircraft equipment module is implemented with the objective to build SM to provide experimental flight test capabilities for research experiments as explained in the introduction, for example to measure the aerodynamic derivatives in flight to compare them with measured wind tunnel results. These requirements follow from accurate measurement of flight conditions and aircraft responses for different selected maneuvers.

Therefore the SM should be equipped with COTS components that are typically based on specific mission requirements. In reality the choice of equipment depends very much on these specific requirements such as flight time and therefore the weight of the battery package and engines or the type of experiment on itself. In this research a selection have been made from the database of the real-built Flying V model built at the TUD. The database inside the MMG could be easily extended if needed for specific requirements. The selected equipment is based on the most important components and also the heaviest, as shifting these components will influence the weight & balance most. The components are extracted as .step files from the CATIA file database. Not only its position is now important for the mass properties of the model, but the code includes also a check if the current equipment fits in the selected scaled size of the model, putting a constraint on the design. These components used in this work are subdivided into:

- flight control system
- propulsion system
- landing gear
- scientific instruments equipment

Examples of equipment used in the real-built Flying V SM can be found in Appendix D. The Flight control systems are used for down-link data requirements and mainly include control and telemetry equipment, more specifically: GPS, attitude, heading, airspeed and acceleration data for aircraft positions and rates; servos; and energy packages such as control power. The flight control system is a computer to process the pilot commands and vehicle sensor inputs to command the control surfaces.

Most SM require a complete avionics package to fly the aircraft. High-quality sensors are used to collect information about the state of the model for use in control and post-test data analysis, these are categorized as scientific instruments. A GPS receiver provides aircraft position and velocity information through the telemetry downlink. Air data booms are used to measure total pressure, static pressure, static temperature, angle of attack, and angle of sideslip. The propulsion system is general the heaviest category as this include the engine/nacelle and batteries. The amount of batteries needed depend much on how long the flight test will take. The landing gear systems include the nose gear retraction and its leg and also the gear computer.

The step files of the selected components taken from the database are then read inside the equipment module and have their assigned mass (usually defined in the production sheet). The component can then kept as it is, this then directly indicates if the component does fit inside the SM. Or it can be scaled to the desired input as

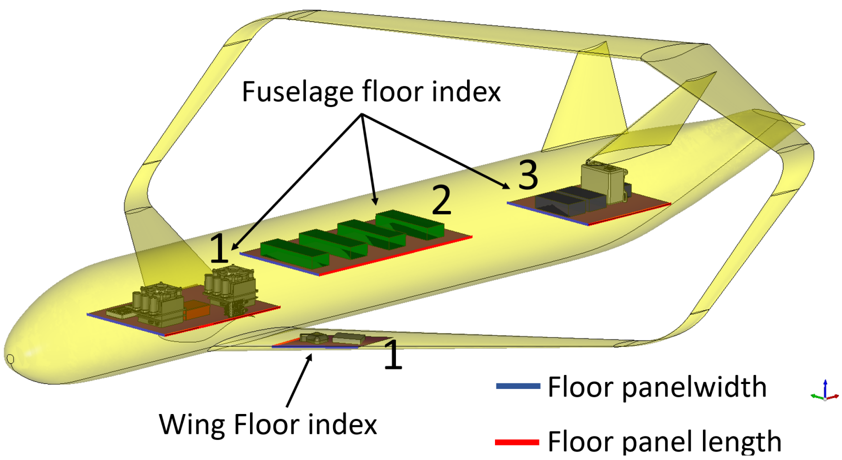

Figure 4.10: Visualization of the reference lengths for components that belong to a floor.

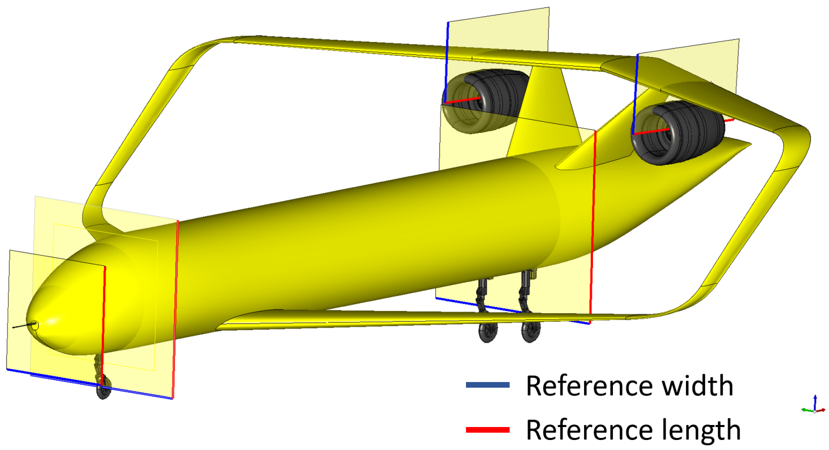

Figure 4.11: Visualization of the reference lengths for components that are externally located or not belong to a floor in the wing or fuselage.

given as input in the data input reader (scale factor n=1.0, by default the as-built dimensions). The component can be positioned with an orientation angle as given in the input file. The component is then classified into a floor component, fuselage or wing external component, see Figures 4.10 and 4.11. The following parametric inputs are given to the components that belong to a floor:

- index of the floor to place the component
- the parametric length as a fraction of the floorpanel length
- the parametric width as a fraction of the floorpanel width

Additionally for components which are external to the wing or fuselage the following inputs should be given to the component, in order that the components scale equally for different scale factors of the SM:

- plane location as a fraction of the leading edge length or fuselage length
- the plane angle which defined the orientation of the component relative to the wing or the fuselage
- the parametric length as a fraction of the plane length to place the component
- the parametric width as a fraction of the plane length to place the component

4.4 WEIGHT AND BALANCE

Now that all the individual components can be created as needed by specific design requirements, the weight & balance properties can be estimated per wing/fuselage or for the aircraft. A final assembly can be created for different SM, for any scale-factor and with different internal structure.

After assembly of the SM, the mass and inertia are estimated based on physics based approach and therefore expected to be within a small margin from a real-built model. A comparison with a real-built Flying V SM is given in Chapter 6. It is expected that the difference is smaller for the weight than for the inertia. This is because the inertia includes the distance arm squared to the center of gravity. Designers are able to quickly determine the effect of adding components or moving them around in the airframe with respect to the weight and inertia targets.

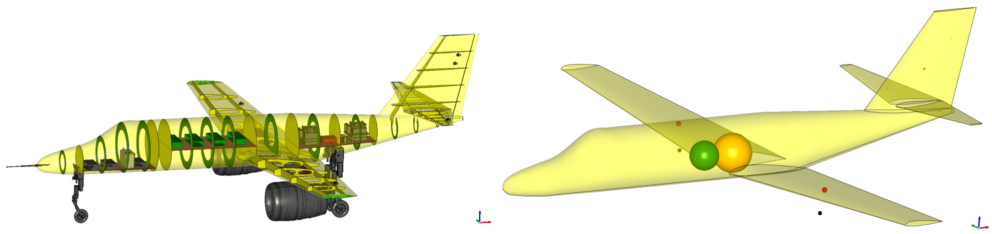

(a) (b)

Figure 4.12: Example of a Cessna Citation II SM (a) final assembly and (b) the aircraft CG in *orange*; the wings CG in *red*, wings equipment CG in *black* and the fuselage equipment CG in *green*.

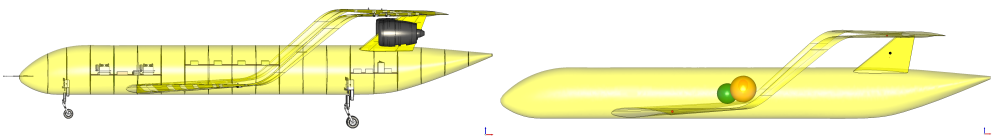

(a) (b)

Figure 4.13: Example of a Parsifal $\frac{1}{18}$th (0.056) scaled SM (a) final assembly and (b) the aircraft CG in *orange*; the wings CG in *red*, wings equipment CG in *black* and the fuselage equipment CG in *green*.

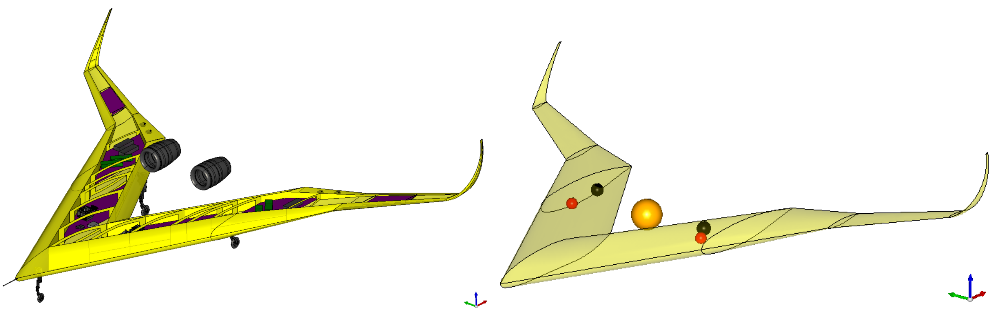

(a) (b)

Figure 4.14: Example of Flying V scaled SM (a) final assembly and (b) the aircraft CG in *orange*; the wing CG in *red* & the equipment CG indicated in *black*.

5 AUTOMATE FINITE ELEMENT MODEL GENERATION

In the previous chapter an appropriate methodology is identified and developed to design the structural components of SM, position COTS components to estimate the mass, inertia and the associated CG of SM. However, the initial input for structures is based on initial structural sizing design rules for the material, spars and rib pitch by Raymer [36]. The final mass distribution for the structure can be different based on requirements on stiffness and strain from structural analysis results, this is known as structural sizing.

The pre-processing of the structure includes all the steps to prepare the model for the structural analysis. Therefore the parametric model has to be meshed, properties and loads must be applied and the structure must be constrained. An activity diagram, shown in Figure 5.1, gives a summary of the steps that are taken to automate the process. Each of the steps in the activity diagram will be further discussed in the following sections, in order to clarify the code build-up.

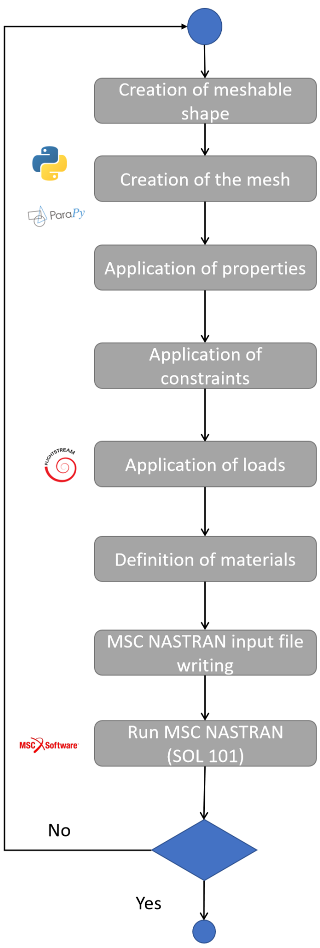

Figure 5.1: Activity diagram describing the structural sizing process workflow and interface with different software.

5.1 MESHABLE SHAPE

There are various components intersecting with the skins, in this case spars and ribs for the wing and frames and bulkheads for the fuselage. The components divide the surfaces into small surfaces called geometric mesh elements. This geometry needs to be prepared to perform structural analysis, for which a structural solver is needed. MSC Nastran is used as the solver in this research, see Appendix F for more details. The Nastran solver has to respect the following requirements for the surface:

1. vertices common to 2 adjacent edges must be shared by the two edges
2. duplicated elements must be avoided
3. each node must belong to a mesh element
4. free edges must be avoided

Shell elements are typically used to model structures in which one dimension (the thickness) is significantly smaller than the other dimensions and the stresses in the thickness direction are negligible. The element is then used to model bending and in-plane deformations. The spar, rib web, frames, bulkheads and skins are modelled as two-dimensional shell elements. Typical shell elements used in structural analysis are triangular (CTRIA) or quadrangular (CQUAD), see Appendix E for more detail on element classification.

Triangular elements can be used in highly irregular surfaces, because this type of element is better adaptable to be used in local transition zones. However, triangular elements are known that they can lead to a very inaccurate solutions. This is because the elements are subjected to over-stiffness, making the model to be more rigid than the real structure is [38]. Moreover, they have a poor convergence rate, therefore typically a very fine mesh is required to produce good results. Creating a non-structured mesh is easily done, however this should be avoided as much as possible. Therefore triangular elements are only used in parts of the model which are known as more irregular surfaces.

Quadrilateral elements with 4 nodes (CQUAD4) could lead to more accurate results. It should not only have 4 edges, but also the aspect ratio of the elements should be controlled as much as possible. The aspect ratio is the ratio between the height a and the length b of the element. If the aspect ratio is high (more than 30 degrees) shear locking can become a dominant effect, making the element more stiff than it in reality is. The problem is known to be less significant under normal or

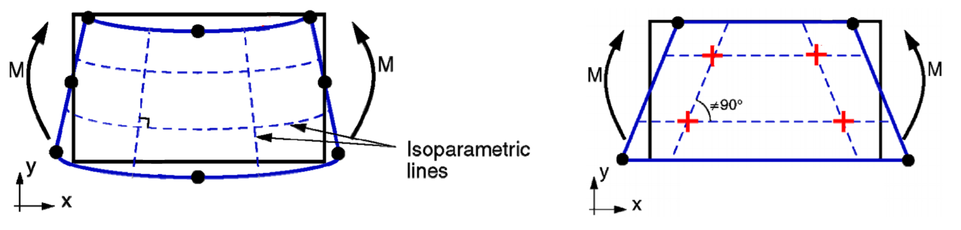

(a) A CQUAD8 element

(b) A CQUAD4 element

Figure 5.2: Overly stiff behaviour results from energy going into shearing the element rather than bending it, called shear locking (a) The element edges can assume a curved shape, the angle between deformed isoparametric lines remains equal to 90° (implies ϵ_{xy}=0 (b) The element edges must remain straight, the angle between the deformed isoparametric lines is not equal to 90° (implies $\epsilon_{xy} \neq$0).

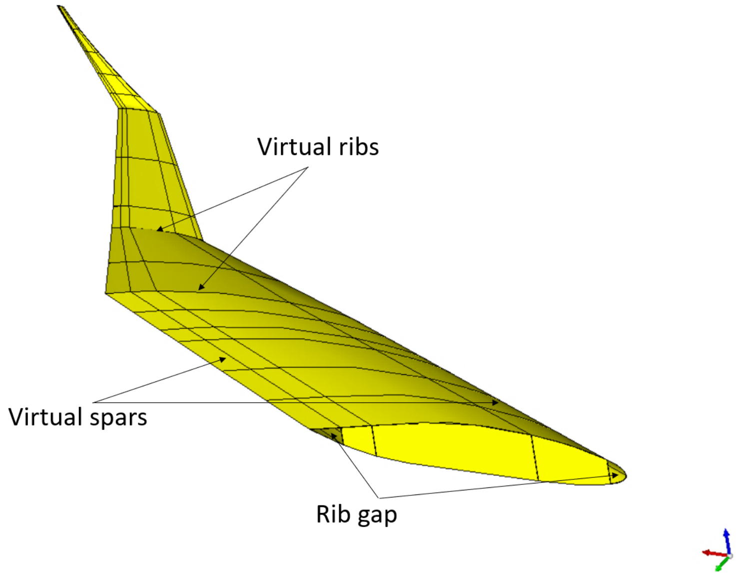

Figure 5.3: Virtual spars at the leading and trailing edge showing the effect on the ribs and skin and in contrary virtual ribs on the spar.

shear loads, or for CQUAD8 elements [39]. However, the problem with 8-node quad is that these elements have mid-size nodes and this can create problems with non-regular meshes and the grid construction is more difficult, see Figure 5.2b. Since the aspect ratio can be controlled for both wing and fuselage, in this work the CQUAD4 element is chosen.

In order to adhere to these requirements, there is the preference to have a shape that consists of mostly quadrilateral faces. Moreover, there is the need to automatically mesh the shape of the aircraft model having these four-sided faces. Generating a structured mesh for an aircraft geometry which has faces with four edges is difficult. In these cases a finer discretization of the structure is necessary, in which the geometry must be split into four sided faces.

The categorization of spars and ribs in virtual components was explained in the previous chapter. The virtual spars are used in the structure through the input files with the objective to divide the surface (skins and ribs) in order to have a meshable shape. No material or mass properties are assigned to the virtual spars, so this will not effect the weight & balance but only solve meshing problems. A virtual spar is created by default at 7% (leading edge zone) and 90% (trailing edge zone) chord-wise direction, or the user can manually set them in the input file. By inserting the virtual spars, a fully structured mesh is obtained and results in a feasible mesh, see Figure 5.3. The virtual spars make it possible to divide the ribs and skin structure in 4-sides elements to have better mesh control. The exclusion of the small area of the rib at leading and trailing edge section of the wing will have little influence on the analysis. Virtual ribs are used to get a correct mesh of the spars. These virtual ribs are at positions of wing kinks if there is no real rib at that location, meaning that some extra edges are created.

Another problem is the connection of the relevant components between the wing and the fuselage, in case there is a fuselage. For structural analysis, the connection must be modeled to guarantee the force transmission between the connected components, assuming a structural connection exists only between the bulkhead of the fuselage and the spar of the wing. Splitter bulkheads are generated at locations of user defined spars and virtual spars. In contrary, splitter spars are generated at locations where frames or bulkheads intersect with the wing, see Figure 5.4. This

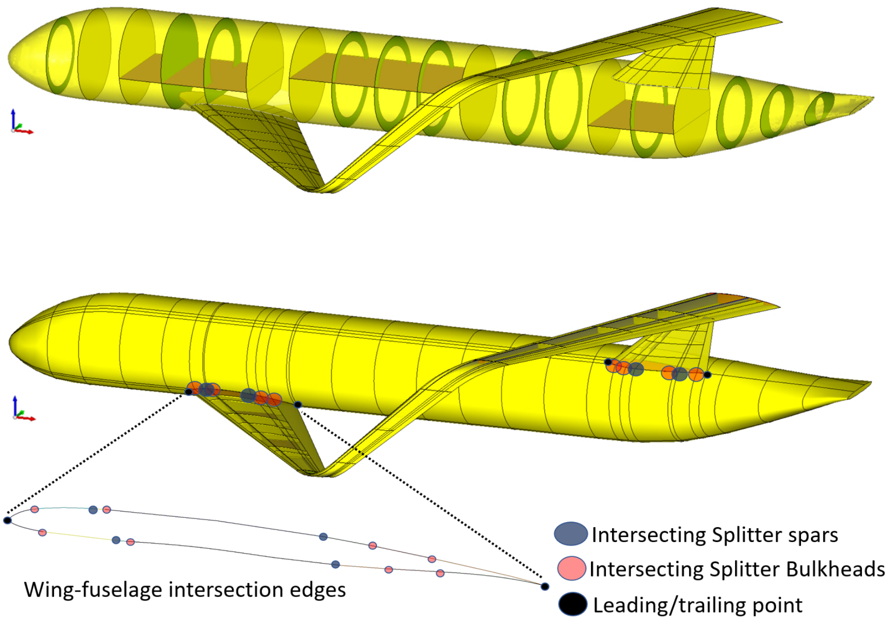

Figure 5.4: Vizualization of splitter spars and splitter bulkheads for wing-fuselage connections.

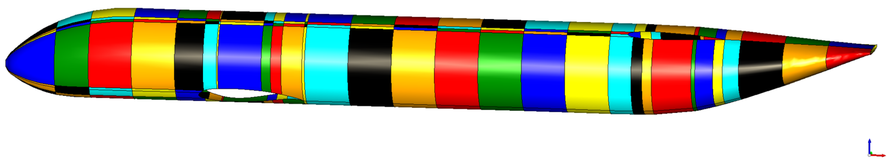

Figure 5.5: Geometrical faces of the fuselage structure group with the help of splitter bulkheads for correct wing connection.

then creates a shape of the fuselage having four-sided faces and it assures a correct load distribution from wing-to-fuselage and vice versa in case the model is glued in these locations to derive the loads per node at these locations. In case of the fuselage an algorithm uses some extra splitter curves to split the fuselage in a shape having quad faces, see Figure 5.5.

5.2 SHAPE BUILDER

Once that all the FE primitives are defined for the wing and the fuselage together with the splitter spars and splitter bulkheads, the final FE model should have edges on which nodes can be attributed. Fusion is the process of coupling components together which will adhere to the requirements to not have duplicated elements and avoidance of having free edges. The structural elements are fused through specific ordered operations to end up with the shape that can be meshed. Since in this research the wing and fuselage are decoupled the fusion steps are different. But if the full-aircraft mesh should be considered the fusion steps can be easily combined. First all the skins are fused together that are defined in the FE structural components. In the next steps the spars and virtual spars are fused with the wing´s outer shell. Then the ribs and virtual ribs are fused with the wings skin and spars. The evolution of the fusion steps for the components are stored and creates additional edges. Afterwards the virtual spars, virtual ribs and the small rib areas at leading and trailing edges are removed from the model. Additionally this modified shape is then fused with the splitter spars and the virtual wing-fuselage-rib to form an equal number of edges at the location where the wings intersect with the fuselage as explained in section 5.1. These splitter spars and virtual ribs are removed from the model after the fusion, as these do not have assigned physical properties.

5.3 MESH BUILDER

Like the structure is defined through an input file, so is the grid also provided by an input file inside the MMG. A parametric description of the model also needs a parametric description of the mesh, such that changes to the mesh density can be made, if desired. This allows rapid generation of mesh and reduces errors in translating data to the MSC Nastran input file. High element density is often used to improve the accuracy of the solution in regions where the stress gradients are high. During a FE analysis study usually a balance between computational resources available and accuracy of the results has to be achieved. The spacing between elements can be reduced at locations where it is believed that stresses will be higher in order to get an accurate solution. In the input file the number of nodes or the pitch of the nodes to assign to the edges are described. Pitch mesh control can be applied to the spanwise edges, leading edges, trailing edges and boxwise edges regarding the mesh, see Figure 5.10. In order to be parametrically defined, the value is given as percentage of the length of the root chord edge. Alternately, a number of nodes can be defined directly on the specified edge group. This option can be selected in the mesh input file. For the fuselage structure the pitch mesh control can be applied on the longitudinal edges, lateral pitches, the bulkhead & frame inner edges (as the outer edges is part of the fuselage skin) and the fuselage-wing pitch as these are the edges where the fuselage intersects with the wing. The fuselage-wing pitch shall be equal for the fuselage and the wings to create the same number of nodes on the intersection edges, see Figure 5.11.

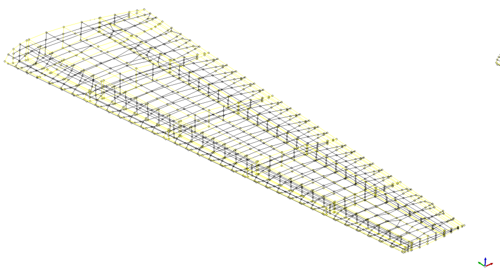

Figure 5.6: Coarse mesh having low density of nodes.

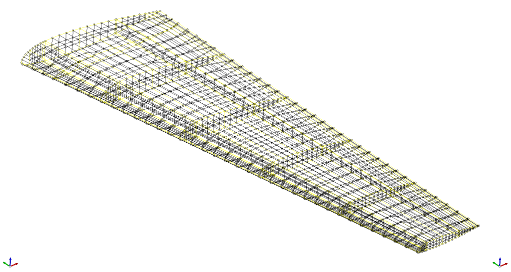

Figure 5.7: Higher density of nodes in chordwise edges.

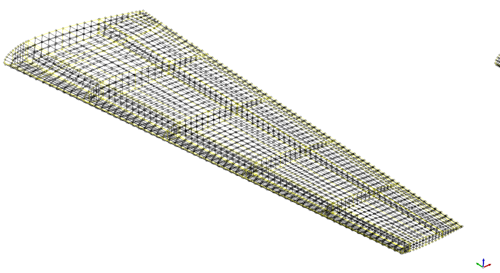

Figure 5.8: Higher density of nodes in spanwise edges.

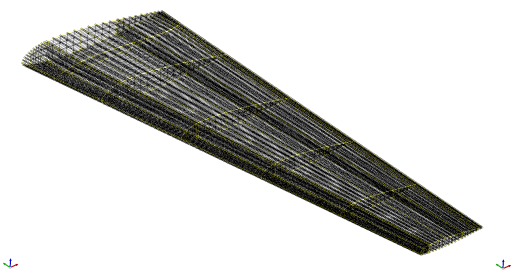

Figure 5.9: Refined mesh having high density of nodes.

Figure 5.10: Example of mesh control for a wing.

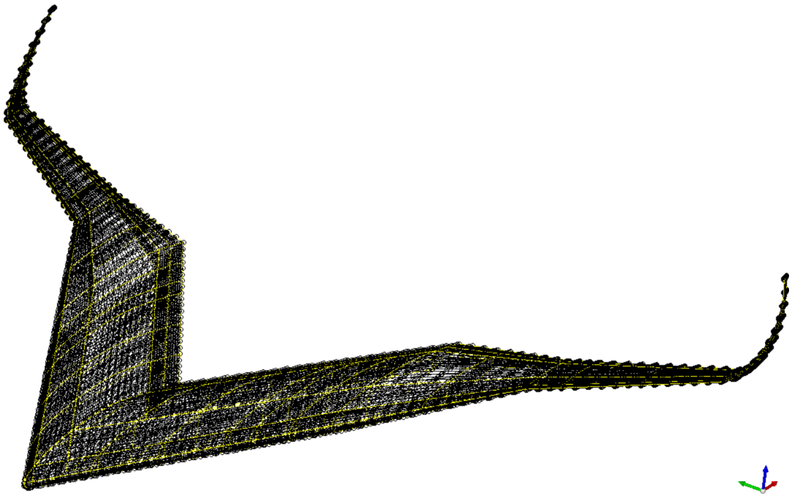

(a) Flying V

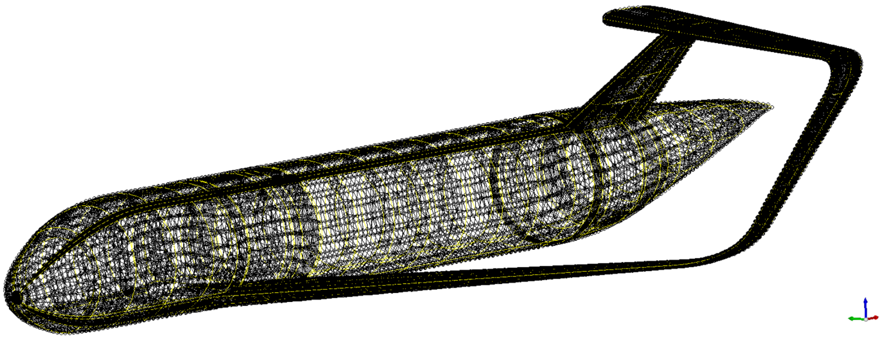

(b) Prandtl-plane

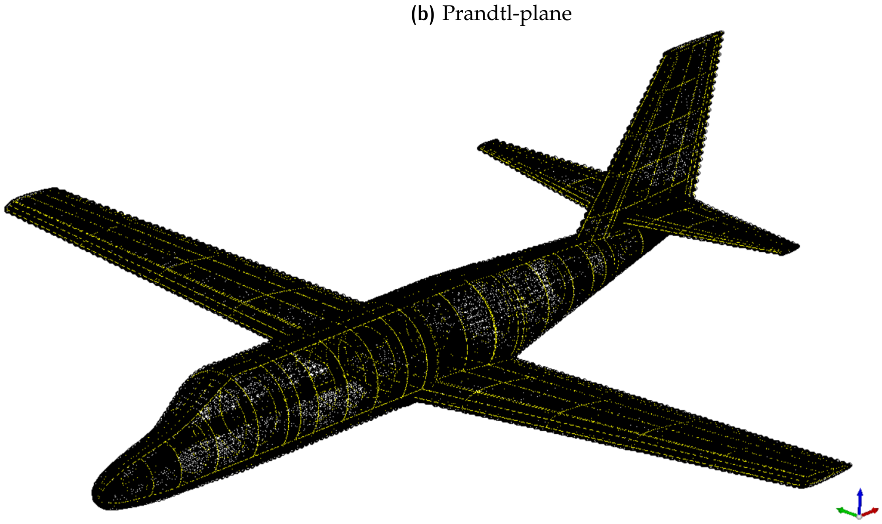

(c) Cessna Citation II

Figure 5.11: Example of structural mesh for different aircraft models.

5.4 MATERIALS AND PROPERTIES

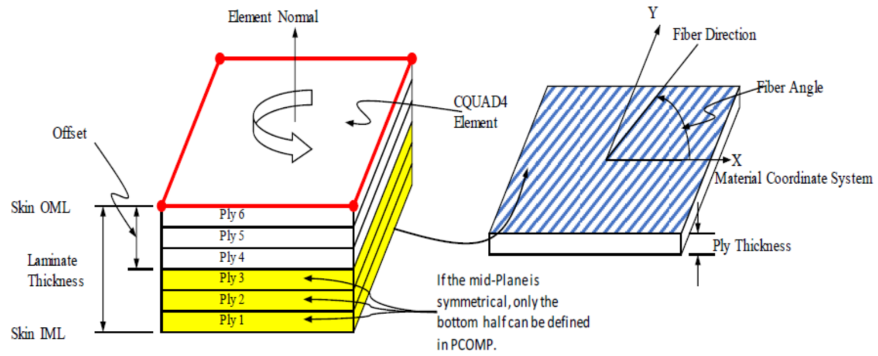

Figure 5.12: An overview of the PCOMP definition.

In this research work focus is on composite materials as most SM are built from this material. In general, composites can be modeled using single layer shells, multi-layer shells (continuum shells) and/or solids. In case of solids, each ply needs to be modeled with at least one solid element. This requires a huge number of solid elements to model a simple plate. The majority of the real life parts are modeled with single layer shell elements. Analysis of composite shells is very similar to the solution of standard shell elements. A single layer shell element is modeled as composite by assigning a composite property (i.e. PCOMP or PCOMPG) to it. PCOMP and PCOMPG are similar. but where PCOMP will not have any associativity between different PCOMPs where as PCOMPG will maintain associativity between PCOMPs in different zones [39]. In this research the PCOMP card is used, based on the assumption that this is sufficient when the cross section or thickness is uniform through out the model. Composite material properties in general are modeled with an orthotropic material model (MAT8), see Figure 5.12.

The strength and stiffness of a composite depends on the orientation of the reinforcing fibers. Both the longitudinal and transverse modulus of elasticity influences the total stiffness of a composite. $E1$ is the modulus of elasticity in longitudinal direction, also defined as the fiber direction or 1-direction. $E2$ is the modulus of elasticity in lateral direction, also defined as the matrix direction or 2-direction. $NU12$ is the poisson's ratio (ϵ_2/ϵ_1 for uniaxial loading in 1-direction). $G12$ is the in-plane shear modulus. $G1Z$ is the transverse shear modulus for shear in 1-Z plane.

Table 5.1: Material properties of carbon/epoxy composite.

	Value
Classification	
Material type	Volume 2F: Polymer-Matrix Composites
Sub-class	Carbon/Epoxy
Common Name	AS4/3501-6 145-UT (bleed)
Form	Tape
Composite Class	Ply/Lamina
Modulus Property set	
ply angles	[0, 45, -45, 90, 0, 45, -45, 90]
E1	137e9
E2	10.2e9
NU12	0.27
G12	7.0e9
G1Z	7.0e9
G2Z	7.0e9

G2Z is the transverse shear modulus for shear in 2-Z plane. The characteristics of the material mass properties are given in the input file as was already described in Section 4, but for structural analysis also strength properties need to be given to the component. So also these material properties are given in the input file to create the geometry inside the MMG.

It is possible to vary the material properties per lifting surface and also for skins, ribs, spars, bulkheads and frames individually. The strength properties of the material chosen to test the methodology in this research and inserted in the JSON file are summarized in Table 5.1 [40]. These values can be easily changed and given any number as the user wants.

5.5 BOUNDARY CONDITIONS

In the previous section the meshable shape creation, mesh control and composite material properties were discussed. For each mesh group the material, ply thickness and stacking sequence is defined. The model needs also the loads that act on the structure and boundary conditions. The boundary conditions characterizing the analysis depend very much on the type of aircraft. In almost all full-scale aircraft (scaled or not) the wingbox carries through the fuselage so that both wings form a continuous beam (it might be subdivided into sections that are joined, but when they are joined, they form a continuous beam). The fuselage then connects to the wing through various different designs (depending on the location of the wing relative to the fuselage), but generally, there are two heavy frames in the fuselage that line up with the spars of the wingbox so that the shear load from the spars can be transmitted into these heavy frames and then into the remainder of the fuselage. For SM the load path can be totally different, in this research the constraint points are located at points where the parts are glued together. These are typically the locations where the wing and fuselage connects, or at locations where wings intersect, see Figures 5.14 and 5.15. An unconventional model involves different constraints than a conventional model. For conventional wings like the Citation II the boundary conditions concern the root section, where the wing is clamped to the fuselage.

5.6 AERODYNAMIC LOADS

Aerodynamic loads might be modelled as points loads to ribs and/or spars. However, in this research work lift loads are applied as pressure loads, which pressure distribution is expected to be a better approximation of the real situation. Therefore a mapping method is needed between the aerodynamic model and structural model. The aerodynamics loads can be analyzed by an aerodynamic flow solver. Examples of such flow solvers are VSAERO or Flightstream [15]-[16]. In this work, Flightstream has been chosen for the coupling of loads to the structural mesh.

Flightstream is a high fidelity aerodynamics tool for aircraft designers. The code has a vorticity based flow solver that uses the surface mesh to produce accurate solutions in a fraction of the time required by full volume mesh CFD solvers [41]. Figure 5.16 shows an example of aerodynamic analysis results in Flightstream for three different SM.

Once the solver has converged, the flow data around the geometry in the solver can be analyzed through the use of streamlines, section planes and spatial probe points. With the latter case, users can probe for the flow conditions in the fluid

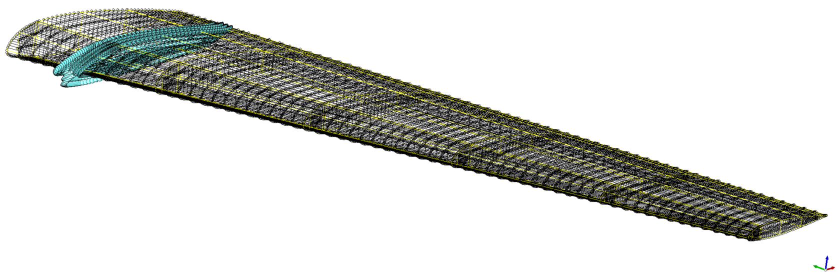

(a) Constraint on a Citation II wing

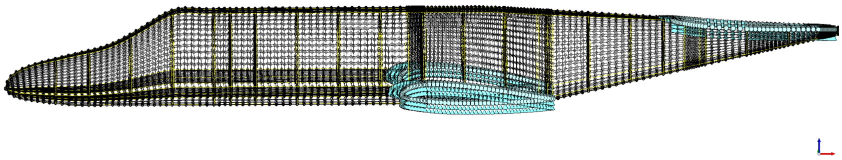

(b) Constraints on a Citation II fuselage.

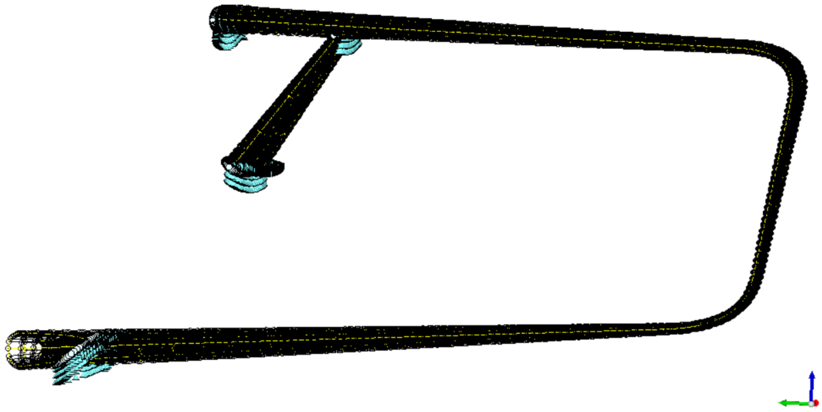

(a) Constraint on a Prandtl-Plane wing

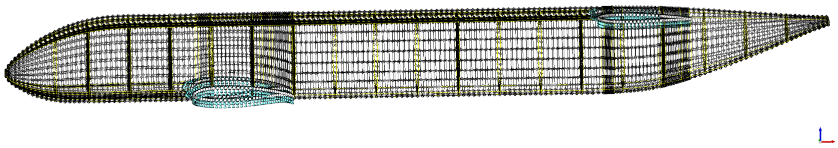

(b) Constraints on a Prandtl-Plane fuselage.

Figure 5.14: SPC constraint forces on different types of structural meshes.

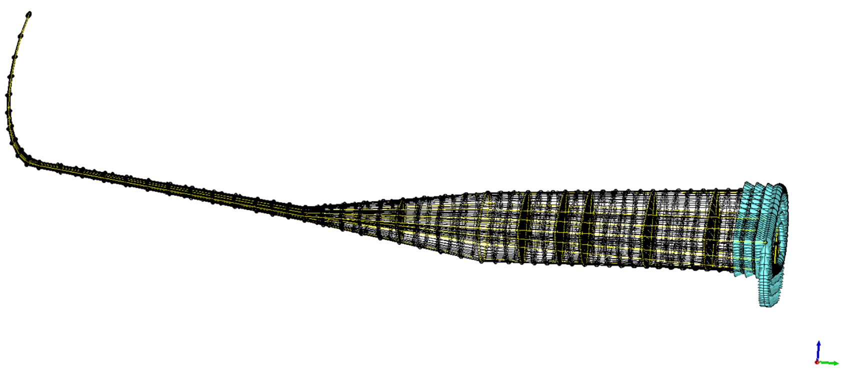

Figure 5.15: Constraints on a Flying V wing.

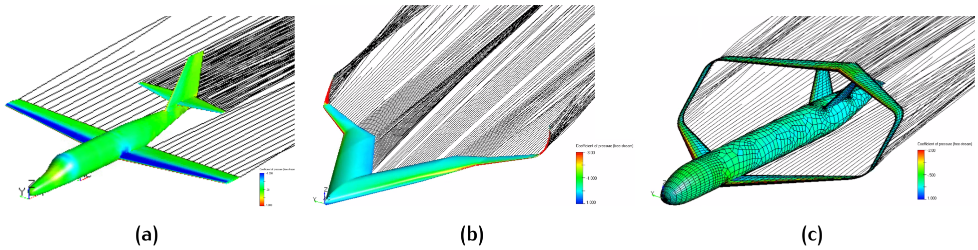

Figure 5.16: Flightstream Aerodynamic analysis (a) Citation II (b) Flying V (c) Prandtl-plane.

space around the geometry. The user can create individual probepoints in the simulation and edit these coordinates to place the probe at any point in space around the geometry. Users can also import a list of probe points directly from a text file.

Inside the DEE an algorithm has been written to automatically write the probepoints that are exposed to the flow at the center point of the structural mesh faces to a file, see Figure 5.17. This allows the easy creation of probepoints for any mesh (both wings and fuselage) and for any scale size of the model. The probepoints can be imported with the Flightstream GUI opening a dialog box allowing the user to

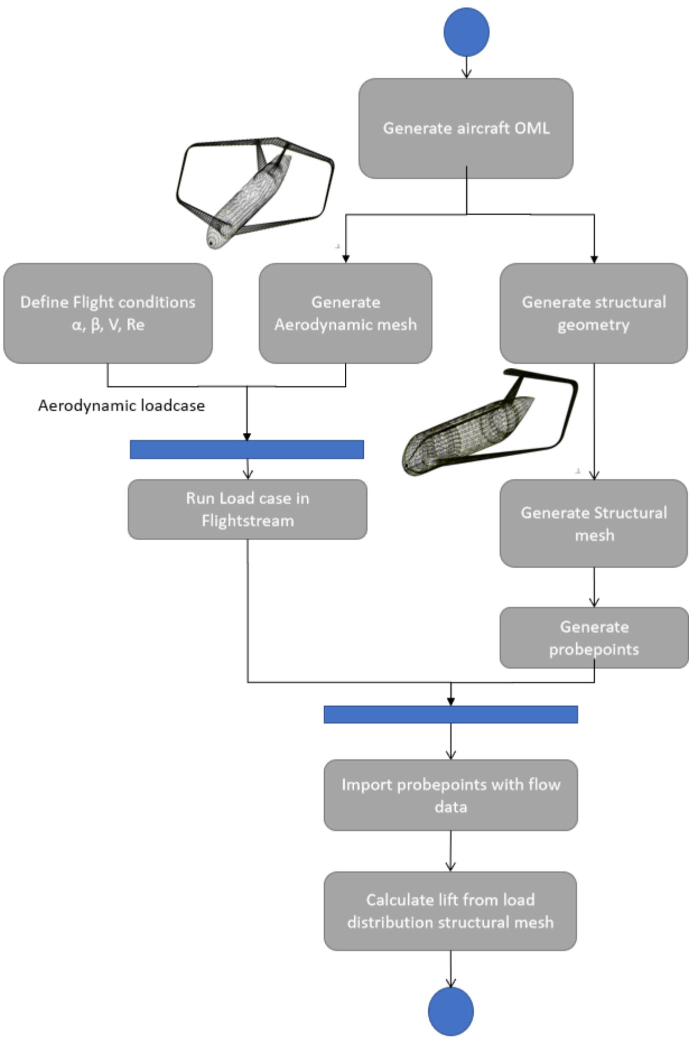

Figure 5.17: Schematic of coupling between aerodynamic load distribution from Flightstream to the structural mesh with the use of probepoints.

Table 5.2: Overview of flow parameters used to derive the pressure.

Symbol	Definition
a	speed of sound
cp	pressure coefficient
M	mach number
p	static pressure at location on the wing
p_∞	freestream pressure
q_∞	freestream dynamic pressure
V	freestream velocity
γ	heat capacity ratio
ρ_∞	freestream air density

navigate to the text file on the system. The file format is a *CSV* text file containing the probe points in the following format (N probe points):

$$\begin{aligned} X1, Y1, Z1, TYPE_1 \\ X2, Y2, Z2, TYPE_2 \\ .... \\ XN, YN, ZN, TYPE_N \end{aligned} \tag{5.1}$$

The parameters XN,YN,ZN indicate the probepoint coordinate location in x-,y- and z-direction. If the value $TYPE_N$ is set to 0 it indicates that the probepoints should be generated for surface type and if set to 1 for volume type. Once a probe has been created and imported, the flow parameters on the probe points can be exported and evaluated.

The first step to compare the loads between the aerodynamic solver and the loads on the structural mesh is to calculate these loads. The flow data from Flightstream is mapped to a pressure distribution on the structural mesh through the probepoints. Flightstream exports the probepoints with their pressure coefficient C_p and mach number M data. The pressure is then calculated as follows:

$$p - p_\infty = cp \cdot \frac{\gamma}{2} \cdot p_\infty \cdot M_\infty^2 \tag{5.2}$$

A definition of the symbols is given in Table 5.2. The relation is based on the isentropic computation using the local Mach number, which in turn is computed from the coefficient of pressure [42]. First, the definition of C_p from Equation 5.3,

$$C_p = \frac{p - p_\infty}{q_\infty} = \frac{p_\infty}{q_\infty}\left(\frac{p}{p_\infty - 1}\right) \tag{5.3}$$

From the definition of dynamic pressure,

$$q_\infty = \frac{1}{2}\rho_\infty V_\infty^2 = \frac{1}{2}\frac{\rho_\infty}{\gamma p_\infty}(\gamma p_\infty)V_\infty^2 = \frac{1}{2}\frac{V_\infty^2}{\gamma p_\infty/\rho_\infty}(\gamma p_\infty) \tag{5.4}$$

And since also $a_\infty^2 = \gamma p_\infty/\rho_\infty$, therefore:

$$q_\infty = \frac{1}{2}\frac{V_\infty^2}{a_\infty^2}\gamma p_\infty = \frac{\gamma}{2} p_\infty M_\infty^2 \tag{5.5}$$

Loads are one critical aspect when performing structural analysis, without accurate loads, stress analysis and sizing is basically meaningless. The verification of the load mapping is treated in Chapter 6.

5.7 LOADS ASSUMPTIONS

As described in Chapter 4 the SM contains equipment to provide experimental flight test capabilities for research experiments. In this context, in case the equipment are placed on a floor the total mass of equipment on that floor is spread equally to the connected grid points where the floor is attached to the ribs. The total mass is then multiplied with the gravitational constant and divided by the number of load points (number of attachment points of the floor to the ribs). The loads can also directly spread to the nodes of a rib or bulkhead in case an engine or landing gear is attached to the rib or bulkhead directly. Or if a component like servo or air data probe is positioned in the SM but not attached to a floor or rib then the closest gridpoint to that load is taken. In case of the engine a moment load is created at the attachment point on the ribs due to the engine offset.

In this research some assumptions are made that affect the analysis. These are summarized:

1. No sideslip angle.
2. The moment due to the engine is equally distributed over the rib grid nodes.
3. The weight of the equipment are modelled as points loads; in this research the assumption is made that the loads from the equipment are taken by the ribs and passed to the skin.
4. The load cases are consired for a 1g steady flight speed, 2.5g and 5g symmetric maneuver.

6 VERIFICATION AND VALIDATION

In this chapter three validation cases are considered for the developed methodology. First, in order to know how well the weight & balance properties can be estimated for different SM, the estimated mass and CG is compared with the real-built flying V model in Section 6.1. Secondly, the error in lift load as a result of load mapping from the aerodynamic model to the structural model is discussed in Section 6.2. Lastly, the correctness of generating the input file for MSC Nastran is checked with Patran in Section 6.3.

6.1 COMPARISON WITH REAL-BUILT FLYING V SM

The real-built SM includes the structural components and COTS components and could therefore be used to validate how well the mass and CG could be predicted by the parametric model in the DEE. Figure 6.1 shows the real-built flying V SM under construction at the manufacturing lab. If the estimated values of the developed physics-based estimation as explained in Chapter 4 are reasonable the methodology can also be used for other sub-scale models in the preliminary design phase. The key dimensions of the physics-based Flying V model are given in Figure 6.2.

An overview of the current equipment used in the real-built Flying V and the physics based model inside the DEE is given in Table 6.1. The selected equipment is based on the most important components and also the heaviest, as shifting these components will influence the weight & balance most. The level of detail in this research work is focused on preliminary design of SM, so the level of detail excludes additional fasteners, adhesives, cabling and paints. It is therefore expected that the difference between the physics based mass estimation and the mass of the real-built Flying V will be within a margin difference.

For example, the material inputs for all the structural components are listed in Table 6.2. For the spars, ribs and floors the aerial weight A_w of the fibers is taken $300 g/m^2$ and for the skins $162 g/m^2$, as this data was also given in the fabrication sheets of the material for the real-built flying V.

Figure 6.1: Left: Flying V model under construction at the manufacturing lab of the TUD. **Right:** Real-built Flying V model.

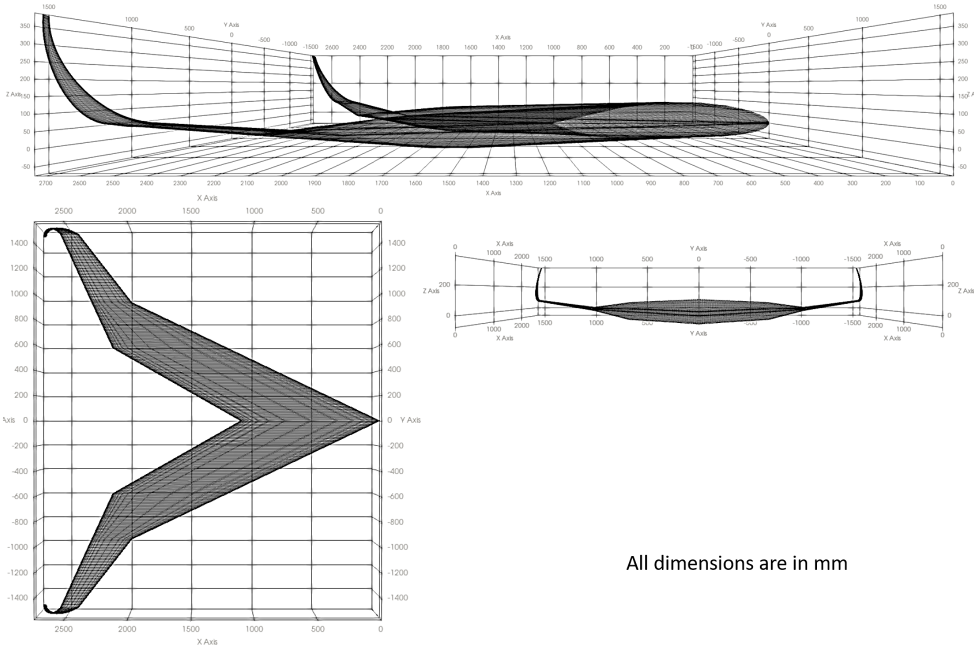

Figure 6.2: The key dimensions of the Flying V model inside the DEE.

Table 6.1: System mass breakdown of heaviest equipment for the real-built flying V SM.

	component	mass [kg]	# components	notes
Flight Control System	Pixhawk	0.033	1	Pixhawk 4
	Receiver	0.024	1	Rex-12
	Telemetry	0.022	1	RF RFD868+
	Secondary Computer	0.070	1	Raspberry Pi 3B+
	Servo	0.026	6	D89MW/HS-5070MH
	Control power	0.173	3	GensAce 2S 4000mAh
	GPS antenna	0.033	1	-
Total group mass		0.86		
Scientific Instruments	Air data probe	0.013	1	-
	Air data computer	0.198	1	-
	GPS	0.094	1	-
Total group mass		0.305		
Propulsion system	Engine	1.135	2	-
	Battery	1.47	4	-
	ESC	0.528	2	-
Total group mass		9.2		
Landing Gear	Nose gear retract	0.335	1	-
	Nose gear leg	0.217	1	-
	Main retract	0.31	2	-
	Main leg	0.500	2	-
	Gear computer	0.048	1	-
Total group mass		2.21		
Total Equipment mass		12.73		

Table 6.2: Mass properties of the structural components used for the Flying V SM.

	material	
	orthotropic	foam*
Skins ***foam only in wingbox sections**		
density [kg/m2]	0.162	0.28
ply number [-]	4	1
thickness [mm]	0.13	3
resin fraction [-]	0.55	-
Spars / Ribs / Floor		
density [kg/m2]	0.300	0.19
ply number [-]	4	1
thickness [mm]	0.13	5
resin fraction [-]	0.55	-

Table 6.3: Comparison between the structural mass groups of the real built and physics based Flying V SM.

	Real-built Flying V [kg]	Physics-based Flying V model [kg]
wing skins	5.92	6.56
main spars	1.87	1.95
main ribs	0.56	0.64
winglets	0.23	0.21
floors	1.29	1.4
Total Structural Mass	9.87	10.76
Total Aircraft Mass	22.6	23.49
Center of gravity [m]		
x	1.49	1.43
y	-0.003	0.001
z	0.040	0.015
Inertia [kg m2]		
Ixx	-	7.12
Iyy	-	5.82
Izz	-	12.72

Based on the previous mentioned assumptions on material properties the code is able to estimate the assembled physics-based mass, CG and inertia. Table 6.3 gives a comparison between the structural mass groups of the real built and physics based Flying V SM and its corresponding CG. In Table 6.3 the equipment mass is added to the structural mass to get the total aircraft mass. The comparison of the inertia is left out as no reference material could be found. An important difference between the physics-based estimated mass and the real-built model can be the choice of resin fraction, which is assumed to be 55%. The real-built flying V SM can have imperfections in the material due to the manufacturing process. The resin fraction is typically about 55% when hand-made and will be lower when lay-up equipment is used [43], see Appendix C for more detail on manufacturing methods. The user can set any value for the resin fraction value which refers to the fibre/resin ratio in terms of volume of fibres to volume of resin.

6.2 AERODYNAMIC LOAD MAPPING

The application of loads are one critical aspect when performing structural analysis. Without an accurate pressure load distribution, stress analysis and sizing is basically meaningless. Therefore, the aim is to provide a validation of the load mapping from the aerodynamic solver to the structural mesh. First, it is important to verify that the aerodynamics loads from Flightstream are correctly mapped to the structural mesh to be used in the structural analysis. Correct mapping means in this case that the load distribution is equivalent to the distribution given by aerodynamic analysis and that the difference between the total lift load given by Flightstream and the calculated load on the structural mesh is within a small error difference.

In general before any design and sizing efforts are conducted on new or modified SM designs, it is critical to determine the entire loads envelope that the SM will be subjected to during the flight test. Critical load cases might be:

1. flight maneuvers
2. propulsion loads
3. landing gear loads
4. ground handling loads & control surface loads

Typical flight maneuvers include pitching, yawing, rolling and various control surface movement combinations needed to accomplish the flight mission profile. A

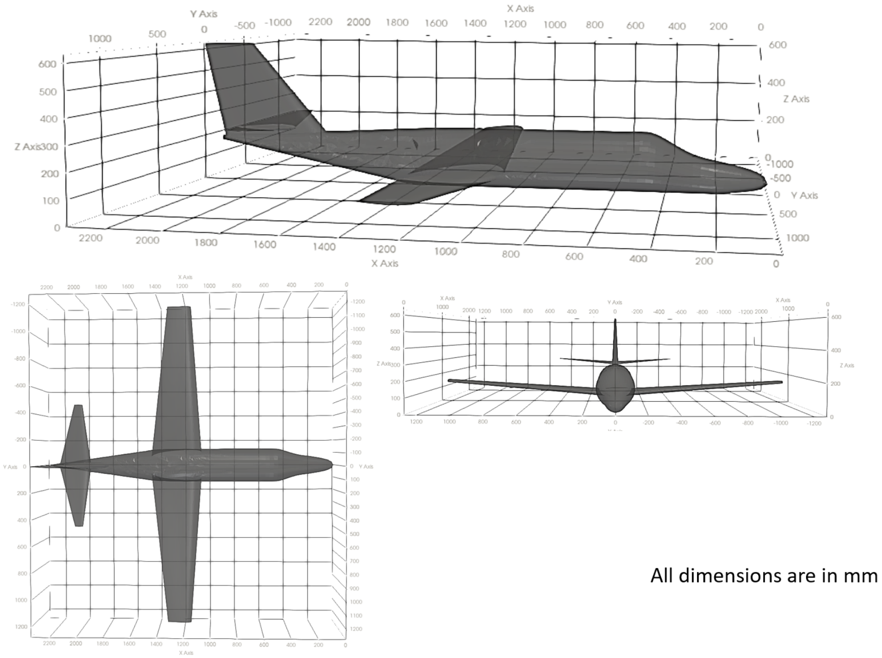

Figure 6.3: The key dimensions of a $n = 0.16$ scaled Citation II SM.

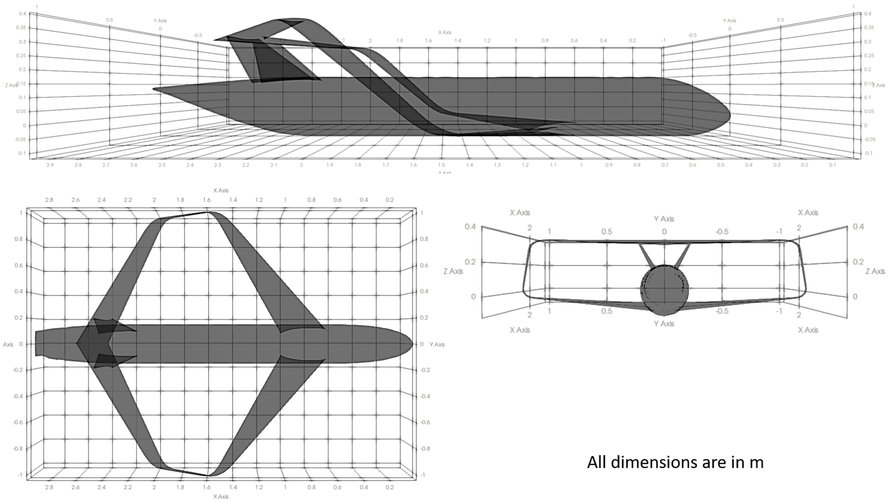

Figure 6.4: The key dimensions of a $\frac{1}{18}$th scaled Prandtl-plane SM.

SM must be designed for all of these expected limit maneuver loads and resulting aircraft ultimate loads. The exploration of design load cases can be a research in itself. Therefore the verification of the load mapping are only shown for a 1g steady flight condition and a 2.5g symmetric pull-up manoeuvre for the Cessna Citation II and Flying V. The key-dimension for both models are given in Figures 6.3 and 6.4. The FD Cessna Citation II dimension are given in Figure 3.2. The scale sizes from the FD Cessna Citation II (15.92m) used to analyze the aerodynamic load mapping are $n = 0.12$ (1.92m), $n = 0.16$ (2.56m) and $n = 0.20$ (3.2m) with the wingspan in between brackets. To show that the methodology also works for the Prandtl-plane aircraft model a 5g symmetric pull-up maneuver flight condition is used to validate the method.

Since only symmetric maneuvers and gusts (side slip angle β=0) are considered in the current simulations, the SMs structural mesh are reduced to a half model, see

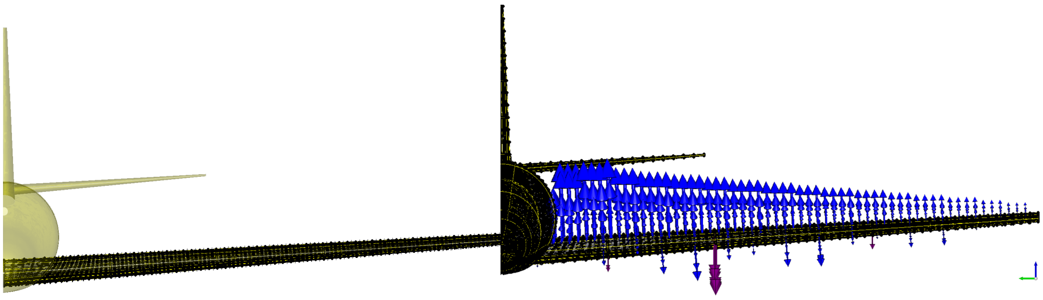

(a) (b)

Figure 6.5: Visualization of (a) probepoints on structural mesh (b) resulting pressure loads (α=3deg, V=41m/s) with equipment point loads for Citation II SM wing.

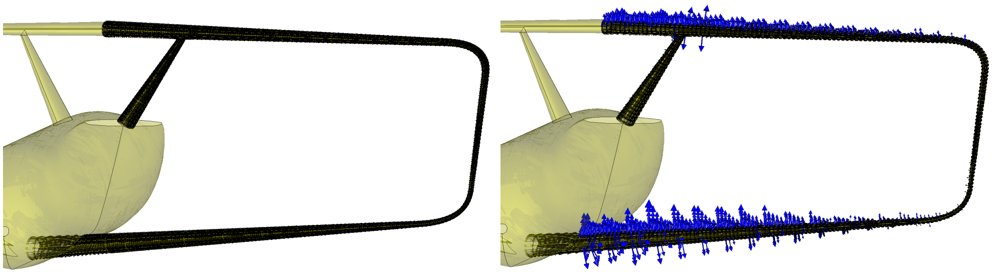

(a) (b)

Figure 6.6: Visualization of (a) probepoints on structural mesh (b) resulting pressure loads (α=8deg, V=50m/s) for the Prandtl-Plane SM wing.

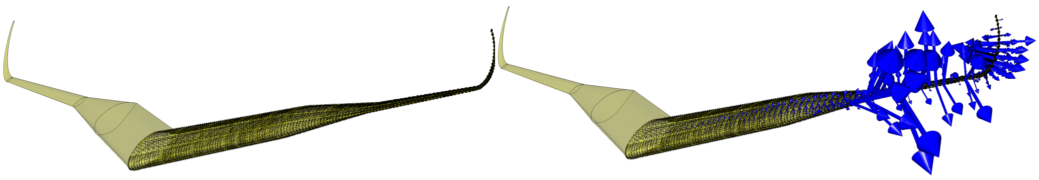

(a) (b)

Figure 6.7: Visualization of (a) probepoints on structural mesh (b) resulting pressure loads (α=11deg, V=32m/s) for the Flying V SM wing.

Figures 6.5, 6.6 and 6.7.

There will be a difference between the structural model and aerodynamic model. This is because there needs to be a mapping mechanism where the linear pressure fields from the aerodynamic solver Flightstream must be mapped to the per face pressure load as needed by the structural solver MSC Nastran. This mapping can make some approximations that may lead to MSC Nastran receiving a load case that is not representative of the condition shown by Flightstream.

Tables 6.4 and 6.5 show the difference in lift load and the estimation error for the main wing of the Cessna Citation and the Flying V wing for a 1g steady flight condition and 2.5g symmetric pull-up manoeuvre, respectively. Table 6.6 shows the lift load comparison for scale sizes of the Citation II and the Prandlt-plane for a 5g symmetric pull-up manoeuvre. In which n refers to the scale factor of the SM. AoA is the angle of attack and V_∞ the freestream flight speed at which the aerodynamic analysis is performed.

Table 6.4: Comparison between the calculated lift on structural mesh and aerodynamic lift for a 1g steady flight condition for SMs of the Cessna Citation II and Flying V.

	n [-]	AoA $[kg]$	V_∞ $[m/s]$	Loadcase $[-]$	Aerodynamic lift [N]	Calculated Lift Structural mesh [N]	Error [%]
Citation II	0.12	1	47	1	92.3	94.3	-2.12
Citation II	0.16	0	47	1	118.3	123	-3.82
Citation II	0.20	0	41	1	139.5	147.8	-5.62
Flying V	-	11	20	1	114	117	2.56

Table 6.5: Comparison between the calculated lift on structural mesh and aerodynamic lift for a 2.5g steady flight condition for SMs of the Cessna Citation II and Flying V.

	n [-]	AoA $[kg]$	V_∞ [m/s]	Loadcase $[-]$	Aerodynamic lift [N]	Calculated Lift Structural mesh [N]	Error [%]
Citation II	0.12	5	50	2.5	224.2	235	-4.59
Citation II	0.16	3	47	2.5	258.9	252	2.73
Citation II	0.20	3	41	2.5	307	300.3	2.23
Flying V	-	5	32	2.5	291	299	-2.67

Table 6.6: Comparison between the estimated lift on structural mesh and aerodynamic lift for a 5g steady flight condition for SMs of the Citation II and the Prandtl-plane.

	n [-]	AoA $[kg]$	V_∞ $[m/s]$	Loadcase $[-]$	Aerodynamic lift [N]	Calculated Lift Structural mesh [N]	Error [%]
Citation II	0.16	7	47	5	456.9	477.4	-4.29
Prandtl-Plane	0.056	8	50	5	580.7	601.5	-3.46

6.3 LOADCASE IN PATRAN

In Chapter 5 the structural analysis steps to run (critical) loadcases are automated based on the requirement to have a short design lead time for SM. All these steps have been implemented inside the DEE, to create the input file for MSC Nastran that constains all the necessary data to describe the model. Once that the input file for MSC Nastran is automatically created, the input file should be evaluated if it maintains its characteristics in the Nastran environment. If the FE analysis results are sufficient realistic it can be used as a constraint in the SM design, see Figure 1.5 and Equations 1.2 and 1.3 in Chapter 1 respectively.

In general, all finite element models used in preliminary SM design phase represent a simplification of the real geometry. These simplifications should be as representative as possible compared to the real-built aircraft at early design phases. Even if the shape of the model in MSC Nastran is the same as the model in ParaPy, the analysis may be incorrect in case the properties of the elements are not attributed properly. However, this can be checked by using the Patran graphical user interface. It should be mentioned that the Patran interface is not needed when running simulations, but it is considered fundamental as a prove of correctness of the FE model generation. Therefore the input file for MSC Nastran is imported in Patran and the several inputs are checked. Of special interest are the material coordinate systems of the composite material and also the pressure loads. This is done for the Flying V and a $n = 0.056$ scale size of the Prandtl-plane SM.

Flying V

Two load cases are considered, one with load factor $n_z = 1$ and the other at $n_z = 2.5$, see Tables 6.4 and 6.5. In the analysis only the aerodynamic load distribution are analyzed and the loads from equipment are left out. In this study it is expected that the situation for a 2.5g case is most critical, as the equipment itself relieves the positive lift force acting on the wing. The PCOMP cards are also checked if this data comply with the material properties, such as thickness, number of ply and the

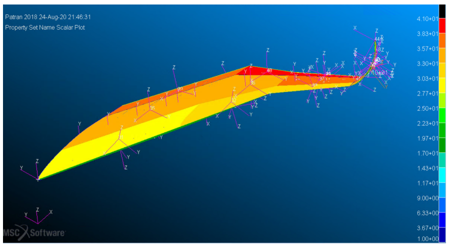

(a) PCOMP sets and material coordinate system of composite material.

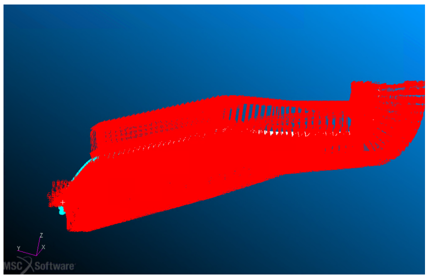

(b) PLOAD4 with B.Cs visualized.

Figure 6.8: Visualization of properties and BCs in the created input file for the Flying V SM in the Patran graphical user interface.

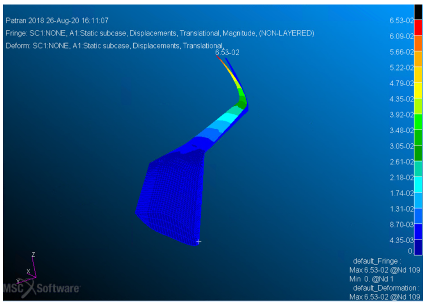

(a) Example of maximum displacement plot. Resulting in 6.53cm deflection with nr_{ply}=4.

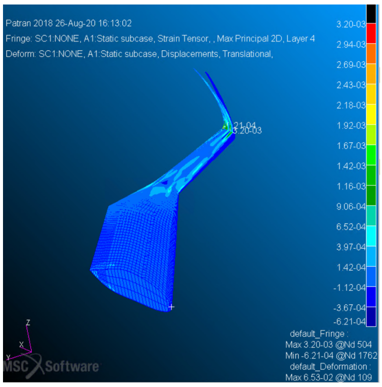

(b) Example of maximum 2D principal strain. Resulting 3200μ strain with nr_{ply}=4.

Figure 6.9: Flying V SM with 4 plies at the top and bottom of the skin nr_{ply}=4 for a load factor of 2.5g.

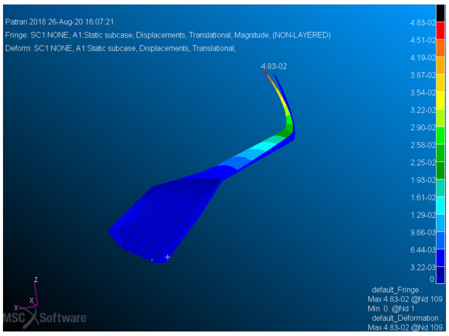

(a) Example of maximum displacement plot. Resulting in 4.83cm deflection with nr_{ply}=5.

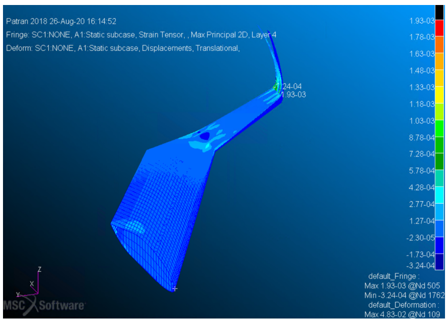

(b) Example of maximum 2D principal strain. Resulting in 1930μ strain with nr_{ply}=5.

Figure 6.10: Flying V SM with 5 plies at the top and bottom of the skin nr_{ply}=5 for a load factor of 2.5g.

material orientation as generated with ParaPy. The division of wing skin in leading edge, wingbox and trailing edge part are clearly visible. In these region different material properties can be assigned, see Figure 6.8. To compare the results only the material properties regarding number of ply is changed for the top and bottoms skin of the flying V.

To know if the model is able to withstand some critical load cases, it should be checked if the units on maximum displacement are realistic and also the values for strains. MSC Nastran does not keep track of the units. Therefore, it is important that the user inputs all of the properties using a consistent set of units. For example, if meters m is defined for locations in grid entries, then the properties, such as areas A, should be in terms of $m2$. From Figures 6.9 and 6.10 it can be seen how the displacement starts clearly after the wing kink, as this is also the region where the load distribution is highest due to the angle of attack and high sweep of the wing. The maximum displacement results in a maximum deflection of 6.5cm when 4 plies are used and 2cm less deflection when 5 plies are used with the orientation of fibers in the [0,45,-45,90,0] direction. The orientation of fibers is based on the data in Table 5.1, but any orientation can be used and defined in the input file to create the structures. A reference value for the displacement of the scaled model of the Flying V or another scaled model is missing, as no good reference material could be found. The 2D maximum principal strain value decreases from 3200μ strain to 1930μ strain. If the wing should be more stiff, it could also considered to add some extra ribs at the section close to the wingtip. The method allows to easily make changes to the design and analyze results with MSC Nastran.

Prandtl-Plane

One example load case is considered with load factor $n_z = 5$ and flight conditions $\alpha = 8\,\text{deg}$ and $V_\infty = 50m/s$. In this study it is assumed that the situation for a 5g case is most critical. In Table 6.6 the aerodynamic load from Flighstream and the calculated total lift load on the structural mesh are compared. From Figure 6.11 it can be seen that the wing model in this case is built mainly from quadrilateral elements, there is only a small region at the intersection of vertical tail with the rear-wing where triangular elements are used. The material orientation and the pressure loads are also checked.

In the analysis the aerodynamic load distribution and the loads from equipment are considered to show the modelling of equipment loads acting on the wing structure, see Figure 6.12. The equipment loads come from the engine or equipment placed on the floors which are equally distributed over the corresponding ribs to which the component is attached. The servo is modelled as point load to the closest node in the wing mesh. Figure 6.13 is a plot showing the displacement and strain distribution.

The results in terms of maximum displacement for the 5g loadcase is 1.72cm in case 4 plies are used in the wing skin with the orientation of plies in the [0,45,-45,90] direction. The 2D maximum principal strain value is 2020μ strain which is lower than the adviced strain of 3500μ by an expert from industry. It can also be seen from the plot that most parts of the wing have order of ten or hundred lower

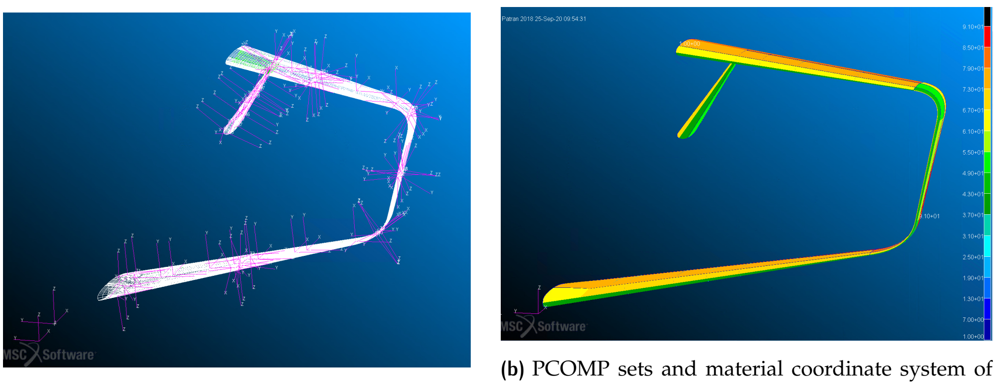

(a) Mesh constists of mainly CQUAD4 elements.

(b) PCOMP sets and material coordinate system of composite material.

Figure 6.11: Visualization of mesh and properties in the created input file for the Prandtl-Plane SM in the Patran graphical user interface.

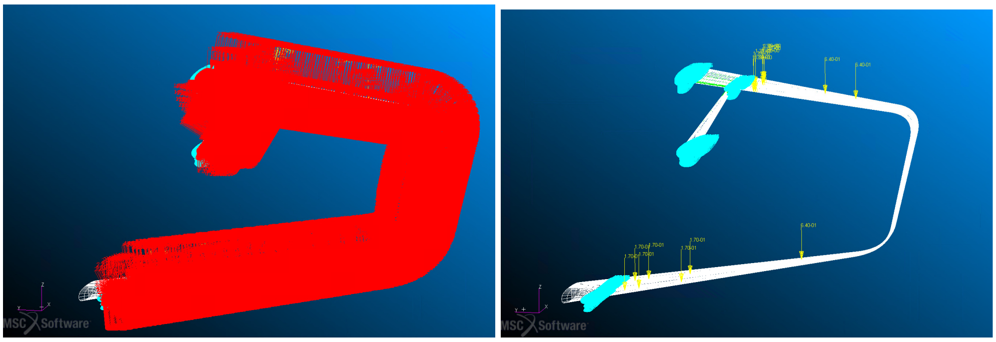

(a) Aerodynamic load distribution. **(b)** Equipment loads modelled as points load.

Figure 6.12: Visualization of loads and BCs in the created input file for the Prandtl-Plane SM in Patran graphical user interface.

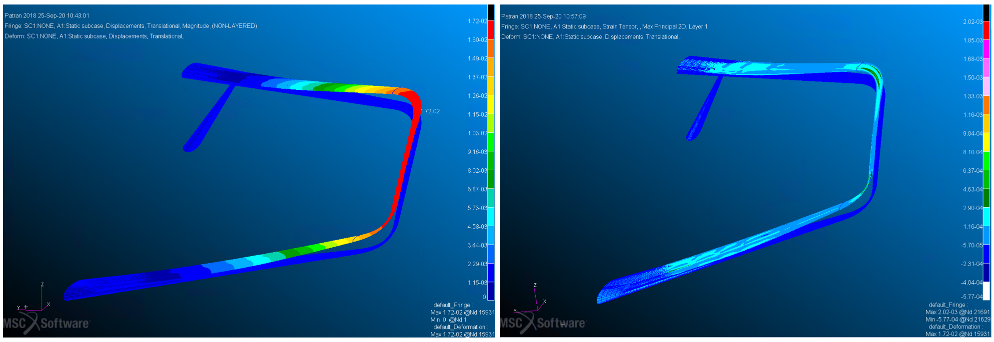

(a) Example of maximum displacement plot. Resulting in 1.72cm deflection with nr_{ply}=4. **(b)** Example of maximum 2D principal strain. Resulting in 2020μ strain with nr_{ply}=4.

Figure 6.13: Prandtl-plane SM $n = 0.056$ displacement and strain plots for a load factor of 5g.

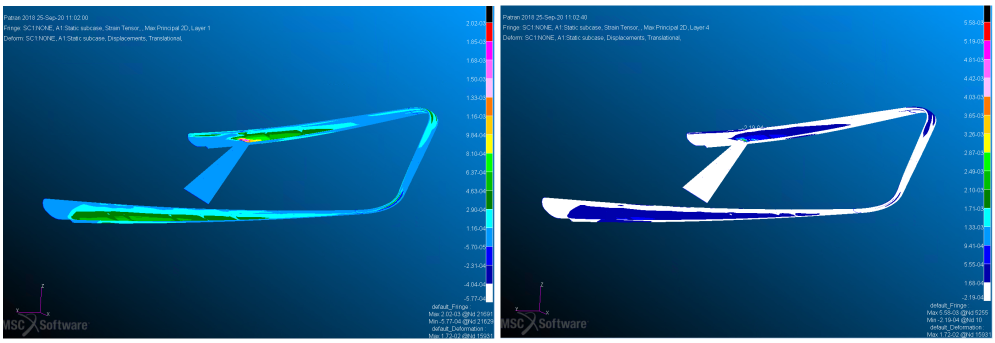

(a) Bottom view maximum 2D principal strain of the first layer. **(b)** Bottom view maximum 2D principal strain of the fourth layer.

Figure 6.14: Prandtl-plane SM $n = 0.056$ scale size with 4 plies at the top and bottom of the skin.

strain values than the maximum value. The connector seems more loaded in the top corner, but the area where the strain seems to be highest is at the bottom skin where the fin and rear wing intersect. The resulting stresses at this region might eventually trigger laminate delamination for even higher load cases, as the strength of the matrix material is substantially smaller than the in-plane strength of layers. Even in a laminate with constant thickness the stresses usually change in different layers due to the different ply angles. Therefore, usually one or a few layers reach their limiting strength earlier than the other layers. Failure prediction based on the failure of the first ply is referred to as first ply failure. After first ply failure has happened, the unfailed layers of the laminate may be able to carry at least a portion of the first ply failure load in a stable condition. As the applied load is increased, the failure progresses from one layer to the next layer, this is usually called progressive failure. Ply stresses and strains in the material directions are functions of the ply angles and therefore the failure envelope depends on the ply angle.

Figure 6.14 shows a bottom view of the maximum 2D principal strains for the first layer and fourth layer. As can be seen from the plot for the first layer, in which the fibers are oriented in the $0deg$ direction (basically the wing span), the layer is highly loaded. While the fourth layer, in which the fibers are oriented in the $90deg$ direction (basically the chordwise direction) shows minimum strain for most parts of the wing. If the strain value should be lowered in some parts of the wing, with the help of the implemented methodology inside the DEE the fiber orientation can be rapidly changed or some extra ribs can be added at the section close to the region where the fin and rear wing intersect. This allows the possibility of studying a large design space for SM in a shorter time in the preliminary design stages.

7 RESULTS

In the previous chapters an appropriate methodology is identified and developed to design the structural components of SM, position COTS components and estimate the mass, inertia and the associated CG of SM. Secondly, the structural analysis capabilities to run (critical) loadcases in a short time were developed and analyzed. The result can be used to ensure that the structure does not fail in flight under critical load conditions for a structural configuration and scale size and indicate if the structure can meet the structural requirements. If this is the case the weight & balance properties can directly be used, if not it might be considered to use different materials or a different internal structure.

As becomes clear adjustments of the structure layout and repeated meshing and FE property loading are needed in each iteration. A KBE approach is used to automate these task. Therefore the preparation of an automatic input file for MSC Nastran allows to consider structural trade studies for different internal configurations and any size scale. As the critical load case or the scale factor increases it is more likely that at some point also the rib pitch or the material properties need to change in order to meet the structural requirements. The required adaptations to the design will change the weight & balance properties of the model, and ultimately the S&C behaviour, see Figure 7.1.

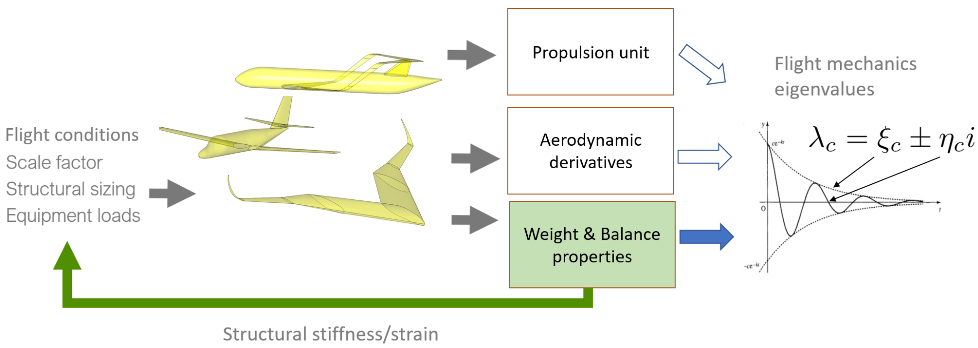

Figure 7.1: Design changes due to structural analysis results and impact on flight mechanics eigenvalues from a weight & balance perspective.

7.1 CASE STUDY 1: CESSNA CITATION II SMs

The citation II is chosen to demonstrate the concept because this full-scale aircraft is co-owned by the TUD and an aerodynamic and weight & balance database does also exist for this full-scale aircraft, therefore also the full-scale eigenvalues are known. The effect of scale sizes and design variables on the mass and inertia is analyzed in Sections 7.1.1 and 7.1.2. The effect of scale size and internal structural configuration on the displacement and strain in Sections 7.1.3 and 7.1.4. Finally, a comparison between the eigenvalues of the Citation FD and SD is given in Section 7.1.5.

7.1.1 Effect of scale size and design variables on the mass

Figures 7.2, 7.3, 7.4 show the effect of mass increase, by changing a design variable, for different SM scale sizes of the Cessna Citation II. The design variables chosen in this study are the number of plies for the skins, the material mass resin fraction and the rib and frame pitch. It should be mentioned that any realistic number for the material properties or mass for the equipment can be given as input. However, in this study the equipment and material properties as defined in Chapter 6 in Tables 6.1 and 6.2 are used respectively. This refers to the same equipment and material that is used as in the real-built Flying V. Moreover, some ballast mass can be added to the SM to change the mass properties.

The horizontal line in the mass graph indicates the constraint for the mass to not exceed the 25kg. This can be the results of regulations by the authorities of the country in which the SFT is performed.

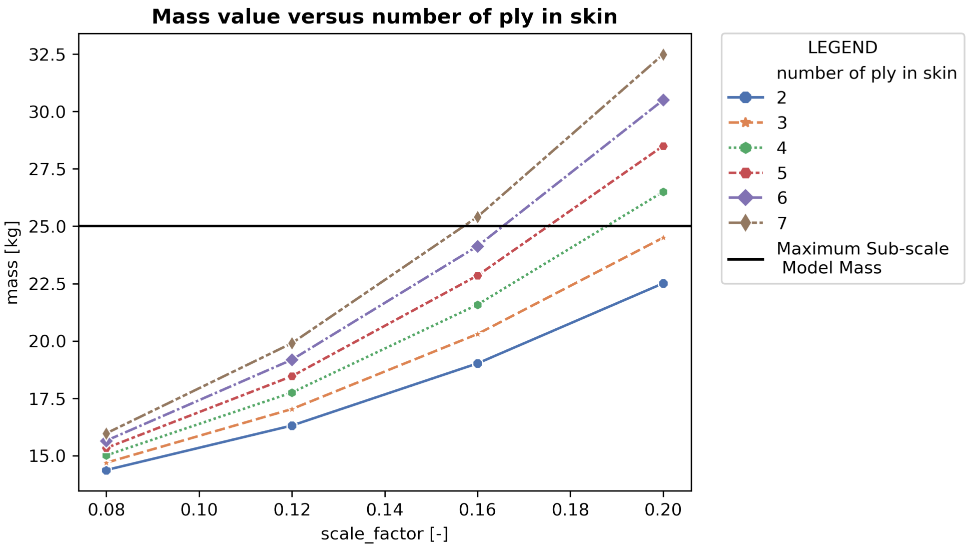

Figure 7.2: Mass for increasing scale size and different number of plies of the Citation II.

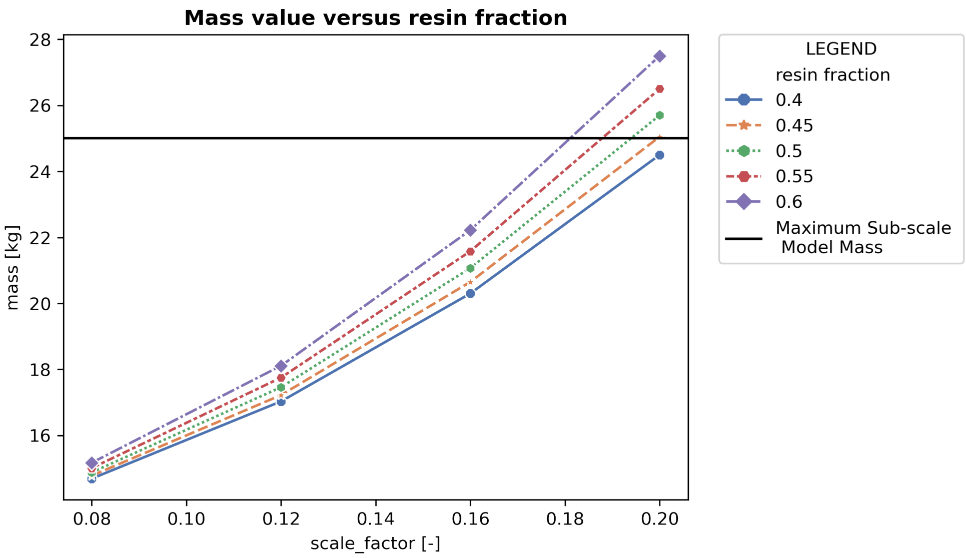

Figure 7.3: Mass for increasing scale size and different material mass resin fractions of the Citation II.

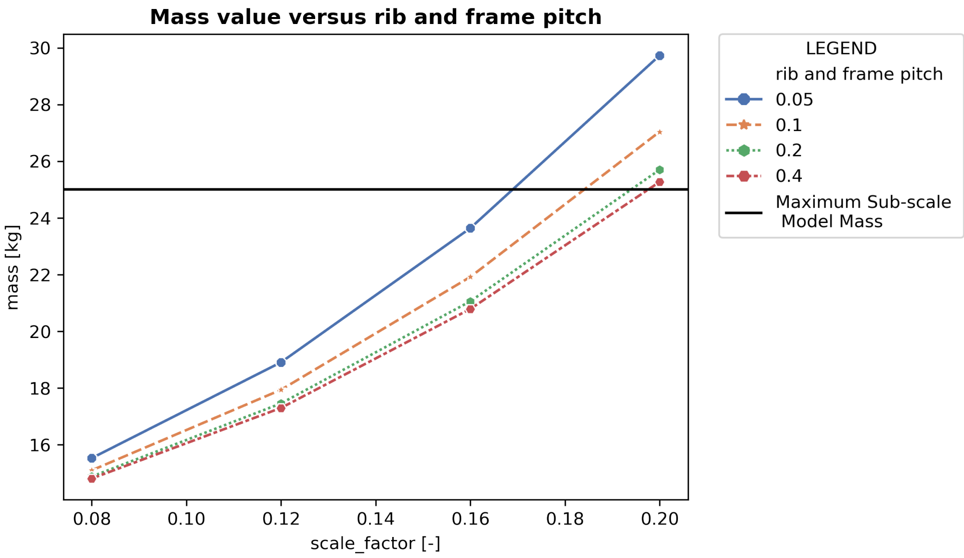

Figure 7.4: Mass for increasing scale size and different rib and frame pitch of the Citation II.

7.1.2 Effect of scale size and design variables on the inertia

Figures 7.5, 7.6, 7.7 show the effect of inertia I_{xx}, I_{yy} and I_{zz} increase, by changing a design variable, for different SM scale sizes of the Cessna Citation II. The design variables are the same as for the mass: the number of plies for the skins, the material mass resin fraction and the rib and frame pitch.

Table 7.1 gives an overview for some scale sizes of the SM model to show the CG for that configuration. The number of ply used for the structural elements in that case is equal to four and the resin mass fraction 55%.

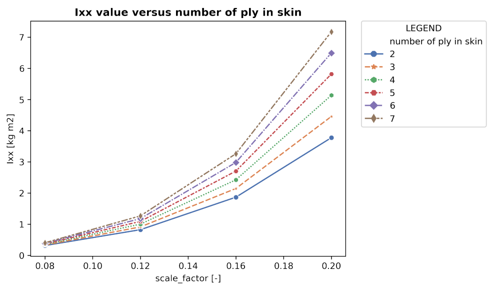

(a) I_{xx} for number of ply.

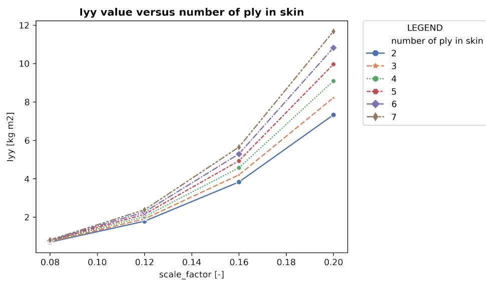

(b) I_{yy} for number of ply.

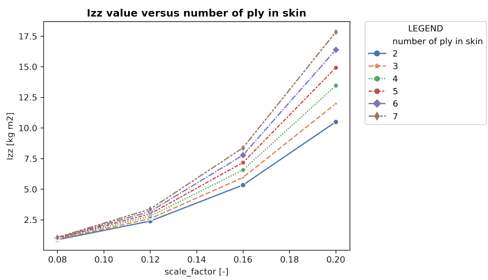

(c) I_{zz} for number of ply.

Figure 7.5: Inertia for increasing scale size and different number of ply of the Cessna Citation II SM.

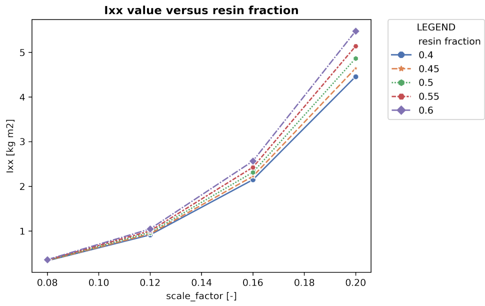

(a) I_{xx} for resin mass fraction.

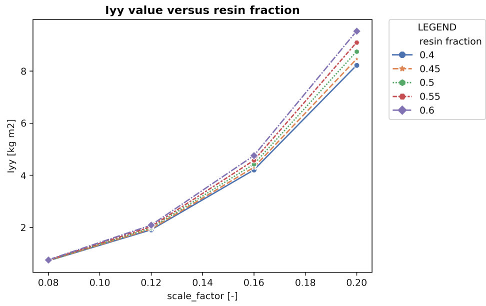

(b) I_{yy} for resin mass fraction.

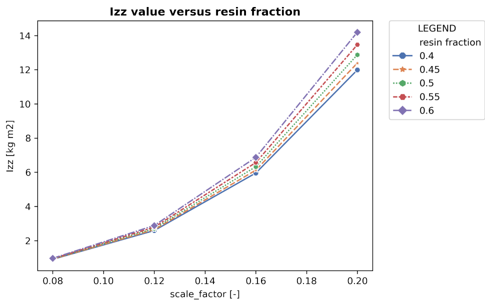

(c) I_{zz} for resin mass fraction.

Figure 7.6: Inertia for increasing scale size and different material mass resin fractions for the skin of the Cessna Citation II SM.

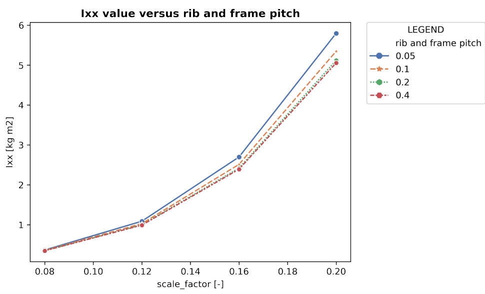

(a) I_{xx} for rib and frame pitch.

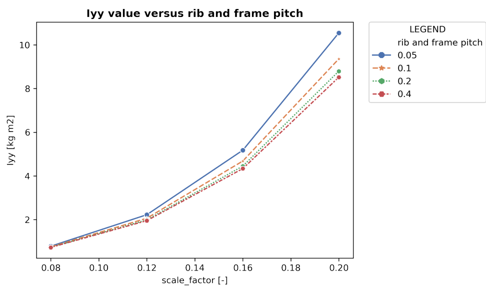

(b) I_{yy} for rib and frame pitch.

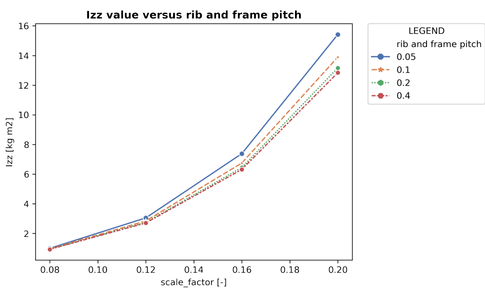

(c) I_{zz} for rib and frame pitch.

Figure 7.7: Inertia for increasing scale size and different rib and frame pitch of the Cessna Citation II SM.

Table 7.1: Mass, Inertia and CG for some scale sizes of the Citation II SM

	Cessna Citation II model		
Physics based estimation	8.8%	13.2%	17.6%
Mass [kg]	15.35	18.53	22.96
Inertia [kg m2]			
Ixx	0.22	1.26	3.11
Iyy	0.91	1.03	5.95
Izz	1.18	3.57	8.55
Center of gravity [m]			
x	0.61	0.93	1.27
y	-0.0008	-0.001	-0.001
z	0.041	0.079	0.119

7.1.3 Effect of scale size on the structural displacement and strain

As was explained at the beginning of this chapter, correct aerodynamic load mapping and generation of the input file for structural analysis in MSC Nastran is important. It is shown that the load mapping error is in most cases lower than 6% and also the generated input file for MSC Nastran was checked in the Patran interface. The influence of different scale factors, plies, internal structure and load cases on the displacement and 2D maximum principal strain can also be checked. The main wing of the Citation II has been selected to show the effect of the different design variables on the maximum displacement and 2D principal strain. Aerodynamic loads will be highest on this wing and expected more critical than for example the horizontal wing, but also all other wing can be checked with the sample principle.

Figure 7.8 shows the effect of selecting a scale factor for the FD the Cessna Citation II (15.92m) for scale sizes $n = 0.12$ (1.92m), $n = 0.16$ (2.56m) and $n = 0.20$ (3.2m) with the wingspan in between brackets. For the current case the increase of wing span and therefore also the aerodynamic loads increase the displacement by less than $1mm$ when more than 4 plies are used in the wing skin and with $4mm$ if 3 plies are used. Having 4 plies in the wing skin for a scale size of 16% results in a displacement of $7mm$ and when having 3 plies in $13mm$.

The same pattern can be noticed for the maximum 2D principal strain. In case the wing skin has 3 plies of fibers the effect of scale factor on the maximum 2D principal strain decreases with 200μ from 700μ strain at $n = 0.12$ to 500μ strain at $n = 0.2$. Having 4 plies the the maximum 2D principal strain decreases with 100μ strain in the same range of scale size. For both the displacement and maximum 2D principal strain it seems that the number of ply and the corresponding orientation has a larger effect on the displacement than the scale factor. Talking about units in mm for the displacement is very small and also the maximum 2D principal strain is a factor 5 to 10 below the adviced allowable for strain of 3500μ strain.

7.1.4 Effect of internal structure and load factor on the structural displacement and strain

The 16% scale size of the Citation II (wing span of 2.56m) has been chosen to analyze the effect of load cases and different internal structure. Three different load cases are considered, a symmetric 1g and symmetric 2.5g and 5g pull-up manoeuvre, see Tables 6.4, 6.5 and 6.6. Four different cases of internal structures have been analyzed: one assuming a full-monocoque structure where only the wing carries the aerodynamic loads, another where only 2 spars are used with no ribs, one with only 4 ribs and no spars and the last one having 2 spars and 4 ribs. For all these 4 different internal configurations also the number of skin plies has been modified

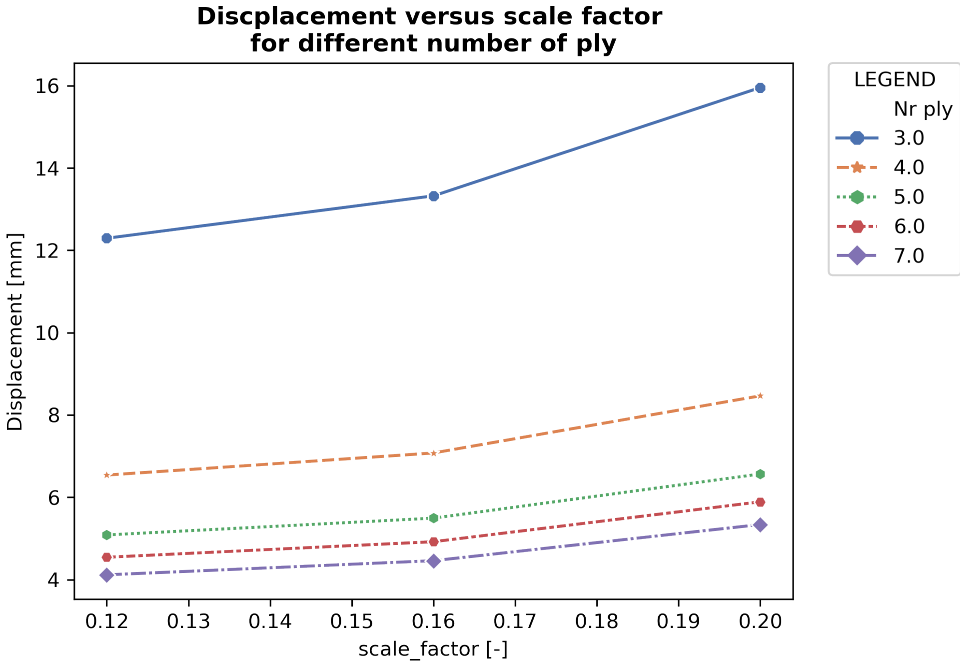

(a) Maximum displacement.

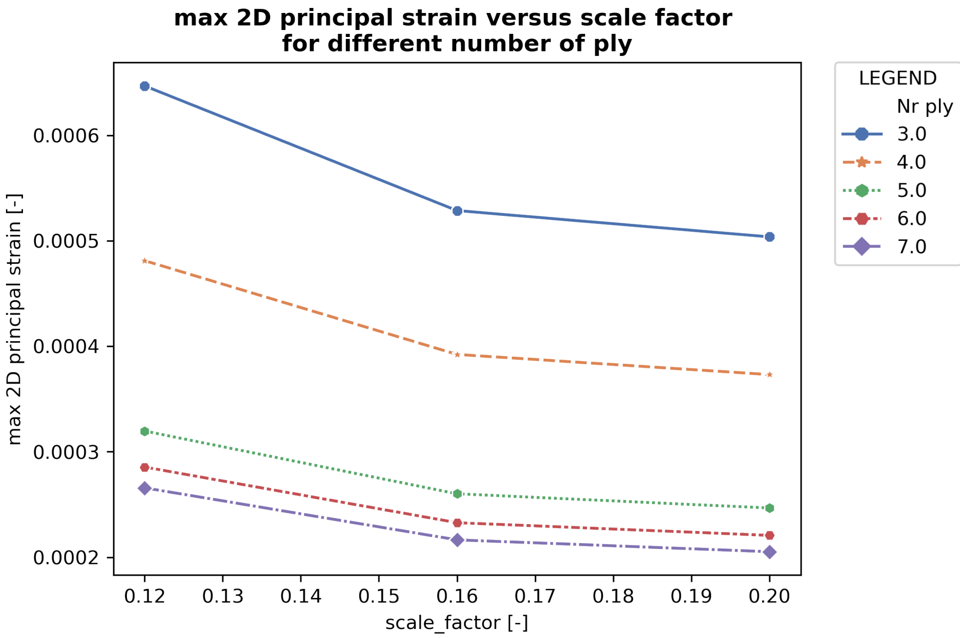

(b) 2D principal strain.

Figure 7.8: Example showing the influence of scale size for different number of ply for FD Citation II ($n_z = 2.5$).

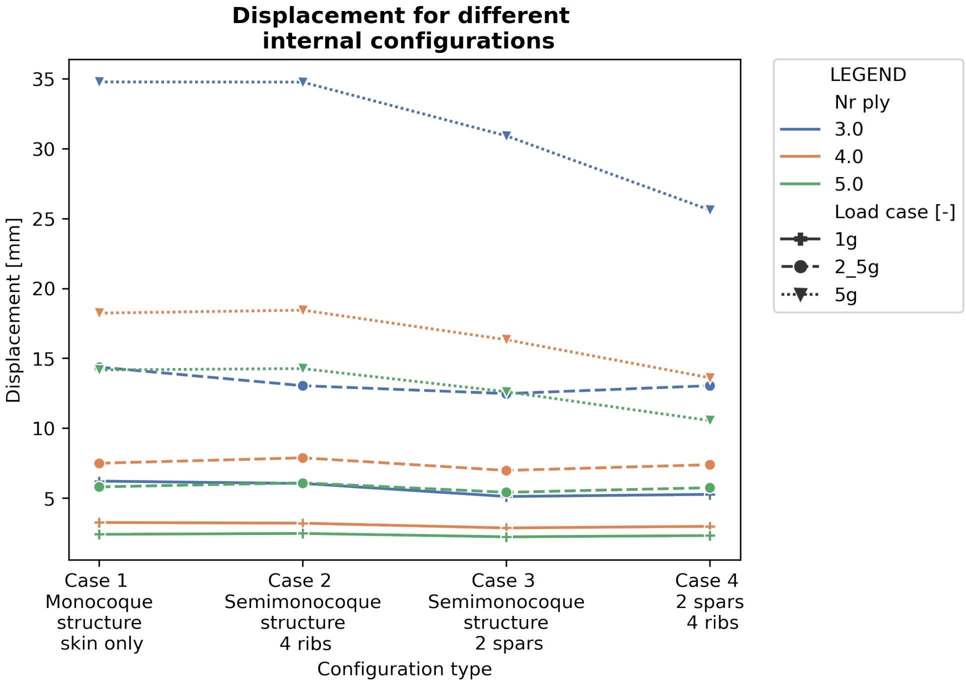

(a) Maximum displacement.

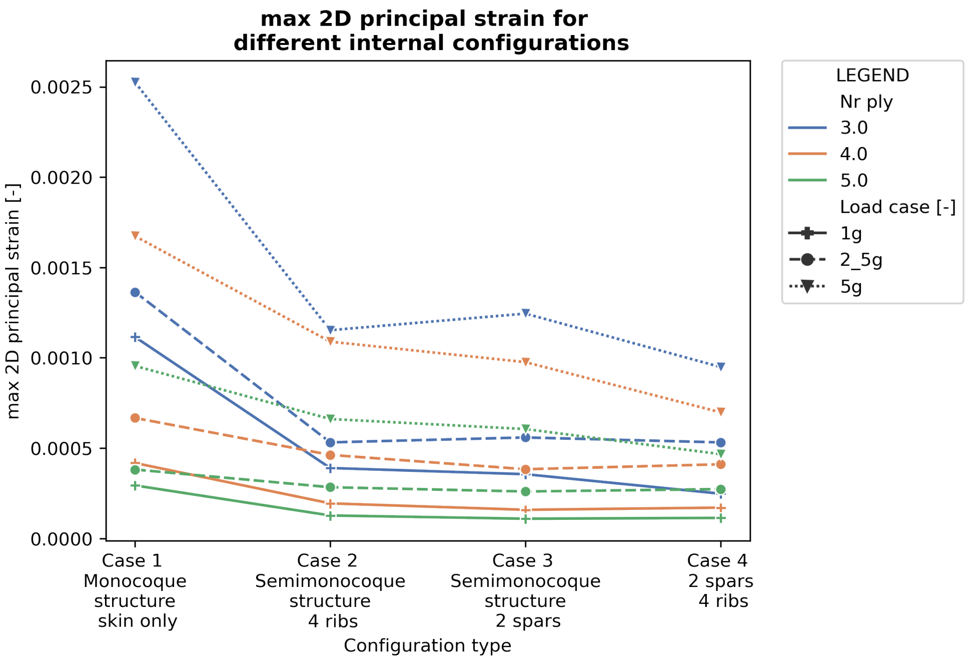

(b) Maximum 2D principal strain.

Figure 7.9: Example of a 16% scale size of the FD Citation II.

ranging from three to five plies oriented as shown in Table 6.2.

As can be seen from Figure 7.9 the displacement is generally not much influenced by the internal structure adding ribs or spars. This could be explained by the fact that the wing span is small compared to wing spans of full-scale models and therefore the spars and ribs have very small effect on the displacement as the skin carries already most of the loads. Therefore for this specific SM case the assumption can be made on a monocoque structure, where the loads are mainly supported through the skin, and where spars and ribs assist in additional stiffness. Ribs and spars might still be needed to simply transfer equipment loads, such as the engine. For the 5g load case with three plies in the wing skin the difference in maximum displacement between a wing having no ribs and spars and one having 4 ribs and spars is almost $1cm$. This could be explained by the fact for higher load case the loads acting on the structure are not only taken by the skin but also transferred to ribs and spars. As can also be seen is that the load case has larger effect on the displacement: analyzing the wing for a 1g load case with three plies at the top and bottom skin seems to result in the same deflection as for a 2.5g load case with 5 plies. And also a 5g load case with 5 plies shows almost similar displacement as compared to a 2.5g load case with three plies. In case the 5g load case is the critical condition and three plies are used in the wing skin the maximum displacement will be $2.5cm$ if the structure consists of 2 spars and 4 ribs. If for the same configuration and load case an extra ply is used in the structure this will decrease the maximum deflection with $1cm$. The effect of load case and internal structure on the maximum 2D principal strain is analyzed and can also be seen in Figure 7.9. For increasing load factor the effect of internal structure on the strain seems to be more significant. For example, considering a 5g load case with four plies and a monocoque structure results in 1700μ and decreases to 800μ in case the wing has 4 ribs and 2 spars. For the 1g and 2.5g load cases the effect of internal structure has less effect on the maximum 2D principal strain.

For some flight manoeuvres even higher load cases must be considered and the structural results can be generated and analyzed in minutes. Combining the results for all different design variables leads to the conclusion that for the citation II SM main wing the load factor is mostly affecting the displacement regarding stiffness constraints and strain regarding strength constraints. The effect of internal structure becomes more important as the load factor increases as the higher loads acting on the skin will be transferred to the internal structure. The material properties or internal structure can be easily modified until the results satisfy the constraints for the motion to be studied.

7.1.5 Comparison of eigenvalues between FD and SD

The following examples of typical aircraft motions show that the flight mechanics behaviour are affected by both the aerodynamic derivatives, propulsion unit and the weight & balance properties of the FD and SD model. The aircraft may experience several types of motion due to an elevator or rudder input. From the full-state-space matrix, which is a fourth order system, the two characteristic longitudinal eigenmotions: the short period and the phugoid can be derived for both the full-scale and the sub-scale aircraft model. The same can be derived for the lateral linear systems and its corresponding eigenvalues (typically three). The slow mode corresponds to the spiral mode, fast mode normally to the aperiodic roll and a oscillatory motion being the Dutch roll. The eigenvalues contain the information of the

Table 7.2: Overview of aerodynamic derivatives of full-scale Citation II and derivatives used in the study of SM to calculate the eigenvalues.

Cma	-0.56	**Czu**	-0.37	**Cyb**	-0.35	**Clda**	-0.230
Cmde	-1.86	**Cza**	-5.74	**Cyp**	-0.03	**Cldr**	0.034
CLa	4.73	**Czad**	-0.0035	**Cyr**	0.85	**Cnb**	0.05
Cxu	-0.028	**Czq**	-5.7	**Cyda**	-0.04	**Cnp**	-0.06
Cxa	-0.48	**Czde**	-0.69	**Cydr**	0.23	**Cnr**	-0.1
Cxad	0.083	**Cmu**	0.07	**Clb**	-0.10	**Cnda**	-0.012
Cxq	-0.28	**Cmad**	0.17	**Clp**	**-0.91**	**Cndr**	-0.094
Cxde	-0.037	**Cmq**	-8.79	**Clr**	**0.24**		

motion expressed as the damping ratio and natural frequency of the eigenmotions, see equation 7.1.

$$\lambda_c = \xi_c + -\eta_c i \tag{7.1}$$

In the DOE it is assumed that the aerodynamic behavior of the FD and SD are the same and the models are trimmed and statically stable around the center of gravity. The trim conditions for the SM can be studied with a higher-fidelity flight mechanics tool PHALANX now that the weight & balance properties can be calculated. However, this is left out in the current work and the assumption is made that the models are trimmed around the center of gravity. Moreover, the same aerodynamic derivatives are used regardsless of their scale size. The DOE then gives insight in selecting the scale size for a given configuration from only a weight & balance perspective. In reality the aerodynamic derivatives will change as the size scale changes, but the model can for example be aerodynamically scaled to result in the same aerodynamic derivatives. The aerodynamic derivatives used in the analysis for both the full-scale and sub-scale are summarized in Table 7.2.

Figures 7.10, 7.11 and 7.12 show the results of mass increase and scale size selection on the damping and frequency part of the eigenvalue. The purple band indicates the domain for equivalence of the damping between the SM and FD, while the blue band indicates the equivalance of the frequency between the SM and FD. It should also be noted that the mass increase in this study is a result of changing the scale factor and the number of plies, but to affect the mass distribution also concentrated masses from equipment can be moved around in the SM or use some ballast weight.

Short period motion

When considering for example the short period, this motion is a rather fast motion. When having an elevator input for example, the aircraft quickly pitches up and down, however airspeed hardly varies during this motion. The I_{yy} value has high influence on this motion, as the motion damps out very quickly (if stable).

$$\begin{bmatrix} C_{Z_\alpha} + (C_{Z_{\dot\alpha}} - 2\mu_c)D_c & C_{Z_q} + 2\mu_c \\ C_{m_\alpha} + C_{M_{\dot\alpha}} D_c & C_{m_q} - 2\mu_c K_Y^2 D_c \end{bmatrix} \begin{bmatrix} \alpha \\ \frac{q\bar{c}}{V} \end{bmatrix} = \vec{0} \tag{7.2}$$

In the matrix the terms C_{Z_α}, C_{m_α} are the static aerodynamic derivatives and can be measured with wind tunnel tests. These derivatives are strongly influenced by the Reynolds number. $C_{Z_{\dot\alpha}}$, $C_{m_{\dot\alpha}}$, C_{Z_q}, C_{m_q} are the dynamic aerodynamic derivatives and are strongly dependent on the Froude number. The terms μ_c and K_Y^2 are mass and inertia derivatives and show the mass effects.

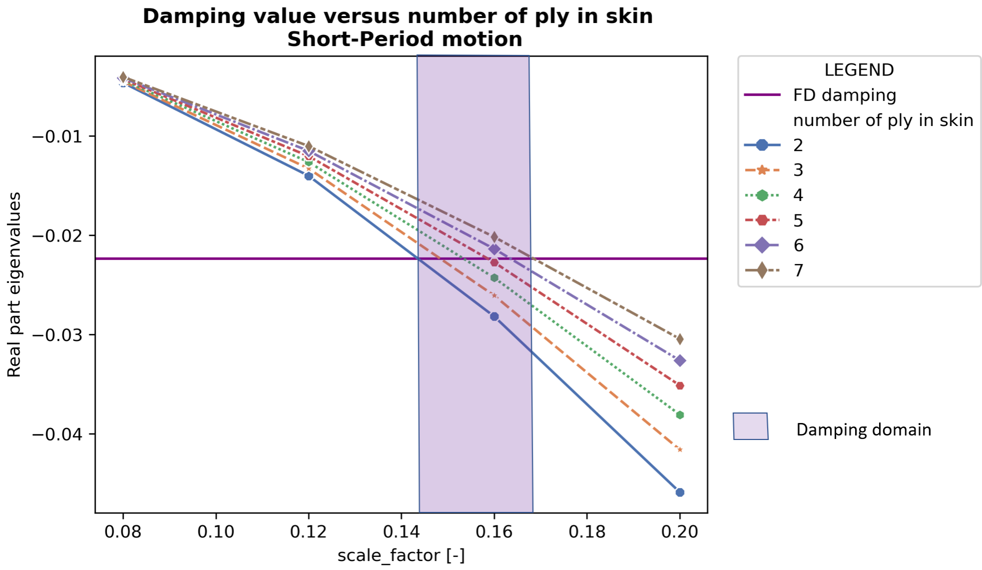

(a) The purple band indicates the domain for equivalence of damping domain between SM and FD.

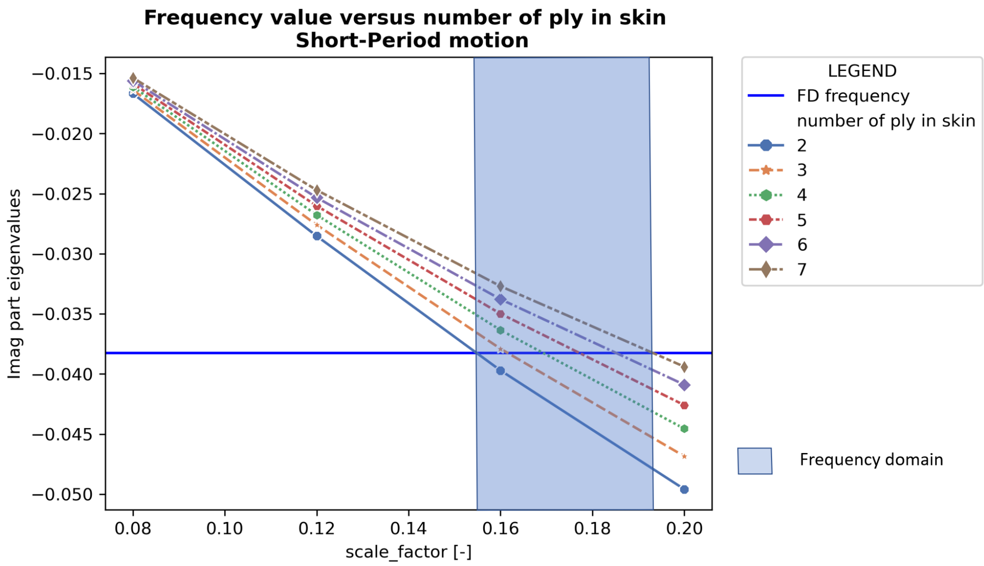

(b) The blue band the frequency domain of the eigenvalue.

Figure 7.10: DOE results for the short-period motion on the effect of mass (by using different amount of plies in the skin) and the scale size on the damping and frequency part of the eigenvalue for a FD Citation II.

From Figure 7.10 it can be seen that for the short period motion with its current configuration of structure and equipment a scale factor in between 14.5% and 17% should be selected to have similarity for the damping value between the FD and SM for the short-period motion. However if one should chose a design having similarity of the frequency and thus the period of the motion, a scale between 15.5% and 19% of FD and SM should be selected.

Phugoid motion

The phugoid motion is a lateral, periodical oscillation resulting from a step input on the elevator. First the airplane pitches up. It starts to climb, losing speed and thus lift. Because of that it pitches down again, builds up speed, lift increases and it pitches up again, starting all over. The most important parameters that vary are airspeed and pitch. The phugoid, if stable, damps out only after quite a long time, therefore it is also called long period motion.

$$\begin{bmatrix} C_{X_u} - (2\mu_c D_c) & C_{Z_0} & 0 \\ C_{Z_u} & 0 & 2\mu_c \\ 0 & -D_c & 1 \end{bmatrix} \begin{bmatrix} \hat{u} \\ \theta \\ \frac{q\bar{c}}{V} \end{bmatrix} = \vec{0} \tag{7.3}$$

In the matrix the terms C_{Z_0} and C_{Z_u} are the dynamic aerodynamic derivatives. The term μ_c is the mass derivative and shows the mass effects. But also the thrust coefficient C_{x_u} affects the motion for example. Regarding the phugoid motion it appears that high scale factors or high mass SM are needed in order to have similarity between FD and SM, see Figure 7.11. With the current weight & balance properties that is not possible for both the damping and frequency value from a weight & balance perspective. It would be interesting to investigate the effect of aerodynamic scaling to see the effect on the eigenvalue, but because of the time constraint of this work this is not possible.

Dutch roll motion

The Dutch roll motion is a periodic motion in which the aircraft sideslips, yaws and rolls.

$$\begin{bmatrix} C_{Y_\beta} - (2\mu_b D_b) & -4\mu_b \\ C_{n_\beta} & C_{n_r} - 4\mu_b K_Z^2 D_b \end{bmatrix} \begin{bmatrix} \beta \\ \frac{rb}{2V} \end{bmatrix} = \vec{0} \tag{7.4}$$

The asymmetric terms μ_b, K_X^2, K_Z^2 and K_{XZ} will now have influence on the motion regarding the weight & balance properties. Also the aerodynamic derivatives C_{y_b} and C_{n_r} affect the motion for example. Usually the motion is stable and will damp out after some time. The period is approximately 2s for the FD Cessna with a time to half amplitude of approximately 2.3s. The motion is initiated with an input on the rudder. For the Dutch roll motion, as can also be seen from Figure 7.12, with the same weight & balance properties as for the other motions for different scale size, a lower scale size between 12.5% and 15% can be chosen to have similarity between FD and SM for the real part of the Dutch roll. The mass or the scale size should be increased if one wants similarity of the frequency domain.

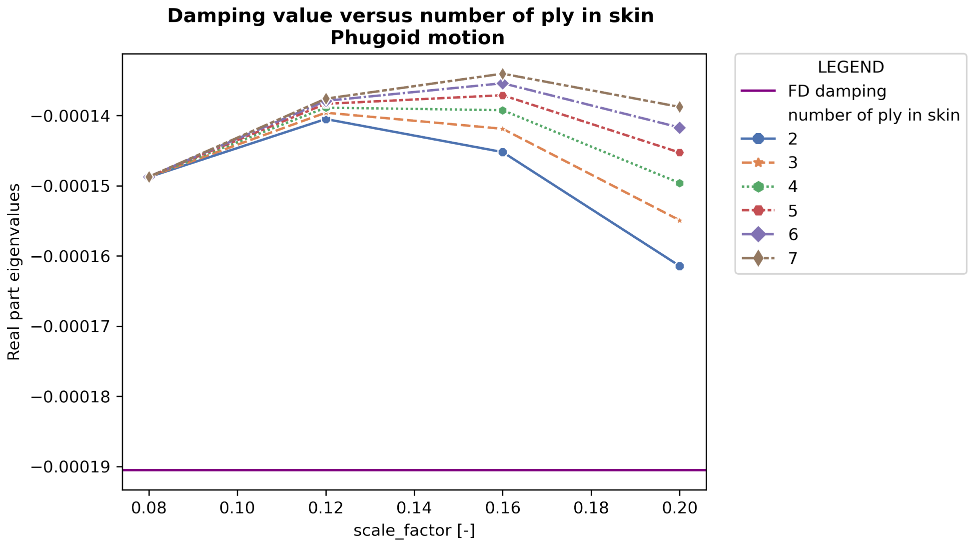

(a) Phugoid motion damping value.

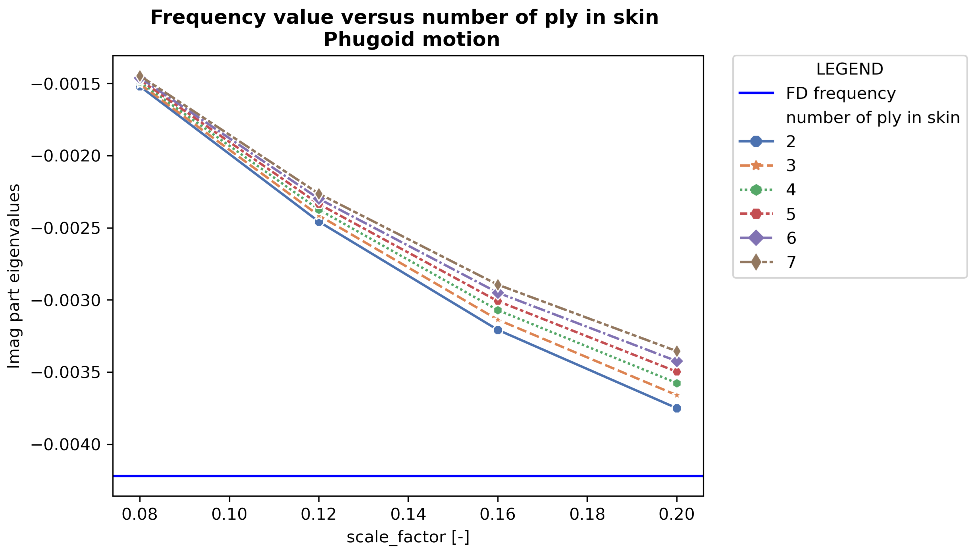

(b) Phugoid motion frequency value.

Figure 7.11: DOE results for the phugoid motion on the effect of mass (by using different amount of plies in the skin) and the scale size on the damping and frequency part of the eigenvalue for a FD Citation II.

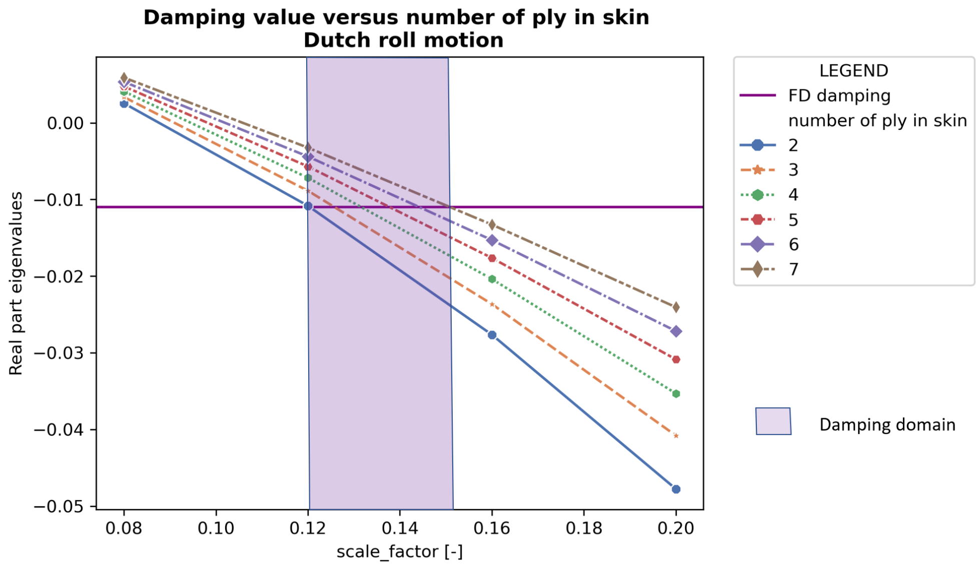

(a)

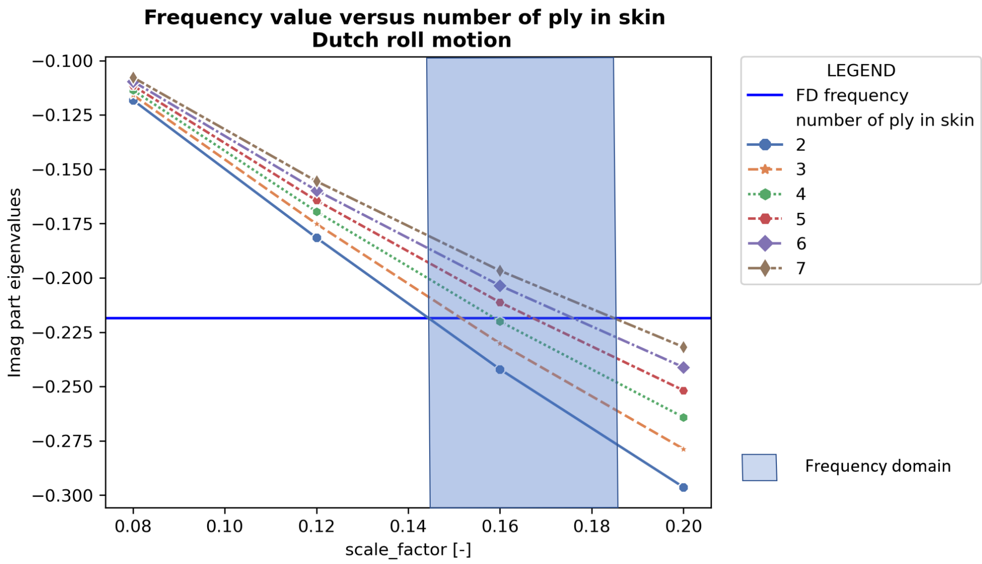

(b)

Figure 7.12: DOE results for the dutch-roll motion on the effect of mass (by using different amount of plies in the skin) and the scale size on the damping and frequency part of the eigenvalue for a FD Citation II.

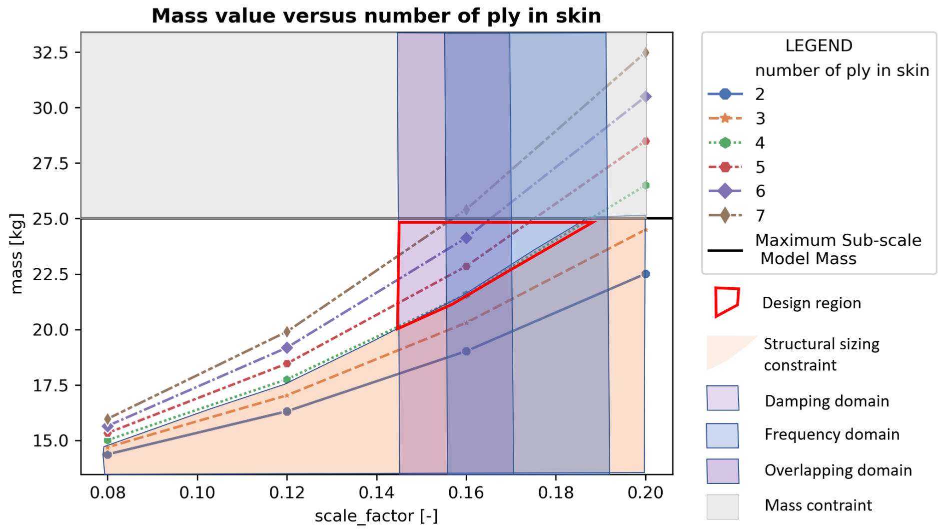

Figure 7.13: Selecting a scale size based on weight & balance properties of the SM in the design region for the short-period motion.

Design space with constraint criteria

The previous plots do not yet take into account the combined effect of selecting an SM with both the damping and frequency domain similar to the FD. Moreover, structural constraints on stiffness and strain as shown in Chapter 6 can also affect the performance of SM. Or maybe even HFQ, although not considered in this study. Taking into account that the mass of the SM can not be higher than 25kg, as a result of regulations, this can put an extra constraint to the design. Therefore it is almost impossible to test the phugoid motion for models with a lower mass than 25kg. If the constraint on maximum mass is increased to 125kg for example a larger scale size with a higher mass can be used to test the phugoid motion. For the short-period and dutch roll it is possible to reach similarity taking into account the mass constraints. If also taking into account structural sizing constraints this might lower the allowable range for the mass or scale size of the model, see Figures 7.13 and 7.14.

In this Design of Experiment (DOE) for example the limit on displacement is sufficient for a minimum of 4 plies in the skins. If the purple and blue band indicating the damping domain and frequency domain are combined, the bands can have an overlapping domain. Now, if the short-period period should be studied a scale factor of around 16% can result in similarity of the motion for both the damping as well as the frequency domain. If there is interest to study the dutch-roll motion it is clear from Figure 7.14 that a larger design area regarding the mass is possible to study the similar behaviour in the damping and the frequency domain. However, there seems little overlapping domain in which both the damping and frequency of the SM are equivalant to the FD. A 15% scale factor should be selected to test for both the damping and frequency.

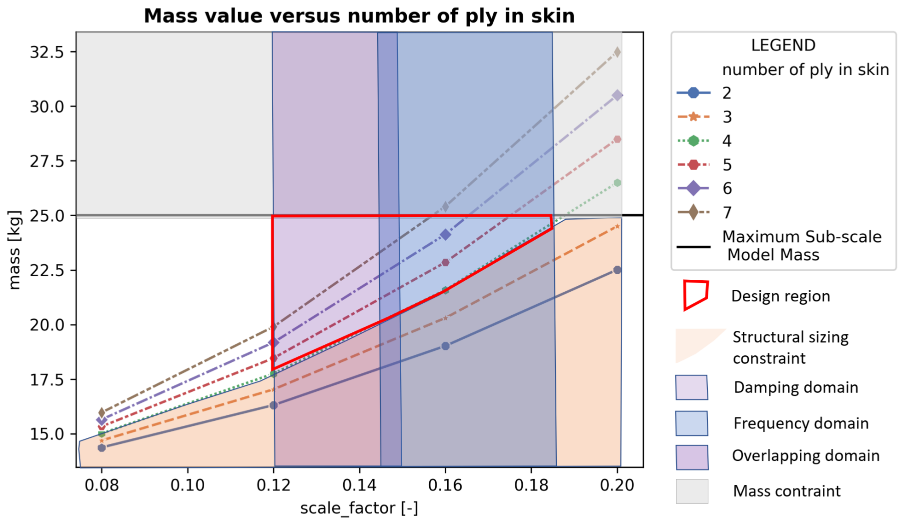

Figure 7.14: Selecting a scale size based on weight & balance properties of the SM in the design region for the dutch-roll motion.

7.2 CASE STUDY 2: FLYING V SMS

The same methodology as is done for the Citation II can be applied on the Flying V. The full-scale data to calculate the damping and frequency parts of the FD eigenvalue could not be found. Therefore in this case study only the effect of material and structure design variables on the mass and inertia are given. If reliable full-scale data is available, the methodology is the same for the Flying V regarding the scale size selection based on the eigenvalue of the FD and SM.

7.2.1 Effect of scale size and design variables on the mass

Figures 7.15, 7.16, 7.17 and 7.18 show the effect of mass increase, by changing a design variable, for different SM scale sizes of the Flying V. The design variables chosen in this study are the number of plies for the skins, the material mass resin fraction and the rib pitch. In this study also the effect of shifting a COTS component is considered. The component studied is the nose landing gear of which the mass of the nose gear is increased from 0.55kg to 0.85kg, while at the same the slightly shifted towards the front of the SM. The movement is based on parametric reference length [0.6, 0.5, 0.4, 0.3] as a fraction of the root chord length.

As expected this will slightly increase the mass by a constant value and have negligible effect on the I_{xx} inertia around the x-axis, but it affects the I_{yy} and I_{zz} inertia mostly. As can be seen from Matrix 7.4 this then can have influence on the Dutch-roll. Also, in this study the equipment and material properties as defined in Chapter 6 in Tables 6.1 and 6.2 are used respectively. The baseline scale factor of $n = 1.0$ does not refer to the FD, but refers to the SM with dimension as in Figure 6.2.

7.2.2 Effect of scale size and design variables on the inertia

Figures 7.19, 7.20, 7.21 and 7.22 show the effect of inertia I_{xx}, I_{yy} and I_{zz} increase, by changing a design variable, for different SM scale sizes of the Flying V. The design variables are the same as for the mass: the number of plies for the skins, the material mass resin fraction and the rib pitch.

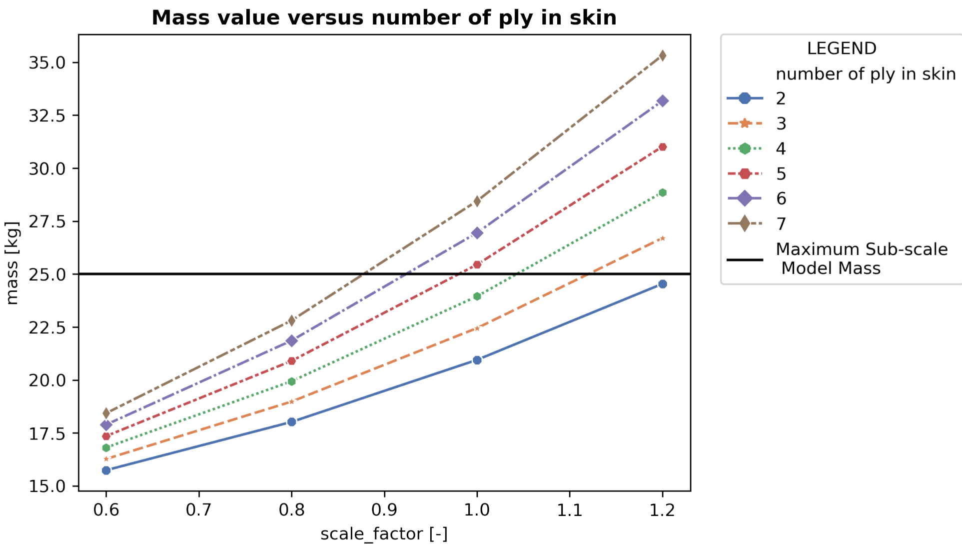

Figure 7.15: Mass for increasing scale size and different number of plies of the Flying V.

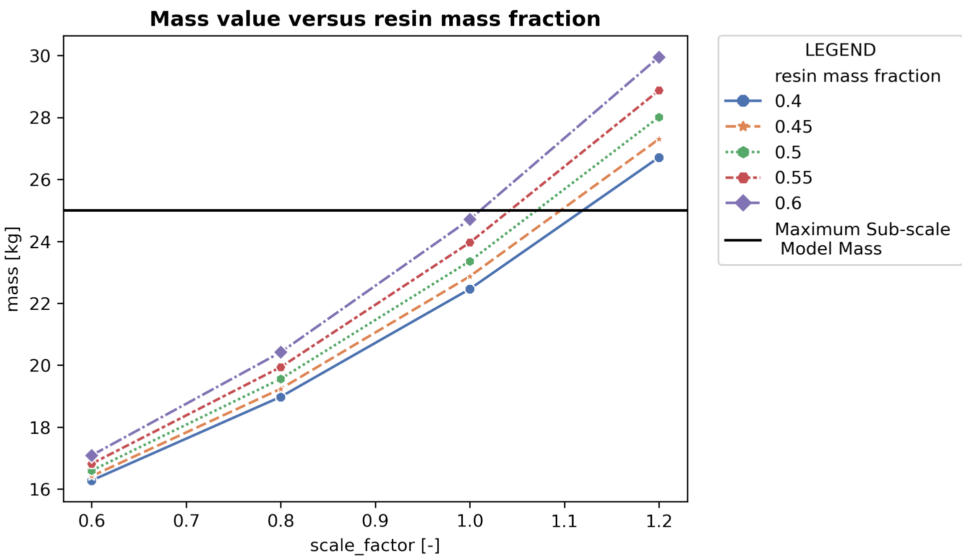

Figure 7.16: Mass for increasing scale size and different material mass resin fractions of the Flying V.

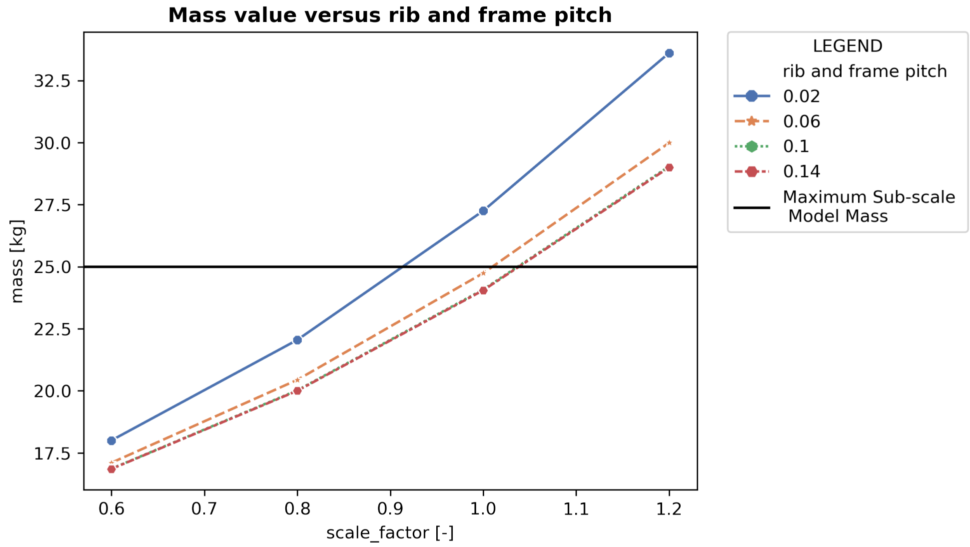

Figure 7.17: Mass for increasing scale size and different rib pitch of the Flying V.

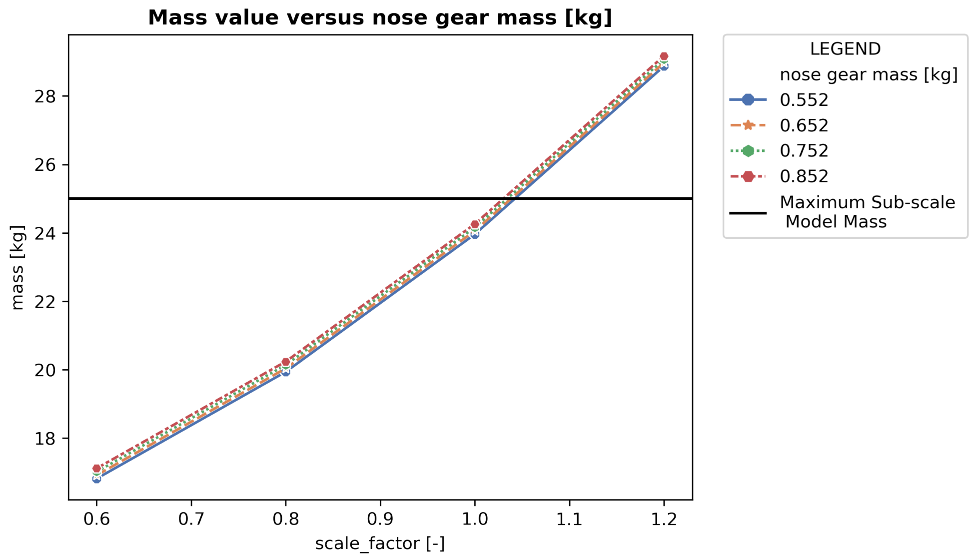

Figure 7.18: Mass for increasing scale size and landing gear mass.

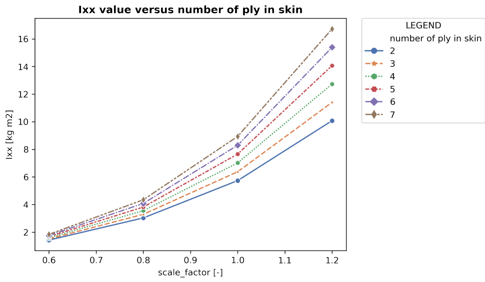

(a) I_{xx} for number of ply.

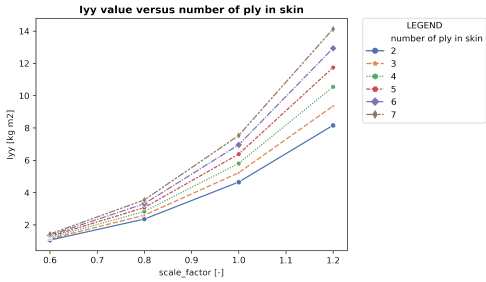

(b) I_{yy} for number of ply.

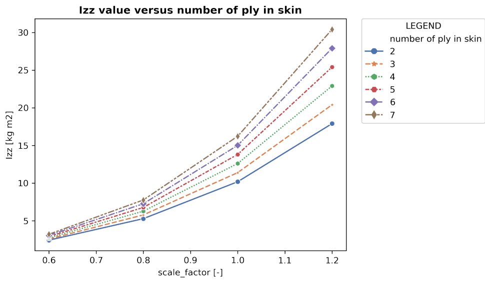

(c) I_{zz} for number of ply.

Figure 7.19: Inertia for increasing scale size and different number of ply of the Flying V SM.

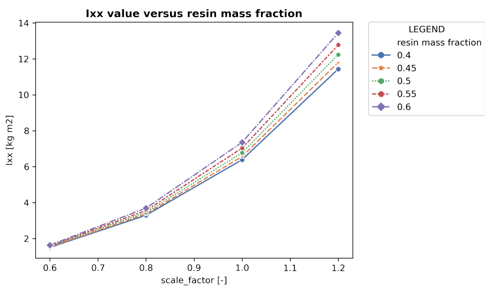

(a) I_{xx} for resin mass fraction.

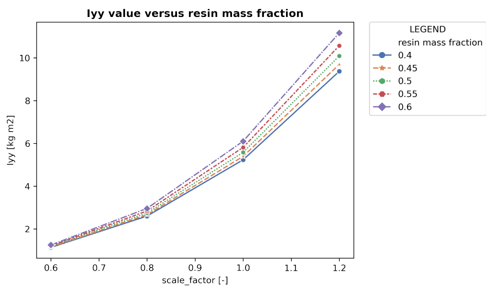

(b) I_{yy} for resin mass fraction.

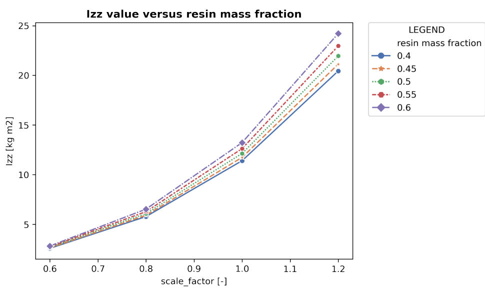

(c) I_{zz} for resin mass fraction.

Figure 7.20: Inertia for increasing scale size and different material mass resin fractions for the skin of the Flying V SM.

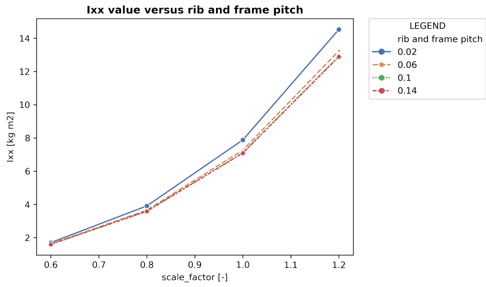

(a) I_{xx} for rib pitch.

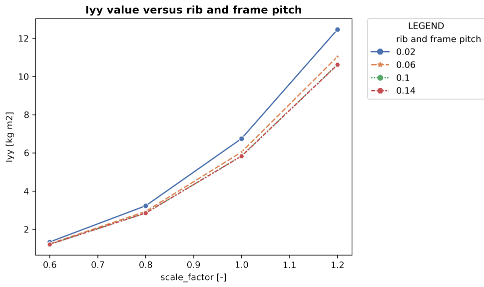

(b) I_{yy} for rib pitch.

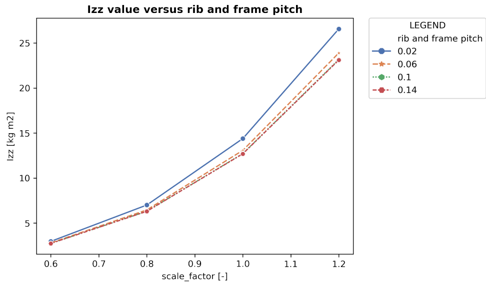

(c) I_{zz} for rib pitch.

Figure 7.21: Inertia for increasing scale size and different rib pitch of the Flying V SM.

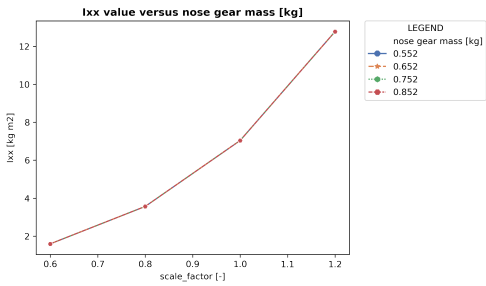

(a) I_{xx} for landing gear mass.

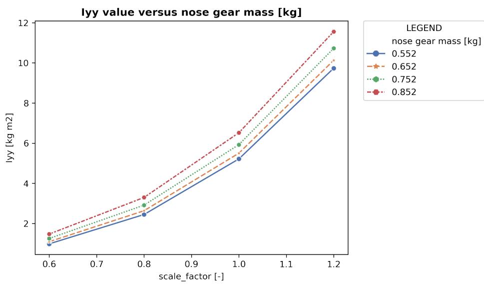

(b) I_{yy} for landing gear mass.

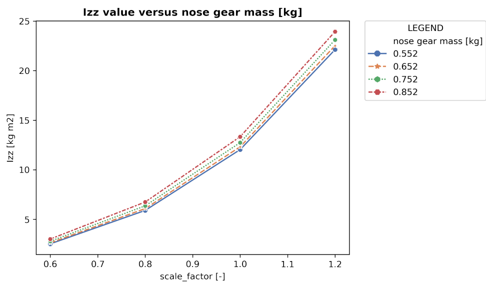

(c) I_{zz} for landing gear mass.

Figure 7.22: Inertia for increasing scale size and landing gear mass of the Flying V SM.

7.3 CASE STUDY 3: PRANDTL-PLANE SMS

The same methodology as is done for the Citation II and Flying V can be applied on the Prandtl-Plane. Realistic full-scale data to calculate the damping and frequency parts of the FD eigenvalue could not be found. Therefore in this case study only the effect of material and structure design variables on the mass and inertia are given. If reliable full-scale data is available, the methodology is the same for the Prandtl-plane regarding the scale size selection based on the eigenvalue of the FD and SM.

7.3.1 Effect of scale size and design variables on the mass

Figures 7.23, 7.24, 7.25 show the effect of mass increase, by changing a design variable, for different SM scale sizes of the Prandtl-Plane. The design variables chosen in this study are the number of plies for the skins, the material mass resin fraction and the rib and frame pitch. Also, in this study the equipment and material properties as defined in Chapter 6 in Tables 6.1 and 6.2 are used respectively.

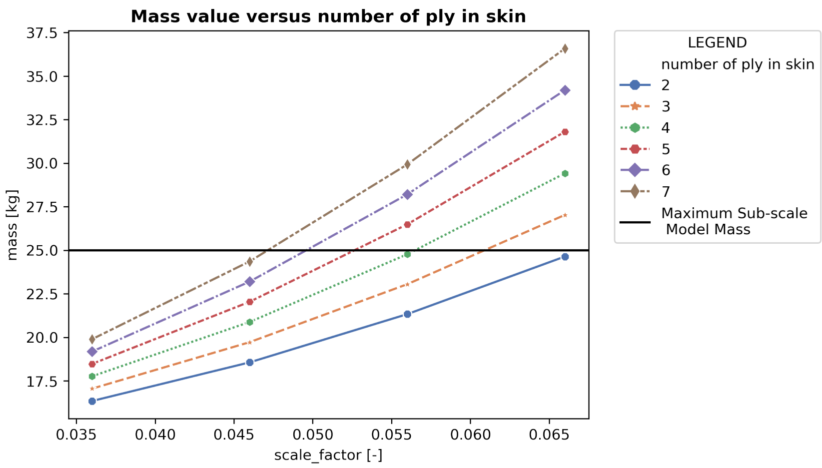

Figure 7.23: Mass for increasing scale size and different number of plies of the Prandtl-plane.

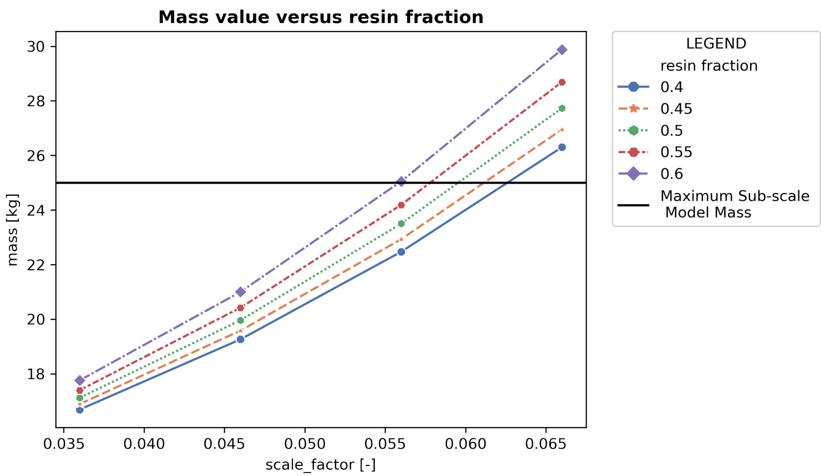

Figure 7.24: Mass for increasing scale size and different material mass resin fractions of the Prandtl-plane.

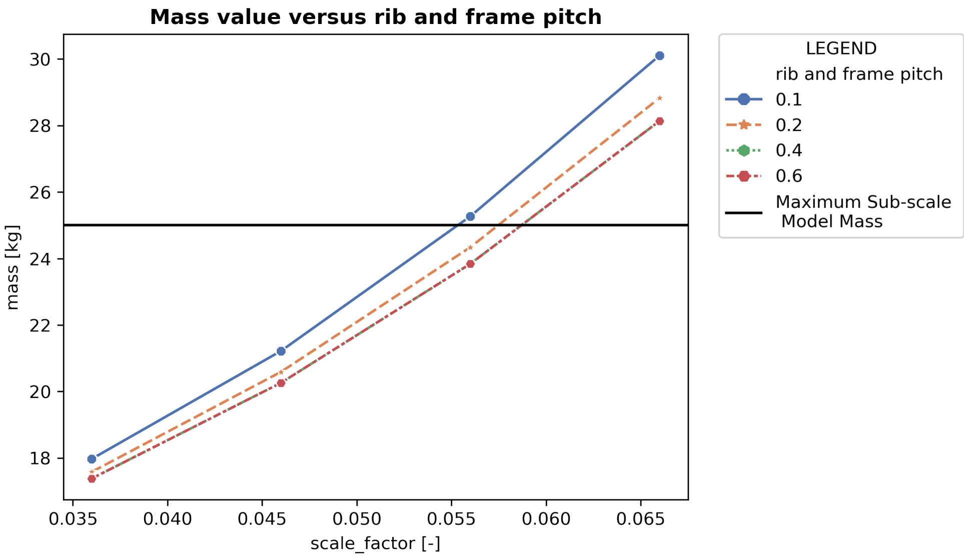

Figure 7.25: Mass for increasing scale size and different rib and frame pitch of the Prandtl-plane.

7.3.2 Effect of scale size and design variables on the inertia

Figures 7.26, 7.27, 7.28 show the effect of inertia I_{xx}, I_{yy} and I_{zz} increase, by changing a design variable, for different SM scale sizes of the Prandtl-plane. The design variables are the same as for the mass: the number of plies for the skins, the material mass resin fraction and the rib and frame pitch.

Table 7.3 gives an overview for some scale sizes of the SM model to show the CG for that configuration. The number of ply used for the structural elements in that case is equal to four. The rib and frame pitch is set to 0.2 and the resin mass fraction 55%.

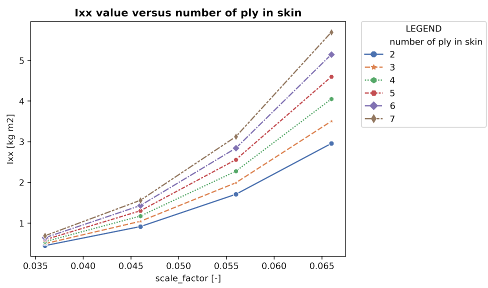

(a) I_{xx} for number of ply.

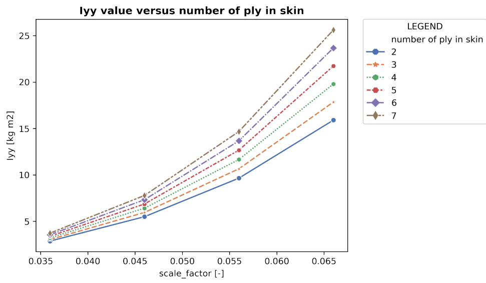

(b) I_{yy} for number of ply.

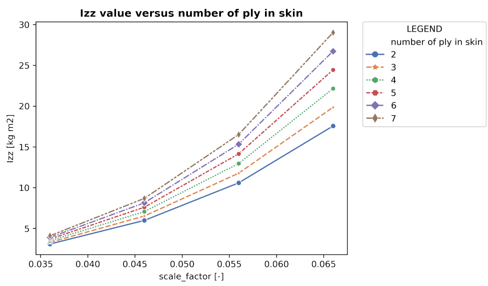

(c) I_{zz} for number of ply.

Figure 7.26: Inertia for increasing scale size and different number of ply of the Prandtl-plane SM.

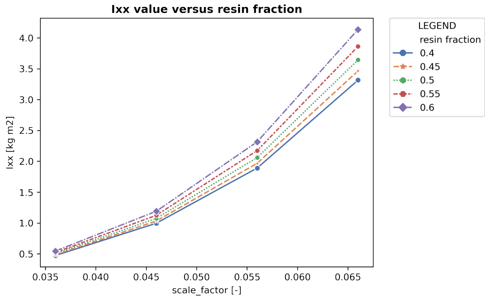

(a) I_{xx} for resin mass fraction.

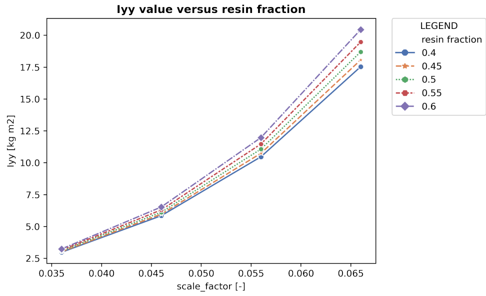

(b) I_{yy} for resin mass fraction.

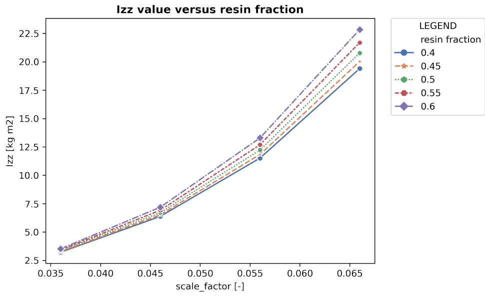

(c) I_{zz} for resin mass fraction.

Figure 7.27: Inertia for increasing scale size and different material mass resin fractions for the skin of the Prandtl-plane SM.

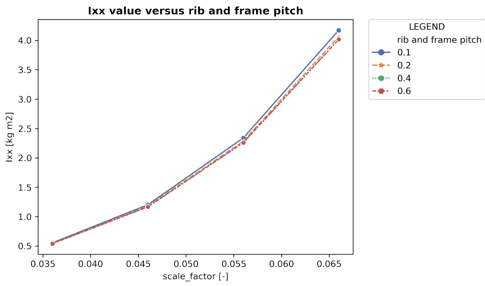

(a) I_{xx} for rib and frame pitch.

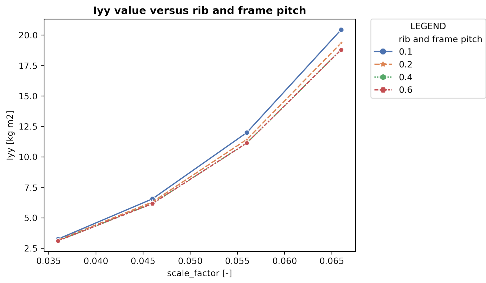

(b) I_{yy} for rib and frame pitch.

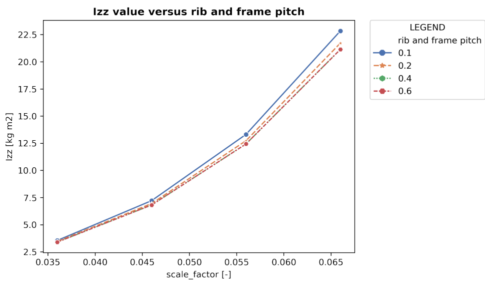

(c) I_{zz} for rib and frame pitch.

Figure 7.28: Inertia for increasing scale size and different rib and frame pitch of the Prandtl-plane SM.

Table 7.3: Mass, Inertia and CG for some scale sizes of the Prandtl-Plane SM.

	Prandtl-Plane model		
Physics based estimation	3.6%	5.6%	7.6%
Mass [kg]	17.82	24.9	35
Inertia [kg m2]			
Ixx	0.54	2.27	6.73
Iyy	3.21	11.76	32.15
Izz	3.49	13.1	36.1
Center of gravity [m]			
x	1.0	1.53	2.1
y	-0.002	-0.0023	-0.002
z	0.043	0.077	0.11

7.4 COMPUTATIONAL TIME

In order that SFT can be effective in the design process, a short design lead time is needed for SM. Therefore one important requirement of the code is that it can set up the weight & balance properties for any scale size and internal structure can be done in a matter of minutes. Besides, the automation of structural input file can aid in structural sizing. Therefore, an example of the time needed for completing the different phases is given in Table 7.4.

Table 7.4: Time required in a design loop from the generation of structure and positioning of equipment to MSC nastran analysis and post-processing.

Design process step	Time [s]
Generate the wing internal structure	5
Generate the fuselage internal structure	5
Generate the wing equipment	15
Generate the fuselage equipment	15
Calculate the model weight & balance properties	20
Fusion and Topology creation	30
Mesh creation	15
Aerodynamic analysis and load mapping	30
Write the BDF file	10
Run FEM Analysis	25
Read results with post-processing script	7
Total Time	**177**

In this table only the time that is needed for the operation in the design loop by the computer is reported. The results are given in seconds and they refer to a Citation II configuration. It is assumed that the user has spend some time to where the equipment shall be placed based on mission requirements. Once this configuration is fixed the weight & balance properties can be determined for different scales and the bdf can be created, without spending time to visualize the shape. This time result is considered sufficient with respect to the code requirements and it allows the possibility of creating sizing loops able to optimize the structure and find corresponding weight & balance properties in just minutes.

In order to make a fair comparison, the time results are compared with the generation of the weight & balance database of the real-built Flying V. Not only this weight & balance sheet is manually edited and therefore more sensitive for errors but also labour intensive. It should be mentioned that the real-built model is eventually built with a lot higher level of detail instead of the preliminary design purposes in this work. Therefore a comparison is made with the time needed to estimate the same level of detail at the preliminary design stage for just one configuration for a selected scale size. This can take more than two weeks for only one type of structural configuration of the SM. In case different types of structural configurations and scale sizes should be considered, every model should be prepared for structural analysis. This requires a lot of time to generate a database. This study shows the time gains obtained from the development of the MMG and how it can enable the efficient assessment of the weight & balance estimation for preliminary designs and preparation of structural analysis file of any given sub-scale design.

8 CONCLUSIONS AND RECOMMENDATIONS

In this chapter an overview of the completed work is provided and conclusions are drawn from the research by reflecting back on the initial research question. Moreover, recommendations are made for further research topics, and also for new developments to extend the methodology.

The aim of the research presented in this report is to apply a KBE approach to estimate the mass, CG and inertia of SM configurations and the create a methodology for automated finite element model generation for structural investigation. The methodology that is developed considers the design of structural elements and selecting and positioning of appopriate COTS components. The automated generated input file for structural analysis should ensure a stiff and safe SM structure in a preliminary design phase. The methods are set up independently from the aircraft configuration, allowing them to be employed for a study on different SM models. In this report models of the Cessna Citation II, Prandtl-Plane and the Flying V are used to demonstrate the methodology.

The research is triggered by the need for a weight & balance module for sub-scale aircraft models to be used in a larger design framework to design representative full-scale unconventional models. The flight dynamics behaviour of such unconventional configurations must be carefully evaluated by studying S&C characteristics to design a safe SM and mitigate risks in flight. The generation of structure and mesh is possible for all the lifting surfaces, any scale size and includes skins, spars, ribs, floors, bulkheads and frames. All the structural elements are not based on any reference system assumption but are automatically created according to the inputs independent of the position and the orientation of the considered wings. From the final assembly the mass, inertia and CG properties can be estimated. In order to take into account structural design requirements in the design the structural analysis steps to run (critical) loadcases are automated based on the requirement to have a short design lead time for SM. The code can interact with results from Flightstream in which flow data is coupled to probepoints on the structural mesh. The methodology showed then the ability to automatically write the input files for MSC Nastran that contain information needed to run static structural analysis. The time needed for creating the assembly with its mass properties, writing the input file, run the simulation and analyze the results of an SM is less than 3 minutes.

In order to test how well the weight & balance properties can be estimated for different SM, the estimated mass and CG is compared with the real-built flying V model. Moreover, the correctness of aerodynamic load mapping and the generated input file for MSC Nastran has been evaluated in Patran if it maintains its characteristics in the Nastran environment. Of special interest in this context is the inclusion of modelling composite material and that the load mapping let MSC Nastran receive a load case that is representative of the condition shown by Flightstream.

If the mass and inertia properties are known of the SM, the aerodynamic derivatives can be gathered from numerical simulation, wind tunnel or from real flight test and can then be used to improve the parameters in the numerical simulation to validate the model. If also similarity can be achieved between the FD and SM the results can be used for further development of SM design. In case of flight tests, Equations of Motion (EOM) are used to convert accelerations and time responses into aerodynamic derivatives using the mass and inertia properties of the designed SM. This provides a method to create multiple SMs taking into account the distribution of masses and inertia, and is necessary to predict the flight dynamics.

The currently implemented tools lead to the following research topics to be suggested:

1. Include the relation of glue and wiring as the scale size increases. This will be especially interesting when suitable design cases are selected and analyzed.
2. Include the structure around control surfaces. Using 2-dimensional shells to model composites works well for continuous structures such as wing and fuselage skins. However, for joints and more complex (and typically, heavier) fittings, local effects become important in a composite layup. In this case, 3D solid elements should be used that allow full interlaminar and through-thickness effects to be simulated. Failure modes such as delamination and interlaminar shear would otherwise be missed.
3. Consideration of detailed structural modelling for global SM finite element model (e.g. stifferener elements if eventually needed, include the effects of rib holes).
4. Identification of critical load cases for SM. propulsion loads, airloads due to engine installation, landing gear impact loads, miscellaneious loads: door loads, ground handling loads, control surface loads. Typical design conditions of the fuselage section are those corresponding to the landing impact of the aircraft. These conditions, usually referred to as "dynamic landing".

BIBLIOGRAPHY

[1] E. Commission, "Flightpath 2050 europe's vision for aviation", en, *technical report European Union, Luxembourg*, https://op.europa.eu/s/olL5, 2011.

[2] IATA, *Forecasts passenger demand to double over 20 years*, Mar. 2016.

[3] J. P. Dorian, H. T. Franssen, and D. R. Simbeck, "Global challenges in energy", en, *Energy Policy*, vol. 34, no. 15, pp. 1984–1991, Oct. 2006, ISSN: 0301-4215.

[4] F. 2. E. V. for Aviation, *The High Level Group on Aviation Research*. Technical report, European Commission, 2016.

[5] V. Handojo, P. Lancelot, and R. de Breuker, "Implementation of active and passive loads alleviation methods on a generic mid-range aircraft configuration", en, p. 15,

[6] J. Ostrower, *What is the Boeing 737 Max maneuvering characteristics augmentation system*, Nov. 2018.

[7] J. Zamboni, R. Vos, M. Emeneth, and A. Schneegans, "Method for the conceptual design of hybrid electric aircraft", en, *AIAA Scitech 2019 Forum*, p. 1587, 2019.

[8] J. F. Gundlach, T. Philippe-André, and F. H. Gern, "Conceptual design studies of a strut-braced wing transonic transport", en, *Journal of aircraft*, vol. 37, no. 6, pp. 976–998, 2000.

[9] A. Frediani, ""lecture series: Innovative configurations and advanced concepts for future civil transport aircraft"", en, *Rhode St-Genèse: Von Kárman Institute for Fluid Dynamics*, 2005.

[10] G. Sacco and C. Lanari, "The three lifting surface configuration concept and lessons learned from the piaggio", en, *Innovative Configurations and Advanced Concepts for Future Civil Aircraft. Lecture Series of Von Karman Institute of Fluid*, p. 180, 2005.

[11] T. Pfeiffer, B. Nagel, D. Böhnke, A. Rizzi, and M. Voskuijl, "Implementation of a heterogeneous, variable-fidelity framework for flight mechanics analysis in preliminary aircraft design", en, *60th German Aerospace Congress (DLRK)*, 2011.

[12] D. Greenwell, "A review of unsteady aerodynamic modelling for flightdynamics of manoeuvrable aircraft", en, *AIAA Atmospheric Flight Mechanics Conference and Exhibit*, p. 5276, 2004.

[13] M. Ghoreyshi, K. Bdcock, and A. Rondch, "Framework for establishing limits of tabular aerodynamic models for flight dynamics analysis", en, *Journal of Aircraft*, vol. 48, no. 1, pp. 42–55, 2011.

[14] C. Jouannet and P. Krus, "Lift coefficient predictions for delta wing under pitching motions", en, *32nd AIAA Fluid Dynamics Conference and Exhibit*, p. 2969, 2002.

[15] J. K. Nathman, *Vsaero User's Manual*. Remond Washington, 1999, vol. 6.1.

[16] Flightstream, *Flighstream User's Guide - fast aerodynamics with fidelity*. Darcorp, 2020, vol. 2020.2.

[17] M. Vahora, G. Ananda, and M. Selig, "Design methodology for aerodynamically scaling of a general aviation aircraft airfoil", en, in *AIAA Aerospace Sciences 2019 Meeting*, American Institute of Aeronautics and Astronautics, 2018, p. 1277.

[18] J. Chambers, *Modeling Flight*. NASA Latest Version: The role of dynamically scale Free Flight Models in support of NASA aerospace programs., 2015, vol. 3.

[19] M. Palermo, "The longitudinal static stability and control characteristics of a flying v scaled model", Master's thesis, TU Delft, Aerospace Engineering, 2019.

[20] F. Bremmers and L. Eveleens, "Free flying scale model flight testing: Future or fiction", *NLR internal document*, vol. 1, p. 24, 2016.

[21] A. Raju Kulkarni, C. Varriale, M. Voskuijl, G. La Rocca, and L. Veldhuis, *Assessment of Sub-scale Designs for Scaled Flight Testing*. AIAA Aviation 2019 Forum, 2019, p. 3089.

[22] J. I. for the Advancement of Flight Sciences and L. R. Center, *A Study of Failure Criteria of FibrousComposite Materials*. NASA, 2001.

[23] A. Raju Kulkarni, G. La Rocca, and L. L. Veldhuis, "Degree of similitude estimation for sub-scale flight testing", en, in *AIAA Scitech 2019 Forum*, San Diego, California: American Institute of Aeronautics and Astronautics, Jan. 2019, ISBN: 978-1-62410-578-4.

[24] A. R. Kulkarni, G. La Rocca, and L. Veldhuis, "Degree of similitude estimation for sub-scale flight testing", Jan. 2019.

[25] EASA, *Prototype Commission Regulation on Unmanned Aircraft Operations*. Aug. 22, 2016.

[26] C. Wolowicz, H. Bowman, and S. James, "Similitude requirements and scaling relationships as applied to model testing", en, *NASA Technical Paper*, p. 65, 1979.

[27] G. La Rocca and M. van Tooren, "'enabling distributed multi-disciplinary design of complex products:a knowledge based engineering approach'", en, *Journal of Design Research*, vol. Vol. 5, no. 3, pp. 333–352,

[28] G. la Rocca, *Knowledge based engineering techniques to support aircraft design and optimization*. PhD thesis, Delft University of Technology.

[29] G. La Rocca, "Knowledge based engineering: Between ai and cad. review of a language based technology to support engineering design.", en, *Advanced Engineering Informatics*, vol. 26, no. 2, pp. 159–179, 2012.

[30] G. La Rocca and M. van Tooren, "'enabling distributed multi-disciplinary design of complex products:a knowledge based engineering approach'", en, *Journal of Design Research*, vol. 5, no. 3, pp. 333–352, 2007.

[31] M. Sansone, "Automated finite element model generation for structural investigation of closed wing systems (parsifal)", Master's thesis, TU Delft, Aerospace Engineering, 2018.

[32] J. de Klerk, "Design and integration of a propulsion system for the prandtlplane", Master's thesis, TU Delft, Aerospace Engineering, 2010.

[33] J. Benad, *Design of a Commercial Aircraft for High-subsonic Speed As a Flying Wing*. Airbus GmbH, Tech. public report; sensitive information censored, 2015.

[34] B. Rubio Pascual, "Engine-airframe integration for the flying v", Master's thesis, TU Delft, Aerospace Engineering, 2018.

[35] M. Claeys, "Flying v and reference aircraft structural analysis and mass comparison", Master's thesis, TU Delft, Aerospace Engineering, 2018.

[36] D. Raymer's, *Simplified Aircraft Design for Homebuilders*. Design Dimension Press, Los Angeles, USA, 2003.

[37] A. Bedford and W. Fowler, *Engineering Mechanics Dynamics*. Pearson, fifth edition in SI Units, 2008.

[38] T. Megson, *Aircraft Structures for Engineering Students*. Elsevier Aerospace Engineering Series.

[39] M. Corporation, *MD Nastran R3 Quick Reference Guide*. MSC Software, 2018.

[40] D. of defense handbook, *Composite Materials Handbook*. Volume 2. Polymer Matrix Composites Materials Properties, 2002.

[41] L. A. Dale, *Potential Flow Theory and Operation Guide for the Panel Code PMARC 14*. NASA, 1999.

[42] J. J.D. Anderson, *Fundamentals of Aerodynamics*. McGraw-Hill Series in Aeronautical and Aerospace Engineering.

[43] H. P. Heslehurst, "Composite fibre volume and weight ratios", en, *Composite Engineer Viewpoint*, 2015.

A PARAPY

The ParaPy software allows engineers to build parametric, rule-based software applications that automate simulation-driven engineering design processes. The company is located in YES!Delft tech incubator in Delft. The objective of the ParaPy software is to capture engineering logic and knowledge rules in a high-level and reusable way. The toolbox includes CAD modeling, meshing and CAE integration to write automatic input files for different discipline software.

The language is built on top of the popular Python language. With a geometry toolbox that uses OpenCascade as reference CAD, it provides access to curves, surfaces and solid modelling operations that are also used in widespread CAD systems, but eliminates manual re-work as much as possible. As soon as the geometry is built and the desired properties derived, it can be pre-processed for a specific discipline thanks to the integrated meshing-toolbox. Primitives, mesh-shapes and corresponding material properties are coupled in a sequential process. The meshing toolbox uses Salome as the reference CAD. The created mesh can then be linked to CAE softwares.

Moreover, there is a lot of flexibility when using ParaPy. They have many open code libraries that can be extended or modified if you need your own specific implementation layer over it. For example in this research work the advantage of an automated coupling of geometry-mesh-MSC NASTRAN input file chain is shown.

Figure A.1: The ParaPy software logo.

B | CLASS DIAGRAM STRUCTURAL COMPONENTS

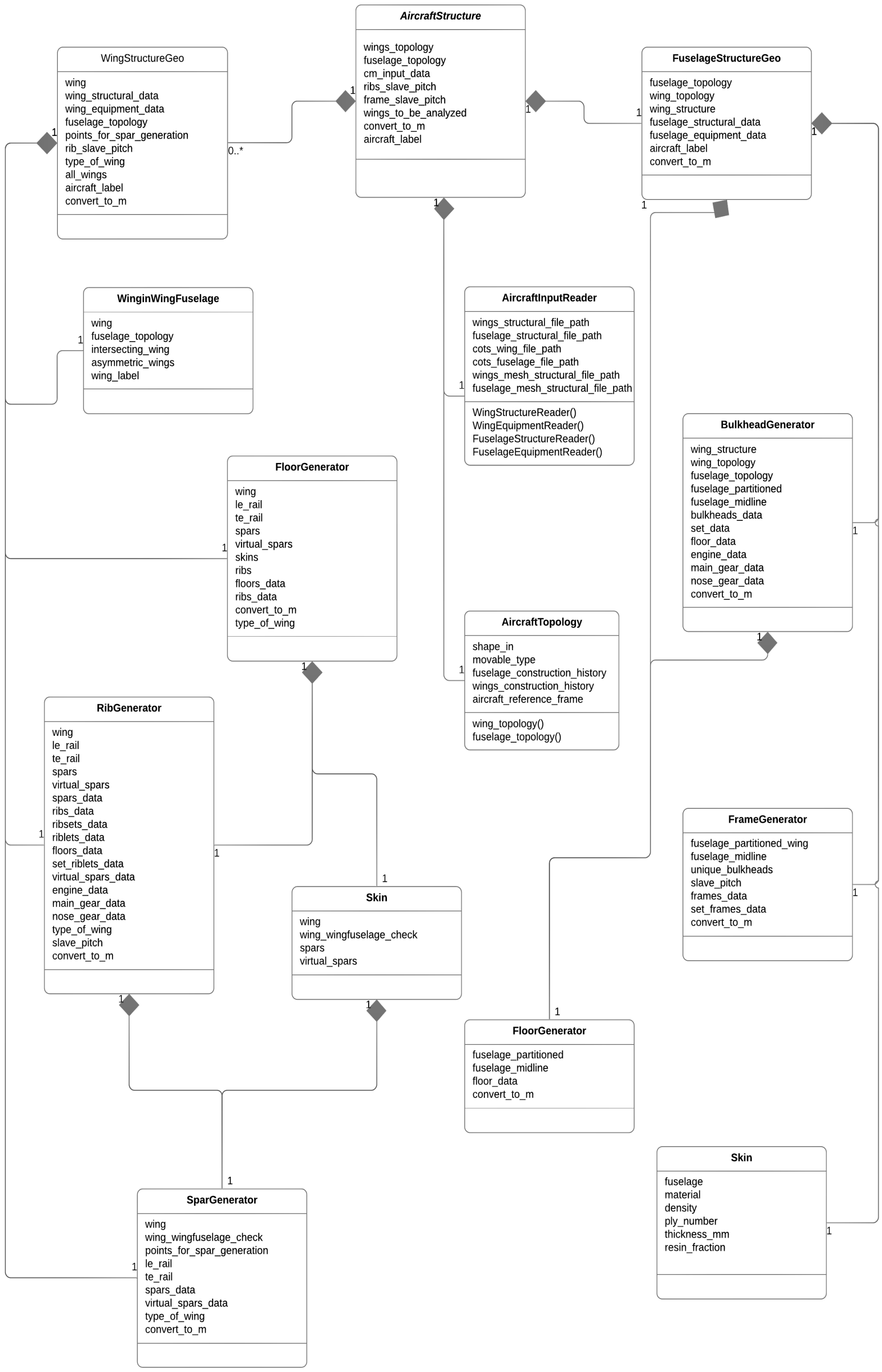

Figure B.1: Class diagram of the structural module.

C COMPOSITE MATERIAL

Different materials can be used in the design of SM, some of the options are wood or metal (isotropic), but most models in practice are built of composites.For Fibre-Reinforced Polymers (FRP)s a variety of materials for the fiber exist which is to be known as the main load carrying element in the composite, for example glass, graphite and boron. The matrix material bonds fibres together. Examples for the matrix material include epoxy, polyester and vinylester resins. Due to the composition, fibre-reinforced materials have higher specific strength and stiffness properties than metals, which makes them suitable for light-weight structures.

Fibre-reinforced composites show directional or anisotropic material properties. This means that a material property, such as strength, at a certain location will differ depending on the direction in which it is measured. Laminates with anisotropic properties, which are symmetric about some orthogonal planes, are called orthotropic laminates. In case of orthotropic material, the material has a specific material density, thickness, resin fraction and number of plies in the stacking sequence. The directional stiffness properties of a laminate can be altered by changing the ply fibre angles or by varying the order of placing the plies (known as the stacking sequence) with certain fibre angles in the laminate. These design variables together with the number of layers and the material type, which can be different for different plies, provide a larger design space than that available when metals are used.

A composite can not contain 100% fibre. In theory, maximum volume fraction can be achieved only if unidirectional fibers are hexagonally close next to each other such that all fibers are touching. The triangular unit cell in Figure C.3 has area $\sqrt{3R^2}$. The unit cell contains an area of fibre which is equal to $\pi R^2/2$. The maximum fibre volume fraction in a unidirectional fibre composite is given with equation C.1.

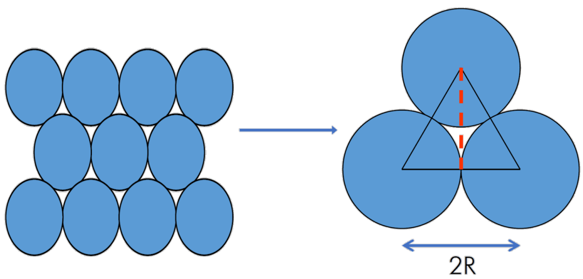

Figure C.1: Theoretical maximum fibre volume fraction.

$$V_f^{max} = \frac{\pi R^2/2}{\sqrt{3R^2}} = \frac{\pi}{2\sqrt{3}} = 0.908 \approx 91\% \tag{C.1}$$

In practice, fibres can not be perfectly aligned, but the accuracy can be improved with more sophisticated manufacturing methods. When composites are fabricated in molds and if the stacking sequence is done manually it can significantly effect the weight and strength properties. Gluing and bonding depends on precise control of temperature and humidity, exact mixing of the adhesive or matrix and careful preparation of the surfaces. In conclusion, the density and strength details depend

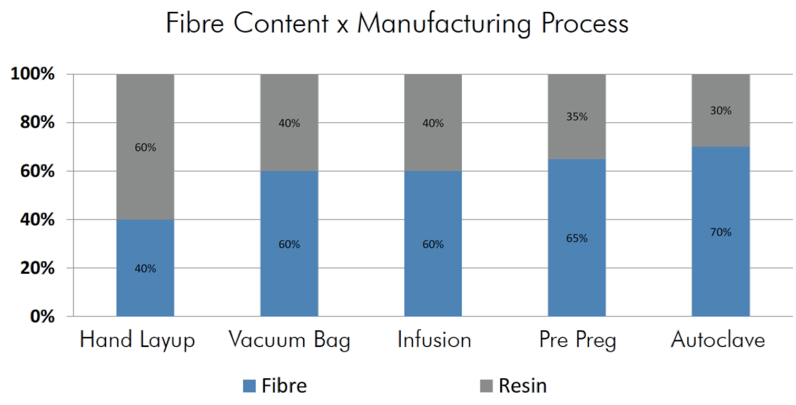

Figure C.2: Typical fiber fraction volumes for different manufacturing process [43].

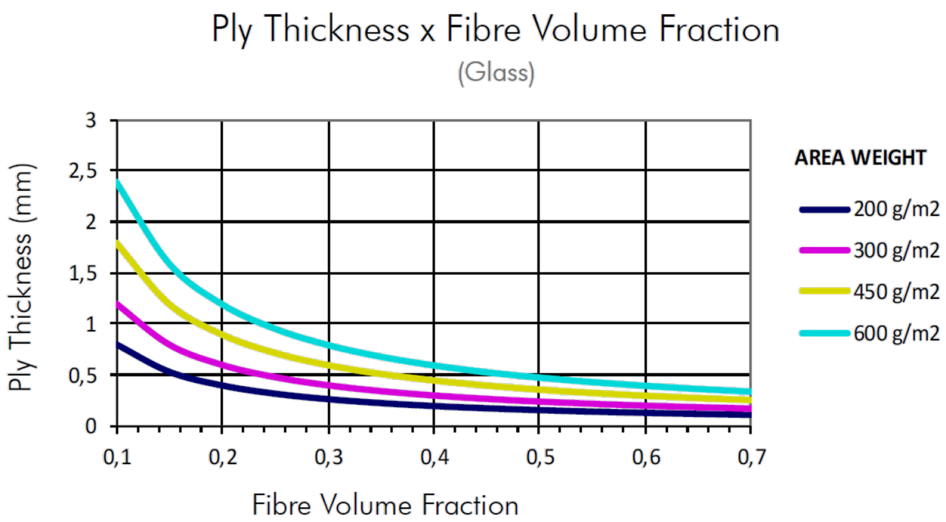

Figure C.3: Fibre volume fraction is inversely proportional to the laminate thickness [43].

very much on the manufacturing process.

When fabricating composite materials and structures from dry fibre and pouring liquid resin onto the fibres, a correct estimation for the ratio of weights of fibre and resin is required to have a correct initial estimate of the weight & balance of the SM. Typical values are given in Figure C.2. Commercial reinforcements are characterised by their areal weight (A_w). This is simply the weight (which is usually given in grams) of $1m^2$ of the reinforcement. A_w depends on many factor such as fiber density and weave style, and is typically given in the fabrication sheet of the manufacturer. The value may range from $100g/m^2$ up to more than $2000g/m^2$. Figure C.3 shows the fibre volume fraction in relation with the laminate thickness for different areal weights. The thickness of a composite laminate depends on the amount of reinforcement and the relative amount of resin which has been included. For a given quantity of reinforcement, a laminate with a high fibre volume fraction will be thinner than one with a lower fibre volume fraction, since it will contain less resin. The typical values such as resin fraction, areal weight and thickness can be any value given by the user.

D EQUIPMENT USED IN FLYING V

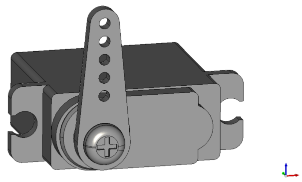

(a) Servo.

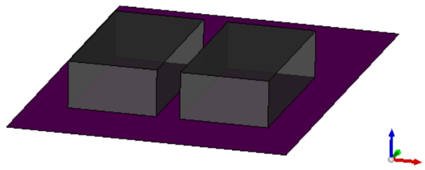

(b) Control power.

Figure D.1: Example components classified as Flight Control systems.

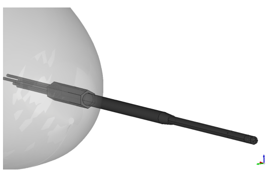

(a) Air data boom.

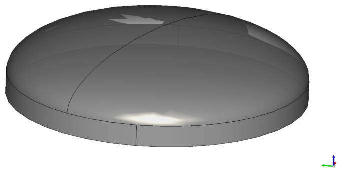

(b) GPS.

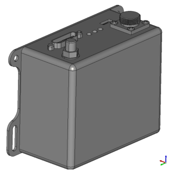

(c) Air data computer.

Figure D.2: Example components classified as scientific instruments.

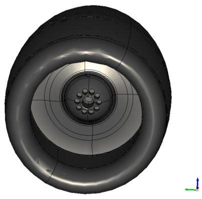

(a) The Engine with nacelle from the front.

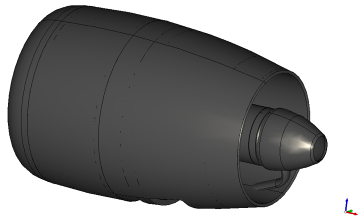

(b) The Engine with nacelle from the side.

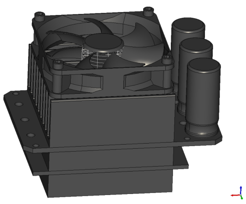

(c) ESC.

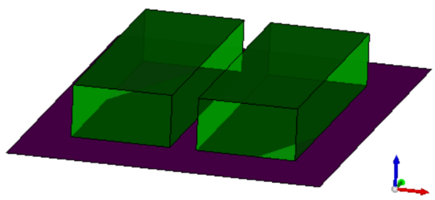

(d) Battery pack.

Figure D.3: Example components classified as propulsion system.

(a) Landing gear.

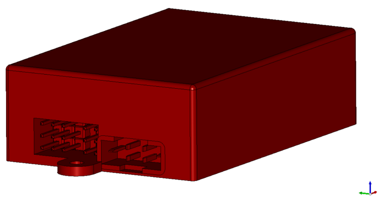

(b) Landing gear computer.

Figure D.4: Example components classified as landing gear systems.

E | FINITE-ELEMENT MODELING

Generating a correct and reasonable FE model is important to carry out FE analysis. The FE method approximates the behavior of a continuous structure with a finite number of elements. The approximated method represents a continuous structure as a collection of discrete elements connected by nodes. The element stiffness matrices are derived from material properties, element properties and the geometry. The stiffness matrices are then assembled into a global stiffness matrix, and together with loads and boundary conditions the nodal displacements can be solved.

Strains and stresses can be computed by the solver as a result of the displacement. As the number of elements increases (decrease the size of the elements), the results become increasingly accurate but the computing time also increases. Solving FE problems is always a balance between accuracy and model size.

There exist a wide range of elements in FE modelling providing flexibility in modeling different geometries and structures. Each element can be classified by the following:

- family
- number of nodes
- degrees of freedom
- formulation

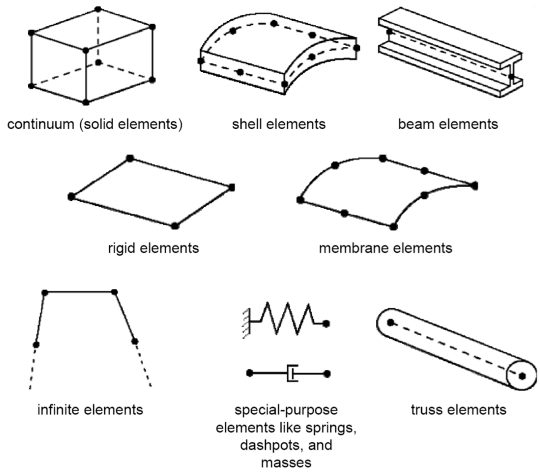

Figure E.1: A family of finite elements used to classify elements.

A family is the broadest classification an element can be put in, see Figure E.1. Shell elements are typically used to model structures in which one dimension (the thickness) is significantly smaller than the other dimensions and the stresses in the thickness direction are negligible. The element is then used to model bending and in-plane deformations. The element number of nodes determines how the nodal degrees of freedom is interpolated over the domain of the element, for example an 8-node or 4-node shell element. The degrees of freedom are for example displacements and rotations. The formulation used to describe the behavior of an element is another broad category that is used to classify elements, being thick/thin shells, small-strain/finite-strain shells or plane strain/stress.

F MSC NASTRAN INPUT FILE

MSC Nastran is a structural analysis solver and requires an input file. The input file contains all the information about the model to be analyzed. The input file is a .bdf or .dat format. The input file can be created with a pre-processing program called Patran. This is a pre- and post-processing software package for FE analysis. However, this could also be written automatically with other software, as is done within the DEE in this research work. In this work a method has been created to automatically write the input file for the geometry, composite materials and pressure loads (PLOAD4). The input file is generally divided into 5 main groups [39]:

1. NASTRAN Statement
2. File Management
3. Executive Control
4. Case Control
5. Bulk Data

The first two section are not mandatory, but optional to change for example some default settings, such as database operations and file management. The other three are mandatory and are explained in the following sections.

EXECUTIVE CONTROL

The Executive control establishes the type of analysis. There are many types of analysis possible, of which some of them are listed below:

1. MSC.Nastran solver for static loads analysis (SOL101)
2. MSC.Nastran solver for vibration analysis (SOL103)
3. MSC.Nastran solver for buckling analysis (SOL106)
4. MSC.Nastran solver for modal complex eigenvalue analysis (110)
5. MSC.Nastran solver for aeroelastic analysis (SOL114)
6. MSC.Nastran solver for structure design and optimization (SOL200)

In this research, the linear static solution has been studied, where a linear relation holds between applied forces and displacements. In practice, this is applicable to structural problems where stresses remain in the linear elastic range of the used material. The requirements regarding structural analysis focus on stiffness and max 2D principal strain. However, with some adaptations to the code other analysis type could be implemented. For example SOL103 and SOL110 if one would like to investigate landing gear impact on the SM.

CASE CONTROL

The Case Control section concerns the outputs and the definition of subcases, which contains the loadset and constraint set. The output requests that are of interest for the analysis can be defined and if other output requests are needed, can be easily added to the code. As regards the outputs, the current implemented output request consider displacement, SPC forces, stress, strain, applied loads, and force. Additionally, to automatically create the HDF5 file (to visualize results in Patran) and print the f06 results file these are also requested from the analysis.

BULK DATA

The BULK data section is the section in which all the information about the model is collected. The section contains the definition of model, loads and constraints. It is actually divided in a few subsections, each collecting the information needed for a particular part of the model. The subsections defined are:

- Properties (PCOMP, PSHELL)
- Elements: CQUAD4, CTRIA3
- Material: MAT8
- Grid
- Loads: PLOAD4, FORCE1, MOMENT
- Constraints: SPC1

In general terms, each line of a bdf file could be divided into 10 consecutive zones each composed by 8 characters. In particular cases, this structure could be modified. An example of a input file for MSC Nastran presenting the typical structure of the data is shown in Figure F.1.

MSC Nastran does not keep track of the units. Therefore, it is important that the user inputs all of the properties using a consistent set of units. For example, if meters m is defined for locations in grid entries, then the properties, such as areas A, should be in terms of $m2$. Therefore in some cases a coordinate of a node needs more than 8 characters, a structure with 16 characters is used for this node, to guarantee that the set value has also the right accuracy in the bdf to be modelled. The 8digit or 16digit spaces are filled with data with respect to Nastran cards. For example, the definition of a material requires a string defining the type of material, an integer as identification number and at the properties which are real numbers in case of the modulus of elasticity in longitudinal and lateral direction or the ply thickness. More details on requirements to correctly fill this data can be found in the MSC Nastran User Guide together with useful examples [39].

```
$ Generated by ParaPy-Nastran interface
$ Date: 2020-08-24T15:45:41
$ Project: main_wing
$ UseCase: my usecase
$
ID project id
SOL 101
TIME 5
CEND
TITLE = my title
SUBTITLE = my subtitle

$ Output requests: 
DISPLACEMENT(PRINT, PUNCH, SORT1, REAL) = ALL
SPCFORCES(PRINT, PUNCH, SORT1, REAL) = ALL
STRAIN(PRINT, PUNCH, SORT1, REAL, FIBER, BILIN) = ALL

SUBCASE 1
$ Subcase name : None
SUBTITLE=None
$ Selects a single-point constraint set to be applied.
       SPC = 116
$ Selects an external static loading set.
       LOAD = 6796
BEGIN BULK 
MDLPRM  HDF5    0
PARAM   PRTMAXIM YES
param,nocomps,-1
SPCADD  116     1       2       3       

LOAD    6796    1.00    1.00    1       1.00    2       1.00    3       

CORD2R* 1               0               0.000000e+00    0.000000e+00    *CRD2A1 
*CRD2A1 0.000000e+00    0.000000e+00    0.000000e+00    1.000000e+00    *CRD2B1 
*CRD2B1 1.000000e+00    0.000000e+00    0.000000e+00    

FORCE   1       109     1       2.53e-010.00    0.00    -1.00   
FORCE   2       1422    1       2.53e-010.00    0.00    -1.00   

PLOAD4  10001   1912    317.63  
PLOAD4  10002   1913    322.71  

SPC1    1       123456  5       
SPC1    2       123456  6       
SPC1    3       123456  7       

CQUAD4  1       1       115     1682    7442    1792    2       0.00    

PCOMP   1       
        1       1.30e-0490.00   NO      
        1       1.30e-04-45.00  NO      
        1       1.30e-0445.00   NO      
        1       1.30e-040.00    NO      

MAT8    1       1.4e+11 1.0e+10 2.7e-01 7.0e+09 7.0e+09 7.0e+09 2.3e+03 
MAT8    2       1.4e+11 1.0e+10 2.7e-01 7.0e+09 7.0e+09 7.0e+09 1.2e+03 
$
$ 8308 GRID POINTS DESCRIBE THE GEOMETRY
$
GRID*   1                               1.687800e+00    0.000000e+00            
*       6.786513e-02    
ENDDATA
```

Figure F.1: Typical structure of an input file for MSC Natran.

G INPUT FILES

The presented input files in this section are of demonstrative type, but of course the user can modify the inputs easily or automatically overwrite them after structural sizing. The format is sensitive to unexpected indentation or spelling, therefore attention must be paid while changing the input file. Example JSON input file for the parametric geometry and mesh building for the wing and fuselage inside the DEE is shown in Listings 1 to 4.

```
–”main˙wing”:–
    ”skin”:
        –”n˙skin”:1,
            ”wingbox˙material”: [”orthotropic”, ”foam”],
            ”wingbox˙density”: [0.162, 0.28],
            ”wingbox˙ply˙number”: [4, 1],
            ”wingbox˙thickness˙mm”: [0.13, 3],
            ”wingbox˙resin˙fraction”: [0.55, 0.0],
            ”top˙material”: [”orthotropic”],
            ”top˙density”: [0.162],
            ”top˙ply˙number”: [4],
            ”top˙thickness˙mm”: [0.13],
            ”top˙resin˙fraction”: [0.55],
            ”bottom˙material”: [”orthotropic”],
            ”bottom˙density”: [0.162],
            ”bottom˙ply˙number”: [4],
            ”bottom˙thickness˙mm”: [0.13],
            ”bottom˙resin˙fraction”: [0.55],
            ”root˙material”: [”orthotropic”],
            ”root˙density”: [0.162],
            ”root˙ply˙number”: [4],
            ”root˙thickness˙mm”: [0.13],
            ”root˙resin˙fraction”: [0.55],
            ”tip˙material”: [”orthotropic”],
            ”tip˙density”: [0.162],
            ”tip˙ply˙number”: [4],
            ”tip˙thickness˙mm”: [0.13],
            ”tip˙resin˙fraction”: [0.55],
            ”ply˙angles”: [0, 45, -45, 90, 0, 45, -45, 90],
            ”E1”: 137e9,
            ”E2”: 10.2e9,
            ”NU˙12”: 0.27,
            ”G12”: 7.0e9,
            ”G1Z”: 7.0e9,
            ”G2Z”: 7.0e9
        ”,
        ”spars”:
            –”n˙spar”:2,
                ”chordwise˙root˙location˙v”: [0.18, 0.68, 0.47, 0.09],
                ”spanwise˙root˙location˙v”: [0.0, 0.0, 0.0, 0.0],
                ”chordwise˙tip˙location˙v”: [0.18, 0.68, 0.5, 0.20],
```

```
                "spanwise˙tip˙location˙v": [1.0, 1.0, 1.0, 0.5],
                "spar˙method˙v": ["2points", "2points", "2points", "2points"],
                "angle˙v": [-45, -30, -30, 0],
                "spar˙span˙ratio˙v": [1, 0.2, 1, 1],
                "properties": –
                    "material": ["orthotropic", "foam"],
                    "resin˙fraction": [0.55, 0.0],
                    "density": [0.3, 0.19],
                    "ply˙number": [4, 1],
                    "thickness˙mm": [0.13, 5],
                    "ply˙angles": [0, 45, -45, 90, 0, 45, -45, 90],
                    "E1": 137e9,
                    "E2": 10.2e9,
                    "NU˙12": 0.27,
                    "G12": 7.0e9,
                    "G1Z": 7.0e9,
                    "G2Z": 7.0e9
                ”
        ”,
        "virtual˙spars":
            –"n˙spar": 0,
                "chordwise˙root˙location˙v": [0.05, 0.94],
                "spanwise˙root˙location˙v": [0 ,0],
                "chordwise˙tip˙location˙v": [0.05, 0.94],
                "spanwise˙tip˙location˙v": [1, 1],
                "spar˙method˙v": ["2points", "2points"],
                "angle˙v": [20, 20],
                "spar˙span˙ratio˙v": [1, 1]
        ”,
        "ribs":
              –"n˙rib": 0,
                  "spanwise˙rib˙location˙v": [0.5, 0.3, 0.57, 0.67, 0.87, 0.95],
                "angle˙rib˙v": [0, 1, 0, 0, 1, 0],
                "rib˙has˙te": ["False", "False", "False", "False", "False", "False"],
                "rib˙has˙le": ["False", "False", "False", "False", "False", "False"],
                "rib˙height˙v": [0.8, 0.8, 0.8, 0.5, 0.5, 0.5],
                "rib˙intersection˙method": ["keep", "wingbox"],
                "rib˙cut˙method": ["ellipse", "circle", "scaled˙curve", ],
                "n˙wingbox˙holes": [0, 0, 0, 2, 2, 1],
                "properties": –
                    "material": ["orthotropic", "foam"],
                    "resin˙fraction": [0.55, 0.0],
                    "density": [0.3, 0.19],
                    "ply˙number": [4, 1],
                    "thickness˙mm": [0.13, 5],
                    "ply˙angles": [90, 45, 0, -45, 90],
                    "E1": 137e9,
                    "E2": 10.2e9,
                    "NU˙12": 0.27,
                    "G12": 7.0e9,
                    "G1Z": 7.0e9,
                    "G2Z": 7.0e9
                ”
            ”,
        "riblets":
              –"n˙rib˙riblet": 0,
```

```
            "spanwise˙riblet˙location˙v": [0.2, 0.82, 0.43],
            "angle˙rib˙riblet˙v": [0, 0, 0],
            "angle˙riblet˙LEz˙v": [10, 5, 10],
            "angle˙riblet˙TEz˙v": [10, 5, 7],
            "riblet˙has˙te": [0, 0, 0, 0, 0, 0],
            "riblet˙has˙le": [0, 0, 0, 0, 0, 0],
            "riblet˙height˙v": [0.7, 0.8, 0.9, 0.8, 0.8, 0.8],
            "riblet˙cut˙method": ["scaled˙curve", "ellipse", "circle"],
            "n˙wingbox˙holes": [0, 0, 0, 2, 2, 1],
            "properties": –
               "material": ["orthotropic"],
               "resin˙fraction": [0.55],
               "density": [0.3],
               "ply˙number": [4],
               "thickness˙mm": [0.13],
               "ply˙angles": [90, 45, 0, -45, 90],
               "E1": 137e9,
               "E2": 10.2e9,
               "NU˙12": 0.27,
               "G12": 7.0e9,
               "G1Z": 7.0e9,
               "G2Z": 7.0e9
            ”
      ”,
      "floor":
           –"n˙floors": 1,
            "floor˙height˙v": [0.1, 0.2],
            "floor˙wingbox˙width˙v": [0.9, 0.8],
            "floor˙start˙location˙v": [0.2, 0.6],
            "floor˙end˙location˙v": [0.4, 0.8],
            "properties": –
               "material": ["orthotropic"],
               "resin˙fraction": [0.55],
               "density": [0.3],
               "ply˙number": [4],
               "thickness˙mm": [0.13],
               "ply˙angles": [90, 45, 0, -45, 90],
               "E1": 137e9,
               "E2": 10.2e9,
               "NU˙12": 0.27,
               "G12": 7.0e9,
               "G1Z": 7.0e9,
               "G2Z": 7.0e9
            ”
      ”,

      "set˙ribs":
           –"n˙set": 0,
            "set˙method": ["all pitch", "number", "pitch"],
            "set˙start˙v": [0, 0.25, 0.25],
            "set˙end˙v": [0, 0.45, 0.25],
            "set˙number": [0, 5, 0],
            "set˙rib˙angle˙v": [0, 0, 0],
            "set˙pitch˙v": [0.2, 0, 0.05],
            "set˙has˙te": [0, 0, 0, 0, 0, 0],
            "set˙has˙le": [0, 0, 0, 0, 0, 0],
```

```
                    ”set˙intersection˙method”: [”keep”, ”wingbox”, ”wingbox”],
                    ”set˙cut˙method”: [”ellipse”, ”circle”, ”ellipse”],
                    ”set˙rib˙height˙v”: [0.8, 0.8, 0.8],
                    ”set˙n˙wingbox˙holes”: [0, 0, 0, 2, 2, 1],
                    ”properties”: –
                        ”material”: [”orthotropic”],
                        ”resin˙fraction”: [0.55],
                        ”density”: [0.3],
                        ”ply˙number”: [4],
                        ”thickness˙mm”: [0.13],
                        ”ply˙angles”: [90, 45, 0, -45, 90],
                        ”E1”: 137e9,
                        ”E2”: 10.2e9,
                        ”NU˙12”: 0.27,
                        ”G12”: 7.0e9,
                        ”G1Z”: 7.0e9,
                        ”G2Z”: 7.0e9
                    ”
            ”,
            ”set˙riblets”:
                –”n˙set”: 0,
                    ”set˙method”: [”pitch”, ”number”, ”all pitch”],
                    ”set˙start˙v”: [0.3, 0.4, 0.35],
                    ”set˙end˙v”: [0.5, 0.6, 0.7],
                    ”set˙number”: [3, 8, 6],
                    ”set˙riblets˙angle˙v”: [0, 0, 0],
                    ”set˙riblets˙LE˙angle˙v”: [10, 0, 0],
                    ”set˙riblets˙TE˙angle˙v”: [-10, 0, 0],
                    ”set˙pitch˙v”: [0.10, 0.0625, 0.1],
                    ”set˙has˙te”: [0, 0, 0, 0, 0, 0],
                    ”set˙has˙le”: [0, 0, 0, 0, 0, 0],
                    ”set˙cut˙method”: [”ellipse”, ”circle”, ”ellipse”],
                    ”set˙riblet˙height˙v”: [0.8, 0.8],
                    ”set˙n˙wingbox˙holes”: [0, 0, 0, 2, 2, 1],
                    ”properties”: –
                        ”material”: [”orthotropic”],
                        ”resin˙fraction”: [0.55],
                        ”density”: [0.3],
                        ”ply˙number”: [4],
                        ”thickness˙mm”: [0.13],
                        ”ply˙angles”: [90, 45, 0, -45, 90],
                        ”E1”: 137e9,
                        ”E2”: 10.2e9,
                        ”NU˙12”: 0.27,
                        ”G12”: 7.0e9,
                        ”G1Z”: 7.0e9,
                        ”G2Z”: 7.0e9
                    ”
            ”
        ”
```


Listing 1: JSON example for a wing structure

In a similar manner, Listing 2 gives an example for the fuselage.

```
–
    "fuselage":–
        "skin":
            –"n˙skin":1,
                "properties": –
                    "material": ["orthotropic"],
                    "density": [0.162],
                    "ply˙number": [4],
                    "thickness˙mm": [0.13],
                    "resin˙fraction": [0.55],
                    "ply˙angles": [90, 45, 0, -45, 90, 0, 45, 0, 90],
                    "E1": 137e9,
                    "E2": 10.2e9,
                    "NU˙12": 0.27,
                    "G12": 7.0e9,
                    "G1Z": 7.0e9,
                    "G2Z": 7.0e9
                ˝
            ˝,

        "bulkheads":
            –"n˙bulkhead":0,
                "bulkhead˙edge˙location˙v": [0.1, 0.9],
                "bulkhead˙intersection˙method": ["keep", "bottom", "top"],
                "properties": –
                    "material": ["orthotropic", "foam"],
                    "density": [0.3, 0.19],
                    "ply˙number": [4, 1],
                    "thickness˙mm": [0.13, 3],
                    "resin˙fraction": [0.55, 0.0],
                    "ply˙angles": [90, 45, 0, -45, 90, 0],
                    "E1": 137e9,
                    "E2": 10.2e9,
                    "NU˙12": 0.27,
                    "G12": 7.0e9,
                    "G1Z": 7.0e9,
                    "G2Z": 7.0e9
                ˝
            ˝,
        "set˙bulkheads":
            –"n˙set":0,
                "set˙method": ["pitch", "number", "pitch"],
                "set˙start˙v": [0.0, 0.45, 0.7],
                "set˙end˙v": [0.0, 0.6, 0.9],
                "set˙number": [0, 4, 6],
                "set˙pitch˙v": [0.0, 0.2, 0.3],
                "set˙intersection˙method": ["keep", "bottom", "top"],
                "properties": –
                    "material": ["orthotropic", "foam"],
                    "density": [0.3, 0.19],
                    "ply˙number": [4, 1],
                    "thickness˙mm": [0.13, 3],
                    "resin˙fraction": [0.55, 0.0],
                    "ply˙angles": [90, 45, 0, -45, 90, 0],
```

```
                "E1": 137e9,
                "E2": 10.2e9,
                "NU˙12": 0.27,
                "G12": 7.0e9,
                "G1Z": 7.0e9,
                "G2Z": 7.0e9
            ”
    ”,
    "frames":
        –"n˙frames":0,
            "frame˙edge˙location˙v": [0.25, 0.3, 0.35, 0.55, 0.7, 0.8, 0.85],
            "frame˙height˙v": [0.7, 0.8, 0.9, 0.8, 0.8, 0.8, 0.8],
            "frame˙intersection˙method": ["keep", "bottom", "top"],
            "frame˙cut˙method": ["scaled˙curve", "ellipse", "circle"],
            "properties": –
                "material": ["orthotropic", "foam"],
                "density": [0.3, 0.19],
                "ply˙number": [4, 1],
                "thickness˙mm": [0.13, 5],
                "resin˙fraction": [0.55, 0.0],
                "ply˙angles": [90, 45, 0, -45, 90, 0],
                "E1": 137e9,
                "E2": 10.2e9,
                "NU˙12": 0.27,
                "G12": 7.0e9,
                "G1Z": 7.0e9,
                "G2Z": 7.0e9
            ”
    ”,
    "set˙frames":
        –"n˙set":0,
            "set˙method": ["number", "pitch", "all pitch"],
            "set˙start˙v": [0.0, 0.5, 0.7],
            "set˙end˙v": [0.0, 0.9, 0.9],
            "set˙number": [0.0, 4, 6],
            "set˙pitch˙v": [0.04, 0.1, 0.3],
            "set˙intersection˙method": ["keep", "keep", "keep", "remove"],
            "set˙cut˙method": ["circle", "circle", "ellipse"],
            "set˙frame˙height˙v": [0.8, 0.9, 0.9],
            "properties": –
                "material": ["orthotropic", "foam"],
                "density": [0.3, 0.19],
                "ply˙number": [4, 1],
                "thickness˙mm": [0.13, 5],
                "resin˙fraction": [0.55, 0.0],
                "ply˙angles": [90, 45, 0, -45, 90, 0],
                "E1": 137e9,
                "E2": 10.2e9,
                "NU˙12": 0.27,
                "G12": 7.0e9,
                "G1Z": 7.0e9,
                "G2Z": 7.0e9
            ”
    ”,
    "floor":
            –"n˙floors": 3,
```

```
                    ”floor˙height˙v”: [0.4, 0.6, 0.4],
                   ”floor˙start˙location˙v”: [0.15, 0.35, 0.7],
                   ”floor˙end˙location˙v”: [0.30, 0.55, 0.8],
                   ”properties”: –
                       ”material”: [”orthotropic”, ”foam”],
                       ”density”: [0.3, 0.19],
                       ”ply˙number”: [4, 1],
                       ”thickness˙mm”: [0.13, 5],
                       ”resin˙fraction”: [0.55, 0.0],
                       ”ply˙angles”: [90, 45, 0, -45, 90],
                       ”E1”: 137e9,
                       ”E2”: 10.2e9,
                       ”NU˙12”: 0.27,
                       ”G12”: 7.0e9,
                       ”G1Z”: 7.0e9,
                       ”G2Z”: 7.0e9
                   ”
               ”
       ”
   ”
```

Listing 2: JSON example for a fuselage structure

The geometry is based on a parametric description and also the mesh is parametrically defined. The mesh control is defined on the base of input provided by the user. Those are the number of nodes or the pitch of nodes to put in each edge. Listing 3 gives an example for the wings mesh controls.

```
"main˙wing":–
    "torsion˙box˙chord˙number": 6,
    "le˙chord˙number": 5,
    "te˙chord˙number": 5,
    "spanwise˙number": 10,
    "web˙number": 3,
    "spanwise˙pitch": 0.08,
    "lewise˙pitch": 0.05,
    "tewise˙pitch": 0.05,
    "boxwise˙pitch": 0.05,
    "spanwise˙method": "pitch",
    "lewise˙method": "pitch",
    "boxwise˙method": "pitch",
    "tewise˙method": "pitch"
  ”
```

Listing 3: JSON example for a wing structure

In a similar manner, Listing 4 gives an example for the fuselage mesh controls.

```
"fuselage":–
      "fuselage˙longitudinal˙pitch": 0.05,
      "fuselage˙lateral˙pitch": 0.05,
      "fuselage˙wings˙pitch": 0.05,
      "bulkhead˙inner˙pitch": 0.02,
      "frame˙inner˙pitch": 0.02
      ”
  ”
```

Listing 4: JSON example for a wing structure